High Magnetic Fields: A Tool for Studying Electronic Properties of Layered Organic Metals

Mark V. Kartsovnik*

Walther-Meissner-Institut, Bayerische Academie der Wissenschaften, Walther-Meissner-Strasse 8, D-85748 Garching, Germany

Received June 9, 2004

Contents

* Phone: (+49)-(0)89-289-142-23. Fax: (+49)-(0)89-289-142-06. E-mail: Mark.Kartsovnik@wmi.badw.de.

1. Introduction

Crystalline organic conductors have been among the most exciting objects in solid state physics and chemistry over the last two decades, providing a laboratory not only for studying virtually all the ground states known in condensed matter physics but also for discovering new ones.

Perhaps the most remarkable feature common to the organic conductors is the reduced dimensionality of the electronic band structure caused by the specific character of their crystal structure.[1] The basic structural units of these materials are partially charged flat organic molecules, for example, tetramethyltetraselenafulvalene, TMTSF, or bis(ethylenedithio)tetrathiafulvalene, BEDT-TTF, or similar donor/acceptor molecules. These units are packed in stacks or in layers separated from each other by counterions. The significant overlap between the molecular π orbitals and the fractional charge transfer from the molecules to the counterions lead to formation of partially filled conduction bands. Due to the chainlike or layered character of the intermolecular overlapping, the conductivity is highly anisotropic, so that the material can be considered as a *quasi-one-dimensional* (q1D) or a *quasi-two-dimensional* (q2D) conductor. Correspondingly, the Fermi surface (FS) of such a material is represented by a pair of open, almost flat sheets perpendicular to the direction of the highest conductivity (q1D case, Figure 1a, ref 2) or a cylinder (q2D case, Figure 1b, ref 3) which is only slightly warped in the direction along its axis parallel to the least conducting direction. In the latter case, the cross section of the cylinder may exceed the size of the first Brillouin zone that gives rise (see, e.g., ref 4) to a multiple connected FS consisting of a smaller cylinder and a pair of open sheets (Figure 1c and d, refs 5 and 6, respectively) or of several cylindrical FSs of smaller cross sections (Figure 1e, ref 7).

The reduced dimensionality combined with relatively low concentrations of charge carriers gives rise to strong electron correlations and numerous instabilities of the normal metallic state. This leads to very rich phase diagrams characterizing different families of the organic conductors or, sometimes, even single

10.1021/cr0306891 CCC: $48.50
Published on Web 10/22/2004

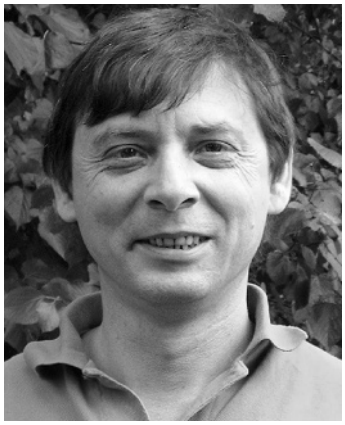

Mark Kartsovnik received his Ph.D. degree in Physics from the Institute of Solid State Physics, Chernogolovka, Russia, in 1990 under the direction of Igor Schegolev. After that he worked at the Institute of Solid State Physics consecutively as a researcher and a senior researcher till 1999. He spent one year as a JSPS postdoctoral fellow at Kyoto University in 1993–1994, working with Takehiko Ishiguro. Between 1996 and 1999 he was working as a visiting scientist at the Walther-Meissner-Institute for Low-Temperature Research in Garching, Germany. Since 2000 he has been a permanent member of the scientific staff of the Walther-Meissner-Institute. His research interests include electronic properties of low-dimensional organic conductors, in particular, high-magnetic-field phenomena in these materials.

compounds. An illustrative example is the phase diagram of the series of q1D radical cation salts $(TMTTF)_2X$/$(TMTSF)_2X$ (where X is an inorganic anion such as PF_6^-, AsF_6^-, ClO_4^-, Br^-) which contains various electronic states ranging from spin–Peierls insulating and Luttinger liquid states to superconductivity (for a review, see, e.g., refs 8–10). Among layered, or q2D, compounds, one should mention first of all the family of the highest-T_c organic conductors κ-$(BEDT\text{-}TTF)_2X$ (with X = Cu[N(CN)$_2$]Cl, Cu[N(CN)$_2$]Br, and Cu(NCS)$_2$)[11–13] and magnetic-field-induced superconductors $(BETS)_2Fe_xGa_{1-x}Y_4$ (Y = Cl, Br)[14–16] also exhibiting fascinating electronic phase diagrams.

Of course, the knowledge of the electronic band structure, in particular, of the FS properties is necessary for understanding the origin of various ground states realized in these materials. Tight-binding band structure calculations using the extended Hückel scheme have been amazingly successful in describing gross features of the FS and provided a good basis for qualitative understanding the relation between crystal structures and electronic properties in many cases (see, e.g., refs 4, 17, and 18). However, such calculations, relying on empirical parameters, do not warrant a priori a correct result. Furthermore, they are unable to describe quantitatively fine features of the band structure; for example, they basically ignore such an important characteristic of layered conductors as the interlayer coupling. Precise first-principles band structure calculations are still a challenging computational problem, due to large unit cells and mixed bonding types, althoughconsiderable progress has recently been demonstrated.[19,20] In this situation, experimental studies aimed to check the theoretical predictions and provide reliable quantitative information on the FS properties are of primary importance.

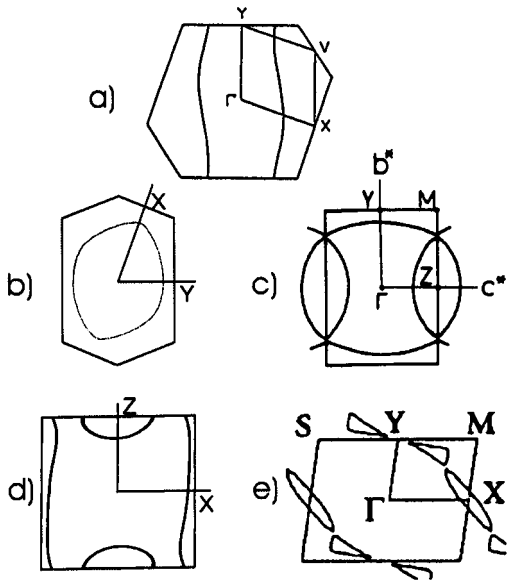

Figure 1. Typical examples of the Fermi surfaces of organic conductors—two-dimensional (parallel to the highly conducting plane) view: (a) $(TMTSF)_2AsF_6$ (Reproduced with permission from ref 2. Copyright 1983 EDP Sciences.); (b) β-$(BEDT\text{-}TTF)_2IBr_2$ (data taken from ref 3); (c) κ-$(BEDT\text{-}TTF)_2Cu(NCS)_2$ (Reproduced with permission from ref 5. Copyright 1988 American Physical Society); (d) α-$(BEDT\text{-}TTF)_2KHg(SCN)_4$ (Reproduced with permission from ref 6. Copyright 1996 EDP Sciences); (e) $(BEDO\text{-}TTF)_2ReO_4\cdot H_2O$ (data taken from ref 7). Brillouin zone boundaries and the principal axes of the reciprocal lattice are also shown.

High magnetic fields have been known for many years as one of the most powerful tools for exploring the FSs of conventional metals.[21–23] The discovery, in 1988, of the magnetic quantum oscillations in the salts κ-$(BEDT\text{-}TTF)_2Cu(NCS)_2$[5] and β-$(BEDT\text{-}TTF)_2IBr_2$[24] has proved this tool to be applicable to the organic conductors and triggered tremendous activities in this direction. It was soon found that not only the quantum oscillations but also the semiclassical magnetotransport experiments can be extremely useful for studying the FSs of these materials. A comprehensive survey of the FS studies of the organic conductors performed up to the middle of the 1990s is presented in ref 25. Some recent interesting cases of the application of the high-magnetic-field techniques, in particular to the salts κ-$(BEDT\text{-}TTF)_2X$ and α-$(BEDT\text{-}TTF)_2MHg(SCN)_2$ (M = K, Tl, Rb, NH_4), have been reviewed in ref 26. Nowadays, high-field experiments have become a necessary ingredient to complex characterization of newly synthesized compounds. They are also extensively used for gaining a deeper insight into electronic properties of already known materials.

The low-dimensional character of the organic conductors leads to important consequences in their response to a magnetic field. In fact, numerous drastic deviations from the conventional three-dimensional (3D) behavior and even qualitatively new effects have been found in these materials. Certainly, one has to understand the nature of these effects in order to correctly interpret the experimental data and obtain useful information.

This article aims to review the physical origin of specific high-magnetic-field phenomena emerging already in the normal metallic state of the organic conductors owing to their extremely high anisotropy and to illustrate how these phenomena can be used for studying the electronic system. The consideration is focused on layered, that is, q2D, compounds; however, some effects related to open FS sheets are also included, since such sheets are often met as a part of the FS in the layered conductors. In section 2 the behavior of the semiclassical magnetoresistance will be discussed. A number of novel effects, in particular related to the field orientation, will be presented. It will be shown that rather simple experiments may give important quantitative information on the exact geometry of the FS and on the anisotropic properties of the conduction system. Section 3 is devoted to quantum oscillations of the magnetization (de Haas−van Alphen, dHvA, effect) and of the resistivity (Shubnikov−de Haas, SdH, effect). As in conventional 3D metals, these oscillations have been widely used in studies of organic conductors. It turns out, however, that the extremely high anisotropy may lead to substantial deviations of the 3D model which should be taken into account in the analysis of experimental data. Recent theories describing the quantum oscillations in two-dimensional (2D) and q2D metals as well as examples of their applications to the organic conductors will be presented. Section 4 provides a brief summary of the most important issues considered in the paper.

2. Semiclassical Magnetoresistance

2.1. Magnetoresistance in Conventional Metals

The theory of galvanomagnetic phenomena in normal metals was basically developed in the 1950s. Since then, the magnetoresistance technique has been very extensively used for about two decades in experimental studies of FSs of many simple metals and some metallic compounds. Detailed reviews of the standard theory are given by Pippard[23] and Lifshitz, Azbel, and Kaganov;[27] the basic principles can also be found in more general textbooks; see, for example, refs 28−31. Here, we will only briefly introduce the most essential points of the semiclassical model. In the following, we will consider electrons in the vicinity of the Fermi level ϵ_F, which are responsible for conducting properties, and assume that scattering processes can be taken into account by introducing a constant relaxation time τ, independent of the electron's momentum and magnetic field. The latter, so-called τ-approximation is not always justified. For example, it ignores oscillations of τ in quantizing magnetic fields, which gives rise to the SdH effect presented in section 3. Nevertheless, this approximation provides a very good starting point for understanding the qualitative behavior of the semiclassical magnetoresistance.

When a magnetic field **B** is applied to a metal, the conduction electrons are subject to the Lorentz force:

$$\mathbf{F}_L = \frac{d\mathbf{p}}{dt} = e\mathbf{v} \times \mathbf{B} \tag{1}$$

where **p**, **v**, and e are, respectively, the electron's momentum, velocity, and charge. From eq 1 it immediately follows that the Lorentz force affects the momentum components in the plane perpendicular to the field; the projection of the momentum on the field direction, p_B, is constant. Further, the Lorentz force does not change the electron's energy, since it is always perpendicular to **v**. Therefore, in the momentum space, the electron motion is described by an orbit lying on the intersection of the FS and the plane p_B = constant, that is, normal to the field direction.

At a low field, the momentum **p** does not change significantly during the scattering time τ. The electron's trajectory is only slightly curved; the characteristic radius of curvature (Larmor radius), $r_L = p_F/eB$ (p_F is the Fermi momentum), is much larger than the mean free path l. In this case it can be shown that, for a current perpendicular to the field, the relative change in the resistivity is

$$\frac{\Delta\rho(B)}{\rho(0)} \propto \left(\frac{l}{r_L}\right)^2 \propto B^2 \tag{2}$$

Let us increase the field so that $r_L \lesssim l$. According to eq 1, the momentum associated with each individual electron will considerably change within the time τ. This obviously results in a varying electron's velocity $\mathbf{v}(\mathbf{p}) = \partial\epsilon(\mathbf{p})/\partial\mathbf{p}$, which depends on the momentum and is always perpendicular to the FS. To calculate the conductivity, now one has to solve the Boltzmann kinetic equation in the presence of both electric and magnetic fields. In the semiclassical τ-approximation the solution yields the conductivity tensor $\sigma_{\alpha\beta}$ in the form

$$\sigma_{\alpha\beta} = -\frac{2e^2\tau}{(2\pi\hbar)^3}\int \frac{df_0}{d\epsilon}\, v_\alpha(\mathbf{p})\overline{v_\beta(\mathbf{p})}\, d\mathbf{p} \tag{3}$$

where α and β stand for x, y, or z; $df_0/d\epsilon$ is the energy derivative of the equilibrium Fermi distribution function; and $\overline{v_\beta(\mathbf{p})}$ is the velocity averaged over the scattering time τ:

$$\overline{v_\beta(\mathbf{p})} = \frac{1}{\tau}\int_{-\infty}^{0} v_\beta(\mathbf{p},t)e^{t/\tau}\, dt \tag{4}$$

One can see from eqs 3 and 4 that the conductivity is determined by the average velocity, which depends on the magnetic field. From eqs 1, 3, and 4 one can numerically calculate the conductivity and, therefore, the resistance of a metal, provided the electron dispersion law $\epsilon(\mathbf{p})$ and, hence, the velocity $\mathbf{v}(\mathbf{p})$ are known. More interesting but, generally, much more complicated is the inverse problem: how to learn something new about the electron dispersion from the experimentally measured magnetoresistance. Lifshitz and co-workers[32,33] have shown that the asymptotic behavior of the conductivity (eq 3) in high magnetic fields is qualitatively determined by the topology of electron orbits on the FS and therefore can give important information about the FS geometry.

The electron motion along a closed orbit in **p**-space can be characterized by a *cyclotron* frequency,

$$\omega_c = \frac{2\pi eB}{(\partial S/\partial \epsilon)_{p_B}} = \frac{eB}{m_c} \quad (5)$$

where S is the orbit area and

$$m_c = (2\pi)^{-1}(\partial S/\partial \epsilon)_{p_B} \quad (6)$$

is a so-called cyclotron mass. In the high-field limit, $\omega_c\tau \gg 1$ (or, equivalently, $r_I/l \ll 1$), the electron completes many turns around the FS before being scattered. Its velocity components perpendicular to the field rapidly oscillate around zero, so that their time-average values tend to zero as the field increases. According to eq 3, this leads to a decrease of the corresponding conductivity components. In the coordinate system with the z axis directed along **B**, the conductivity tensor can be expressed as[32]

$$\sigma_{\alpha\beta}^{\text{closed}} = \sigma_0 \begin{pmatrix} \gamma^2 a_{xx} & \gamma a_{xy} & \gamma a_{xz} \\ -\gamma a_{xy} & \gamma^2 a_{yy} & \gamma a_{yz} \\ -\gamma a_{xz} & -\gamma a_{yz} & a_{zz} \end{pmatrix} \quad (7)$$

where $\gamma = (\omega_c\tau)^{-1} \ll 1$, σ_0 is the conductivity at zero field, and a_{ij} are coefficients determined by characteristics of the material and usually have the order of unity.

By taking the inverse of the tensor in eq 7, one obtains that, at the lowest order in γ, the diagonal components of resistivity are independent of B:

$$\rho_{xx,yy,zz}^{\text{closed}} \rightarrow \text{constant} \quad (8)$$

Thus, if all the orbits on the FS are *closed*, magnetoresistance *comes to saturation* at increasing field, for both the transverse (ρ_{xx}, ρ_{yy}) and longitudinal (ρ_{zz}) geometries.

If the FS is open, it is possible to align the magnetic field in such a way that an electron orbit in **p**-space will be open, that is, will cross Brillouin zone boundaries and extend to infinity. If the open orbit is, say, in the x direction (and, as before, $\mathbf{B}||\hat{\mathbf{z}}$), the y-component of the velocity does not oscillate around zero. Therefore, the time average of v_y does not vanish and the conductivity components σ_{yy} and σ_{yz} tend to finite values at increasing field:[32,33]

$$\sigma_{\alpha\beta}^{\text{open}} = \sigma_0 \begin{pmatrix} \gamma^2 a_{xx} & \gamma a_{xy} & \gamma a_{xz} \\ -\gamma a_{xy} & a_{yy} & a_{yz} \\ -\gamma a_{xz} & -a_{yz} & a_{zz} \end{pmatrix} \quad (9)$$

at $\gamma \ll 1$. The diagonal resistivity components in this case are

$$\rho_{xx}^{\text{open}} \propto (\omega_c\tau)^2 \propto B^2 \quad (10)$$

$$\rho_{yy,zz}^{\text{open}} \rightarrow \text{constant} \quad (11)$$

Thus, the magnetoresistance measured in the direction of an *open orbit increases* quadratically with field.

The qualitative difference between the behavior of ρ_{xx} in eqs 8 and 10 allows for probing the FS topology by means of a careful examination of the dependence of magnetoresistance on the magnetic field and electric current orientations. It should be noted that three-dimensional FSs are often quite complex, and this makes the measurement and analysis of angular diagrams of magnetoresistance very difficult and time-consuming. Such experiments have significantly contributed to studies of FSs of conventional metals (see, e.g., ref 21).

2.2. Cylindrical Fermi Surface

In this section, we will consider magnetoresistance behavior associated with a FS in the form of a cylinder slightly warped along its axis. Such a FS is, for example, typical of salts with the β-type packing of organic cation radicals.[1,25,34] In particular, as we will see, β-(BEDT-TTF)$_2$IBr$_2$ appears to be an ideal model object demonstrating all the basic effects. In many other compounds the FS consists of either multiple cylinders or a combination of a cylinder and a pair of corrugated planar sheets.[1,17,25,35] Therefore, the magnetoresistance properties introduced here can often be observed in such materials as well.

We will start with the most remarkable phenomenon, angle-dependent magnetoresistance oscillations, which provide a simple and, at the same time, extremely effective method of investigation of q2D FSs. After that we will consider the behavior of the nonoscillatory magnetoresistance background when the field is rotated (a) with respect to the plane of highly conducting layers and (b) within this plane. It will be shown what additional information about the electronic system can be obtained from this behavior.

Before proceeding further, the following comments should be made. First, it turns out that the most interesting, qualitatively new effects are observed in magnetoresistance measured with the current directed perpendicular to the plane of highly conducting layers, that is, in the *interlayer resistance* geometry. Fortunately, it is the interlayer resistance that can be most reliably measured in highly anisotropic layered compounds, using the conventional four-probe dc or low-frequency ac techniques. Indeed, let us consider a typical experimental geometry, as shown schematically in Figure 2a. Single crystals of organic metals are usually platelets with dimensions $\sim 1 \times (0.1-1)$ mm^2 in the plane of highly conducting molecular layers, and a thickness (i.e. the size in the direction perpendicular to the layers) ~ 0.1 mm. To measure the interlayer resistance $R_\perp$, one applies a current I via two leads attached, by a conducting paint, to the opposite lateral surfaces of the sample and records the voltage U on the adjacent pair of voltage leads. Given that the resistivity anisotropy ratio is, typically,

$$\rho_\perp/\rho_{||} \sim 10^3 \text{ to } 10^5 \quad (12)$$

($\rho_\perp$ and $\rho_{||}$ are the resistivities across and within the layers, respectively; in the plane of the layers the resistivity anisotropy is usually only $\sim 1-5$), the

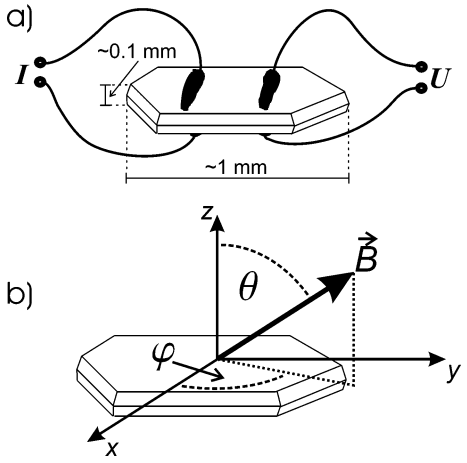

Figure 2. (a) Typical scheme of four-probe resistance measurements. Current I is applied through the opposite flat faces parallel to the highly conducting layers in the crystal; voltage U is measured between the same faces. Such a geometry provides a reliable evaluation of the interlayer resistance in the highly anisotropic layered organic conductors (see text). (b) Conventional definition of the magnetic field orientation by the tilt angle θ and the azimuthal angle φ.

current distribution is roughly equivalent to that in an isotropic rod with a cross section of $1 \times (0.1-1)$ mm^2 and length of 10^2-10^4 mm and, thus, can be taken as perfectly homogeneous. The resistance is then, obviously, determined as $R_\perp = U/I$. By contrast, the *in-plane resistance* measurements are typically much less reliable: the distribution of the current applied, nominally, along the layers is essentially inhomogeneous and strongly depends on the anisotropy ratio (eq 12).[36,37] Moreover, even small deviations of the current distribution from the ideal one caused by crystal imperfections such as microcracks or cavities, which are often met in organic metal crystals, lead to an uncontrollable mixing of the $\rho_\parallel$ and $\rho_\perp$ components. Thus, in what follows we will focus on the interlayer magnetoresistance.

Next, since the crystal orientation in a magnetic field is of primary importance in most of the phenomena discussed in this article, it is worth introducing notations with which the crystal versus field orientation will be defined hereinafter. As shown in Figure 2b, we introduce the coordinate system with the xy plane parallel to the plane of the molecular layers and the z axis normal to this plane. In cases of a strongly anisotropic in-plane conductivity, the x axis will be directed along the highest-conduction direction. The field orientation is defined by a polar angle θ, between the field direction and the z axis, and an azimuthal angle φ which is formed by the projection of the field on the xy plane and some characteristic direction in this plane, for example, the direction of molecular chains.

2.2.1. Angle-Dependent Magnetoresistance Oscillations (AMROs)

From the presented above results of the standard model one would, at first sight, expect a rather simple orientational dependence of the magnetoresistance in a layered metal with a cylindrical, only slightly warped, FS. Indeed, with tilting the field from the z axis (that is normal to the layers and, hence, parallel to the axis of the Fermi cylinder) toward a direction parallel to the layers, the topology of the electron orbits in **p**-space, which are always perpendicular to **B**, simply changes from closed (at θ not too near to $\pi/2$) to open (at $\theta \approx \pi/2$). Therefore, one could expect a gradual change from the regime described by eq 8 to that given by eqs 10 and 11, as described, for example, in refs 28 and 33.

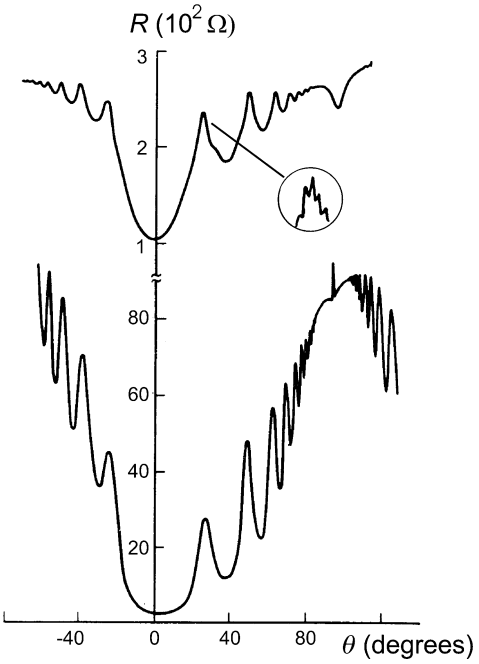

Figure 3. Angular dependence of the magnetoresistance of β-(BEDT-TTF)$_2$IBr$_2$ measured along (upper curve) and perpendicular to (lower curve) the highly conducting layers, at $T = 1.4$ K and $B = 15$ T.[38] The semiclassical magnetoresistance exhibits strong oscillations (AMRO). The weak, as compared to the AMRO, Shubnikov–de Haas oscillations at θ corresponding to the first AMRO peak are shown in the inset, in an enlarged scale.

However, already one of the first experimental studies[38] of the magnetoresistance anisotropy in a clean sample of the layered superconductor β-(BEDT-TTF)$_2$IBr$_2$ has shown a much more complex behavior. Figure 3 shows the resistance measured with the current applied along and perpendicular to the highly conducting ab plane (upper curve and lower curve, respectively) at the magnetic field $B = 15$ T rotating in the ac^* plane (where $c^* \perp ab$). The most obvious difference from the simple scenario mentioned above is the presence, in both curves, of a regular series of strong oscillations. Soon after this observation, similar oscillations were found[39] in another layered superconductor, θ-(BEDT-TTF)$_2$I$_3$, implying that they are a general property of q2D metals.

The basic features of these *angle-dependent magnetoresistance oscillations* or, shorter, *AMROs* can be summarized as follows:[38-40]

(i) The positions of the peaks in the magnetoresistance are unaffected by temperature or magnetic field strength and repeat periodically in the scale of tan θ.

(ii) The AMRO amplitude is much stronger for the interlayer resistance than for the intralayer one (see Figure 3).

(iii) The field dependence of the interlayer magnetoresistance is qualitatively different at the field orientations corresponding, respectively, to the dips and to the peaks of the oscillations. In the dips, $R_\perp(B)$ is sublinear, tending to saturation, whereas in the peaks it increases with field without saturation, approximately proportional to B^2.

(iv) The SdH oscillations, which are much smaller in magnitude than the AMROs (see the expanded $R(\theta)$ fragment in Figure 3), are strongly enhanced in the AMRO peaks.

Feature (i) indicates that the AMRO phenomenon must be associated with a specific geometry of the electron orbits in a tilted magnetic field rather than with phase transitions or a field-induced quantization of the energy spectrum (the latter, so-called Landau, quantization gives rise to the SdH oscillations whose angular position changes with the field strength). Feature (ii) suggests that the AMROs are primarily a property of the interlayer resistivity ρ_{zz}. The first, very important step in understanding the geometrical nature of AMROs was made by Yamaji.[41] He considered electron orbits on a weakly warped Fermi cylinder determined by the simplified dispersion law:

$$\epsilon(\mathbf{p}) = \frac{p_x^2 + p_y^2}{2m} - 2t_\perp \cos(p_z d/\hbar) \qquad (13)$$

with $t_\perp$ ($\ll \epsilon_F$) and d being the interlayer overlap integral and interlayer period, respectively, and noticed that the difference, ΔS, between the largest and the smallest areas of electron orbits on this cylinder oscillates with tilting the field:

$$\Delta S(\theta) \approx \frac{8\pi m t_\perp}{\cos\theta} J_0\left(\frac{p_F d}{\hbar}\tan\theta\right) \qquad (14)$$

where $p_F = (2m\epsilon_F)^{1/2}$ is the in-plane Fermi momentum and J_0 is the zeroth order Bessel function. In particular, for $\tan\theta > 1$ the Bessel function can be approximated as

$$J_0(\chi) \approx \sqrt{2/\pi\chi}\cos(\chi - \pi/4) \qquad (15)$$

and, therefore, $\Delta S = 0$; that is, *all the orbits have the same area* when[41]

$$|\tan\theta| = \frac{\pi\hbar}{p_F d}(n - {}^1/_4), \quad n = 1, 2, \ldots \qquad (16)$$

At angles satisfying this condition, the system becomes similar to a perfectly 2D metal in the sense that the energy spectrum is completely quantized into a series of Landau levels. This should lead to a dramatic enhancement of the SdH and dHvA oscillations, as, indeed, was observed in the experiment.[25,38,40]

As to the strong increase of the resistivity, it was proposed[41] that the complete Landau quantization also gives rise to an enhanced interlayer resistivity at the angles satisfying eq 16. However, it should be noted that the AMROs are observed even at conditions when the quantization effects, such as SdH oscillations, are completely suppressed due to strong scattering or high temperature. Therefore, the nature of AMROs is more likely semiclassical, without involving the Landau quantization.

Indeed, Yagi et al.[42] have succeeded in simulating the AMRO effect by numerical integration of the semiclassical expression of the form in eq 3 for the interlayer conductivity $\sigma_{zz}(B)$, assuming the simplified dispersion relation in eq 13. They have also obtained the analytical formula for the conductivity illustrating the angular oscillations:

$$\sigma_{zz} = \sigma_{zz}^\circ \sum_{n=-\infty}^{\infty} \frac{J_n^2(p_F d\tan\theta/\hbar)}{1 + (n\omega_c\tau)^2} \qquad (17)$$

where J_n is the n-th order Bessel function, $\omega_c = eB\cos\theta/m$ is the cyclotron frequency in the tilted field, and $\sigma_{zz}^\circ = \sigma_{zz}(B = 0)$. In high fields, $\omega_c\tau \gg 1$, the dominant contribution to the sum in eq 17 is generally given by the term with $n = 0$. However, at the tilt angles satisfying the condition in eq 16 the numerator of this term vanishes, which leads to a sharp decrease in the conductivity and hence to a peak in the resistivity $\rho_{zz} \approx 1/\sigma_{zz}$. The field dependence $\rho_{zz}(B)$ has been shown[42] to change qualitatively on moving from an AMRO peak to a dip, in agreement with the experiment [see feature (iii) of the AMROs above]. Similar results describing the AMRO behavior have been obtained by Peschansky et al.[43] for a generalized q2D spectrum.

Qualitatively, the physical origin of the AMROs can be understood from the following consideration.[3] In the high-field limit, $\omega_c\tau \gg 1$, the conductivity σ_{zz} essentially depends on the interlayer velocity v_z averaged over the period of the electron motion on the closed orbit (see eqs 3 and 4). The latter, in turn, is determined by the dependence of the orbit area S on the position in **p**-space:

$$\overline{v_z} = \overline{\partial\epsilon/\partial p_z} = -\frac{\partial S(P_z)/\partial P_z}{(\partial S/\partial\epsilon)_{P_z}} = -\frac{\partial S(P_z)/\partial P_z}{2\pi m_c} \qquad (18)$$

where P_z is the point at which the plane of the orbit intersects the p_z axis, and the cyclotron mass m_c defined by eq 6 monotonically increases proportional to $1/\cos\theta$ in the q2D case. The derivative $\partial S(P_z)/\partial P_z$ is, generally, also finite, so that the interlayer conductivity σ_{zz} saturates at a finite value with increasing the field. However, at the angles satisfying Yamaji's condition in eq 16, $\partial S(P_z)/\partial P_z \approx 0$. This leads to the vanishing averaged velocity $\overline{v_z}$ and, hence, vanishing σ_{zz}. An explicit analysis shows[43] that, at Yamaji's angles, the interlayer resistivity rapidly increases,

$$\rho_{zz} \propto B^2 \qquad (19)$$

as long as $1 \ll \omega_c\tau \ll \epsilon_F/t_\perp$, tending to saturation only at $\omega_c\tau > \epsilon_F/t_\perp$.

As will be shown below (see sections 2.2.2 and 3.1.1), for β-(BEDT-TTF)$_2$IBr$_2$ the ratio $\epsilon_F/t_\perp > 10^2$ while $\omega_c\tau \simeq 3-7$ for clean samples in fields of 10−15 T. Therefore, the dependence $\rho_{zz}(B)$ is expected to be approximately parabolic at Yamaji's angles in this field range, in agreement with the experiment.[40]

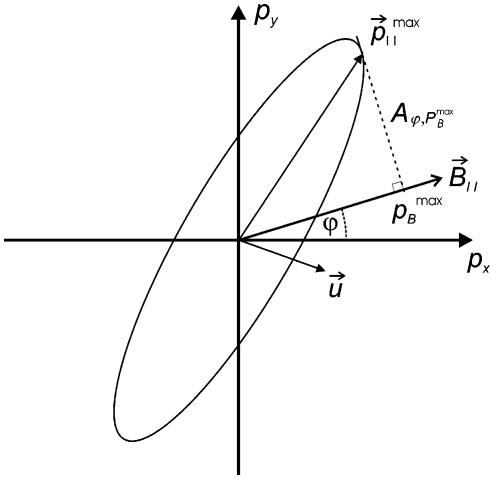

Figure 4. Schematic view of the transverse cross section of a cylindrical FS. $\mathbf{B}_{||}$ is the field component parallel to the xy plane; $\mathbf{p}_{||}^{\max}$ is the in-plane component of the Fermi momentum whose projection on the direction $\mathbf{B}_{||}$ attains the maximum value $p_B^{\max}$; $\mathbf{u}$ is the in-plane component of the interlayer hopping vector $\mathbf{h} = (u_x, u_y, d)$; see eqs 20 and 21.

Thus, the AMRO phenomenon can be successfully interpreted in terms of the semiclassical transport model as a kind of periodically repeating dimensional crossover between a strongly anisotropic, but still 3D, transport and an almost ideally 2D case with a vanishingly small interlayer transfer.

The condition in eq 16 for the AMRO peaks can be generalized for a more realistic dispersion relation:

$$\epsilon(\mathbf{p}) = \epsilon(p_x,p_y) - 2t_\perp \cos[(p_z d + p_x u_x + p_y u_y)/\hbar] \quad (20)$$

where $\epsilon(p_x,p_y)$ is an even function of p_x and p_y corresponding to a convex cross section of the FS; u_x and u_y have the meaning of in-plane components of an oblique *hopping vector* $\mathbf{h} = (u_x, u_y, d)$ along which electrons are effectively transferred between the layers. In this case, eq 16 should be modified to the form[3]

$$|\tan\theta| = [\pi\hbar(n - {}^1/_4) \pm (\mathbf{p}_{||}^{\max}\cdot\mathbf{u})]/p_B^{\max} d \quad (21)$$

where the sign in the $\pm$ is the same as the sign of $\tan\theta$ and the meaning of $\mathbf{p}_{||}^{\max}$ and $p_B^{\max}$ is illustrated in Figure 4: $\mathbf{p}_{||}^{\max}$ is the in-plane Fermi momentum whose projection on the field rotation plane, determined by angle φ, takes the maximum value, denoted as $p_B^{\max}$. From the periods of AMROs measured at various azimuthal angles φ, one can determine $p_B^{\max}(\varphi)$ and graphically deduce the shape and size of the FS cross section in the p_xp_y plane. The line $\mathbf{A}_{\varphi,p_B^{\max}}$ perpendicular to the projection of the field rotation plane on the p_xp_y plane drawn at the distance $p_B^{\max}$ from the coordinate origin is tangent to the FS at point $\mathbf{p}_{||}^{\max}$. One has to determine the set of $\mathbf{A}_{\varphi,p_B^{\max}}$ by measuring AMROs at various φ's, and the figure inscribed in this set will give the FS cross section. Such a procedure was for the first time applied to determine the FS of β-(BEDT-TTF)$_2$IBr$_2$[3].

As was noted in ref 44, in the case of a regular shape of the FS cross section, when it can be described by the "superelliptic" parametric form, $|p_x/p_1|^\alpha + |p_y/p_2|^\alpha = 1$, the value $p_B^{\max}$ can be analytically expressed via the principal semiaxes p_1 and p_2:

$$p_B^{\max}(\varphi) = \frac{\sin\varphi + \cos\varphi[(p_1/p_2)^\alpha \cot\varphi]^{1/(\alpha-1)}}{[(p_1\cot\varphi/p_2^\alpha)^{\alpha/(\alpha-1)} + p_2{}^{-\alpha}]^{1/\alpha}} \quad (22)$$

The exponent α should be greater than 1, since eq 21 is applicable only to convex cross sections. At $\alpha = 1$ the shape of the "superellipse" is a rhombus; at $\alpha \to \infty$, it approaches a rectangle. For an elliptical shape, $\alpha = 2$ and eq 22 is simplified to[45]

$$p_B^{\max}(\varphi) = [(p_1\cos\varphi)^2 + (p_2\sin\varphi)^2]^{1/2} \quad (23)$$

It should be noted, however, that organic conductors have generally rather low-symmetric crystal structures and irregular FSs. Therefore, for exact determination of the FS, it is preferable to use the direct graphical procedure described above. This can be of special importance when, for example, nesting properties of the FS are in question.

In addition to the determination of the FS cross section, eq 21 gives a possibility to estimate the direction of the hopping vector $\mathbf{h}$ or, in other words, the orientation of the characteristic plane of warping of the FS[3]. This is given by the asymmetry of the positions of AMROs with respect to $\tan\theta = 0$.

The presented semiclassical description of the AMRO effect[3,42,43] is utterly related to the interlayer resistance. The in-plane resistance is predicted to change in a monotonic manner with the tilt angle θ.[43] To check this, Kurihara[46] has performed a quantum mechanical analysis of both σ_{zz} and σ_{xx}, based on the eigenvalues of the model q2D Hamiltonian in a tilted magnetic field. The result obtained for σ_{zz} essentially coincides with that of the semiclassical model. In the expression for σ_{xx}, a term oscillating periodically with $\tan\theta$ has been obtained. However, this term seems to be of the order of the SdH oscillations and become unimportant when Landau quantization effects are suppressed due to scattering or temperature. Thus, the relatively strong oscillations seen in the upper curve in Figure 3 are most likely caused by the presence of the interlayer conductivity component in what is called "in-plane resistance" R_a.

We have shown that the AMRO phenomenon is an extremely powerful tool, not only providing qualitative information on the topology of the FS (as is the case of ordinary 3D metals) but also enabling direct quantitative evaluation of its exact shape and size. Unlike magnetic quantum oscillations, such as dHvA or SdH effects, they do not rely on the field-induced quantization of the energy spectrum and therefore can be observed at lower fields and higher temperature. Nowadays the AMROs are routinely used in Fermiology of metallic charge-transfer salts. A number of important examples are reviewed in refs 25, 26, and 47. Some more recent illustrative examples are FS studies of new materials, β-(BDA-TTP)$_2$SbF$_6$[48,49] and (BEDT-TTF)$_2$Br(DIA),[50] and detection of cylindrical FS pockets at low temperatures in originally

q1D compounds, $(TMTSF)_2FSO_3$[51] and $(DMET\text{-}TSeF)_2Au(CN)_2$.[52] It is worth noting that the AMROs have also been observed and applied for FS studies in other classes of q2D materials such as the high-T_c superconductor $Tl_2Ba_2CuO_{6+\delta}$,[53] the triplet superconductor Sr_2RuO_4,[54−56] intercalated graphite,[57,58] and a modulated heterostructure superlattice.[59]

2.2.2. Magnetoresistance at High Tilt Angles

Let us now separately consider the behavior of the nonoscillating background of the interlayer magnetoresistance. As seen from Figure 3, the general tendency for the background is to grow with increasing θ. This has a simple physical explanation. With tilting the field, the electron orbits, whose orientation is strictly determined by the direction of **B** (see eq 1), cross more and more **p**-space unit cells in the p_z direction, which causes the interlayer velocity to oscillate more rapidly. This is clearly seen if we use, for example, the simplified dispersion relation in eq 13. The oscillations of the velocity,

$$v_z = \frac{\partial \epsilon}{\partial p_z} = \frac{2t_\perp d}{\hbar} \sin\left(\frac{p_z(t)d}{\hbar}\right) \tag{24}$$

are determined by the rapidly changing $p_z(t)$ component. As a result, the average over the cyclotron period $\overline{v_z}$ decreases with increasing θ, leading to a decrease of σ_{zz} and, correspondingly, an increase of the interlayer resistivity.[60]

With tilting the field, the electron orbits become elongated and the cyclotron frequency decreases:

$$\omega_c(\theta) = \omega_{c0} \cos\theta \tag{25}$$

where $\omega_{c0} = eB/m_c(\theta=0)$. While ω_{c0} is, as usually, supposed to be much bigger than the scattering rate $1/\tau$, the actual frequency $\omega_c(\theta)$ becomes smaller than $1/\tau$ at low enough cos θ. In the limit $\omega_c(\theta)\tau \ll 1$, the electron can only traverse a small part of the long closed orbit within the time τ. Averaging the velocity v_z over the whole cyclotron period is no longer appropriate; rather, one should use explicitly the scattering time. Thus, the averaged v_z will be determined by the product $\omega_1\tau$, where $\omega_1 \cong \omega_{c0}p_F d/\hbar \sim \omega_{c0}$ is the frequency of crossing one unit cell in **p**-space, which is almost independent of θ at strongly tilted fields. Therefore, the angle dependence of the magnetoresistance is expected to flatten at $\theta_1 < \theta < \pi - \theta_1$,[60] where $\theta_1 \cong \arccos(1/\omega_{c0}\tau)$. Obviously, the AMROs, whose existence relies on the periodic motion on closed orbits (see eq 18), are suppressed at the same angles. From the data of refs 3 and 38 the characteristic angle θ_1 is estimated as $\approx(80-82)°$ for β-$(BEDT\text{-}TTF)_2IBr_2$, at the field of 15 T, yielding the parameter $\omega_{c0}\tau \leq 6-7$. From this, the scattering time can be evaluated: $\tau \simeq 10$ ps, if one substitutes the effective cyclotron mass $m_c(\theta=0) = 4.2m_e$ (m_e is the free electron mass) determined from magnetic quantum oscillations.[40,61] This estimation of the scattering time is in good agreement with the value obtained from the SdH data (see section 3.5.1).

With θ coming even closer to $\pi/2$, that is, when the field approaches the orientation exactly parallel to the layers, the interlayer magnetoresistance in Figure 3 exhibits a sharp peak. The height of the peak can amount to 30% of the background resistance at $B = 15$ T.[3] Hanasaki et al.[62] have performed a detailed investigation of this feature on β_H-$(BEDT\text{-}TTF)_2I_3$,[63] which is very similar to β-$(BEDT\text{-}TTF)_2IBr_2$ in the crystal and electronic structure,[25,34,64,65] possessing a single cylindrical FS. The width of the peak was found to be independent of the field strength, thus suggesting a geometrical origin of the effect. The peak feature and its dependence on magnetic field have been successfully reproduced in numerical simulations of the semiclassical magnetoresistance[62] based on eq 3 and the q2D dispersion relation (eq 13). The results of the calculations are illustrated in Figure 5.

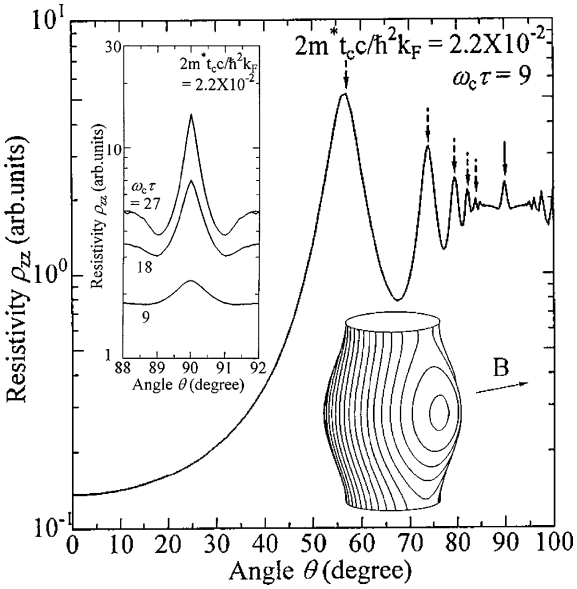

Figure 5. Calculated semiclassical magnetoresistance as a function of the tilt angle. Dashed arrows point to the AMRO maxima, and the solid arrow points to the peak feature at $\theta \sim 90°$. The upper left inset shows the peak feature at different values of the parameter $\omega_{c0}\tau$, that is, at different magnetic fields. The lower right inset shows schematically cyclotron orbits on the warped FS at θ close to 90°. (Reproduced with permission from ref 62. Copyright 1998 American Physical Society.)

To explain the effect, one has to take into account an important topological change in electron orbits at $\theta \to \pi/2$. When the tilt angle reaches the value $\theta_c \sim \arctan(\epsilon_F/2t_\perp)$, a part of the orbits splits, producing small closed loops at the very side of the warped FS, as shown in the inset in Figure 5 and, in another projection, in Figure 6. It was originally proposed[62,66] that it is an effective averaging of v_z over periodic precession on these small closed orbits that gives rise to the peak. Therefore, the latter should appear when the characteristic frequency of the cyclotron motion on these orbits, $\omega_{small} \sim \omega_{c0}(t_\perp/\epsilon_F)^{1/2}$, exceeds the scattering rate $1/\tau$. For the isotropic, parabolic in-plane dispersion (eq 13), the magnetic field at which electrons make at least one complete turn on the small orbit is[62]

$$B \geq B_c = \frac{2\pi\hbar}{ed\tau}\left(\frac{m_c}{2t_\perp}\right)^{1/2} \tag{26}$$

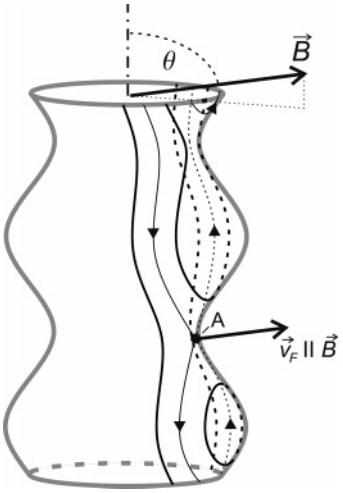

Figure 6. Schematic view of cyclotron orbits on a warped cylindrical FS under a magnetic field almost parallel to the layers. The thin line (with arrows indicating the direction of the electron motion) is the self-crossing orbit which separates the regions of big single-connected orbits (to the left) from those where each orbit is split into a big one and a small closed loop on the edge of the FS (to the right of the self-crossing orbit). The Fermi velocity in the vicinity of the crossing point, A, is nearly parallel to the magnetic field.

To evaluate B_c, we substitute in eq 26 the scattering time estimated above ($\tau = 10$ ps), the interlayer period[34] ($d \approx 15$ Å), and the cyclotron mass and interlayer transfer integral extracted from data on magnetic quantum oscillations[40,61,67] ($m_c = 4.2m_e$ and $t_\perp \simeq 0.35$ meV). As a result, we obtain $B_c \simeq 50$ T for β-(BEDT-TTF)$_2$IBr$_2$. This estimate should also be valid for β_H-(BEDT-TTF)$_2$I$_3$, since the crystallographic and electronic properties of these compounds are very similar. However, the peak feature becomes clearly visible at fields almost an order of magnitude lower for both salts. This implies that making complete closed trajectories is not necessary for the observation of the peak. As suggested in ref 68, more relevant here is the existence of self-crossing orbits which lie on the border separating the split orbits and the rest. An example of such a self-crossing orbit is shown in Figure 6. The Fermi velocity at the crossing point A is exactly parallel to the field direction. Provided the FS warping is very weak, $t_\perp \ll \epsilon_F$, the velocities are nearly parallel to **B** in a relatively large area around point A. According to eq 1, the Lorentz force almost vanishes in this area, so that the electrons do not move on the FS, no matter whether they are situated on the small or big orbits. Obviously, the velocities of such electrons are conserved. Therefore, their contribution to the interlayer conductivity dominates over the contributions from electrons situated far from the self-crossing orbits whose interlayer velocities rapidly oscillate.[60,69] At $\theta = \theta_c$ the z-component of the Fermi velocity at the crossing point is maximum, $v_z^A \simeq 2t_\perp d/\hbar$, which gives rise to a local minimum in the angular dependence of the interlayer magnetoresistance[68] (see Figures 3 and 5). As θ further approaches $\pi/2$, v_z^A rapidly decreases and becomes exactly zero at $\theta = \pi/2$. This results in a sharp peak of the magnetoresistance at $\theta_c < \theta < \pi - \theta_c$.

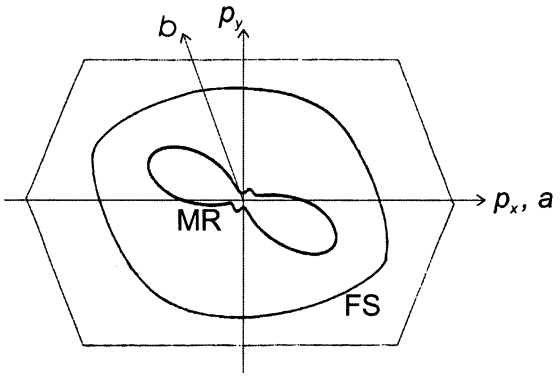

Figure 7. Transverse cross section of the FS of β-(BEDT-TTF)$_2$IBr$_2$ determined from the AMRO experiment[3] and the interlayer magnetoresistance[40] (MR) as a function of azimuthal angle φ plotted in polar coordinates. Thin lines indicate the Brillouin zone boundary and the crystal axes directions.

The width of the peak provides an estimate of the anisotropy ratio $2t_\perp/\epsilon_F$:[62,68] for the dispersion law (eq 13), it is determined as

$$\frac{2t_\perp}{\epsilon_F} \simeq (\pi - 2\theta_c)\frac{\hbar}{p_F d} \tag{27}$$

For the present salts, the width of the peak varies between ≈1.5° and ≈3°, depending on the azimuthal angle φ, which indicates a substantial dependence of the FS warping on φ. This yields the anisotropy ratio $2t_\perp/\epsilon_F$ being in the range ~1/100 to ~1/200. This result is consistent with the value obtained from the beat frequency of the magnetic quantum oscillations[38,40,61,70] (see sections 3.1.1 and 3.5.1).

It is worth noting that the peak feature vanishes in a narrow interval of φ in β-(BEDT-TTF)$_2$IBr$_2$.[3] A similar effect is likely observed in β_H-(BEDT-TTF)$_2$I$_3$[62] and (BEDT-TTF)$_2$Br(DIA)[50] and in κ-(BEDT-TTF)$_2$Cu$_2$(CN)$_3$ under pressure.[71] A more detailed study is necessary to clarify whether it means a vanishing warping of the FS at these φ's (more precisely, losing the coherence of the interlayer charge transport as discussed in section 2.5).

2.2.3. In-Plane Field Rotation

The in-plane cross section of the FS of β-(BEDT-TTF)$_2$IBr$_2$ determined from the AMRO experiments[3] is not very anisotropic: p_F varies as a function of the azimuthal angle φ by not more than a factor of 1.5. Therefore, the electronic properties are not expected to strongly depend on the direction in the highly conducting ab plane. However, the interlayer resistance was found to change by an order of magnitude when the field was rotating in the ab plane.[40] The angular diagram is represented in polar coordinates in Figure 7 along with the experimentally determined FS cross section.

The reason for this surprisingly strong effect of the azimuthal field orientation[72,73] is similar to the mechanism discussed in the previous paragraph in the sense that in both cases so-called "effective" electron orbits which dominate in the total conductivity[60,74] are involved. Let us consider different open orbits perpendicular to the p_xp_y plane which correspond to

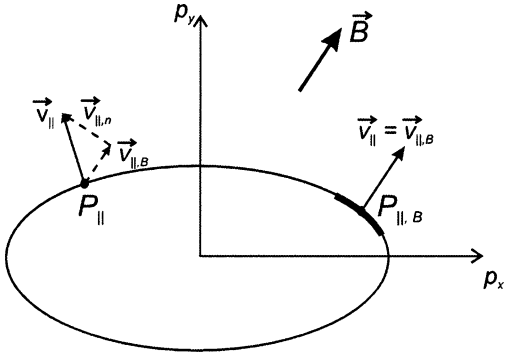

Figure 8. Schematic view of the FS cross section by the plane p_z = constant. At an arbitrary position, e.g., at $P_{||}$, the electrons have a substantial velocity component, $\mathbf{v}_{||,n}$ normal to the in-plane magnetic field, **B**, and rapidly move on the FS along p_z under the Lorentz force (eq 1). The interlayer velocity of such electrons, v_z, averages asymptotically to zero. By contrast, in the vicinity of point $P_{||,B}$ the velocity is almost parallel to **B**. Therefore, the electrons here conserve their momentum and velocity, thus dominating in the total conductivity σ_{zz}.

the electron motion in a magnetic field $\mathbf{B} = (B \cos \varphi, B \sin \varphi, 0)$. The mentioned above small closed orbits, originating from the warping of the FS, will be neglected here, as they are insignificant for a qualitative understanding of the effect. On most of the orbits, electrons have a substantial in-plane velocity component $v_{||,n}$ perpendicular to the field direction, as shown, for example, in Figure 8 for an orbit passing through point $P_{||}$ on the FS cross section. Due to the Lorentz force (eq 1), the momentum component p_z rapidly changes, making the interlayer velocity oscillate around zero. Therefore, the contributions from such orbits to the conductivity σ_{zz} vanish with increasing the field strength. In this situation the orbits in the vicinity of point $P_{||,\mathbf{B}}$, at which the velocity is nearly parallel to **B** (marked by a thick line in Figure 8), dominate in σ_{zz}.[60,74] The relative number of these "effective" orbits obviously depends on the curvature of the in-plane FS cross section at point $P_{||,\mathbf{B}}$: it increases (therefore σ_{zz} increases) with increasing the radius of curvature $\kappa_{FS}(P_{||,\mathbf{B}})$. As shown by Lebed and Bagmet,[74] the interlayer resistivity $\rho_{zz} \approx 1/\sigma_{zz}$ is ultimately determined by the ratio $v_{||}^2(P_{||,\mathbf{B}})/\kappa_{FS}(P_{||,\mathbf{B}})$ at an intermediate field such that $1 < \omega_{c0}\tau \leq (\epsilon_F/t_\perp)^{1/2} \sim 10$.

If the in-plane Fermi velocity component $v_{||}$ is not very anisotropic (as appears to be the case of the present compound), the dependence of the interlayer magnetoresistance on the field orientation within the conducting plane is mostly governed by $\kappa_{FS}(\varphi)$. For an elliptical FS cross section with the main axes $p_{||,max}$ and $p_{||,min}$, the maximum and minimum values of the curvature are related to each other as $(p_{||,max}/p_{||,min})^3$. From the data of ref 3, this ratio can be estimated as $\approx$2.7, which is considerably smaller than the observed anisotropy. This reveals a substantial deviation of the FS shape from an ellipse.

From Figure 7 one can clearly see that the maxima in the magnetoresistance very well correspond to the maxima of the FS curvature, $\kappa_{FS}^{-1}(\varphi)$, in good agreement with the above consideration. However, the matching between the magnetoresistance and $\kappa_{FS}^{-1}(\varphi)$ is not everywhere perfect. For example, despite a rather low curvature of the FS obtained from the AMRO data at $\varphi = 0°$, the magnetoresistance is relatively high, about half of its maximum value, at this angle. Further studies are necessary in order to understand this result.

Finally, a short comment should be made on the field dependence of the magnetoresistance for the field lying in the 2D plane. Theoretical analysis[60,74,75] predicts an unusual, *linear* behavior of $\rho_{zz}(B)$ at intermediate fields $1 < \omega_{c0}\tau \leq (\epsilon_F/t_\perp)^{1/2}$. The conventional quadratic field dependence should be restored only when $\omega_{c0}\tau > (\epsilon_F/t_\perp)^{1/2}$. For the present β-type salts this would correspond to fields $\sim$ 25 T. Indeed, the linear magnetoresistance has been observed in β-(BEDT-TTF)$_2$IBr$_2$ at some field orientations φ.[40] However, at ϕ's corresponding to the region of the main peak of the angular diagram in Figure 7, the dependence $\rho_{zz}(B)$ is definitely superlinear at all fields between 2 and 15 T.[40,66] The reason for such a behavior is not quite clear at present.

2.3. Open Fermi Sheets

FSs of many layered compounds, for example, α-, κ-, and λ-type salts of BEDT-TTF and its derivatives, include, in addition to a cylindrical part, a pair of corrugated sheets which are open in the plane of the layers (see, e.g., Figure 1c,d). This may lead to new features in magnetoresistance in comparison to those considered above. Here we will review effects of magnetic field orientation originating from the existence of open Fermi sheets.

For this purpose, we will consider a FS solely consisting of sheets extended perpendicular to the x axis and warped along the y axis much more strongly than along z axis. In the tight-binding approximation the energy spectrum of such a system is written as

$$\epsilon(\mathbf{p}) = 2t_x \cos(p_x a_x/\hbar) - 2t_y \cos(p_y a_y/\hbar) - 2t_z \cos(p_z a_z/\hbar) - \epsilon_F \quad (28)$$

Here x and z axes are associated with the most and the least conducting directions, respectively, so that the transfer integrals are $t_x \gg t_y \gg t_z$; a_x, a_y, and a_z are the corresponding lattice constants. The dispersion along the x axis is often approximated to be linear near the Fermi level, and eq 28 is written in the simplified form:

$$\epsilon(\mathbf{p}) = v_F(|p_x| - p_F) - 2t_y \cos(p_y a_y/\hbar) - 2t_z \cos(p_z a_z/\hbar) \quad (29)$$

where v_F and p_F are respectively the Fermi velocity and momentum at $t_y = t_z = 0$.

The most prominent examples of such q1D metals with strongly anisotropic coupling between the 1D chains are the Bechgaard salts (TMTSF)$_2$X.[1] Despite a very simple electronic band structure, these compounds exhibit numerous exciting phenomena associated with spin-density-wave states, non-Fermi-liquid behavior, and exotic (most likely triplet) superconductivity (see refs 1, 9, and 76−78 for a review). Our consideration will be restricted to the magnetoresistance behavior in the normal state

which is likely transferable to the case of q2D materials containing open Fermi sheets. Again, we will consider the magnetoresistance measured along the least conducting direction. Basically, three different phenomena, namely, Lebed magic-angle resonances, Danner−Kang−Chaikin oscillations, and the so-called third angular effect, are distinguished in the $(TMTSF)_2X$ salts, depending on whether the field is rotated in the *yz*, *xz*, or *xy* plane, respectively.

2.3.1. Lebed Magic-Angle Resonances

When a strong magnetic field is applied in a plane perpendicular to the chain direction, $\mathbf{B} = (0, B \sin\theta, B \cos\theta)$, the Lorentz force (eq 1) makes electrons move along the Fermi sheets, crossing many Brillouin zones with an almost constant rate $dp/dt \propto v_F$. The frequencies of crossing one Brillouin zone in the p_y and p_z directions are, respectively,

$$\omega_y = \frac{a_y}{\hbar}\left|\frac{dp_y}{dt}\right| = \frac{ev_F a_y}{\hbar} B \cos\theta \tag{30}$$

and

$$\omega_z = \frac{a_z}{\hbar}\left|\frac{dp_z}{dt}\right| = \frac{ev_F a_z}{\hbar} B \sin\theta \tag{31}$$

For a generic value of θ, these frequencies are different and the electron motion is aperiodic. However, as was first noted by Lebed,[79] when the field is directed along a lattice vector, that is, when

$$\tan\theta = \frac{p}{q}\frac{a_y}{a_z} \tag{32}$$

where p and q are integers, the frequencies are commensurate (one can consider this as a kind of a resonance) and the motion in **p**-space becomes periodic. For the $(TMTSF)_2X$ salts characterized by the spin-density-wave instability, this may have important consequences regarding the ground state.[79] It turns out that even in the normal metallic state the transport properties are affected by this periodicity. Naughton et al.[80,81] and Osada et al.[82] were the first to report an anomalous decrease of magnetoresistance in the metallic state of $(TMTSF)_2ClO_4$ at the Lebed magic angles (LMAs) satisfying the condition in eq 32. Later the same effect, but even more pronounced, was found in $(TMTSF)_2X$ with $X = PF_6$ and ReO_4 under pressure[83−86] as well as in some other q1D conductors, for example, $(DMET\text{-}TSeF)_2X$ ($X = AuCl_2$, AuI_2)[87,88] and (BEDT-TTF)(TCNQ).[89] LMA resonances, though less pronounced, have also been found in several q2D materials containing both a Fermi cylinder and a Fermi sheet, κ-$(BEDT\text{-}TTF)_2Cu(NCS)_2$,[90−92] α-$(BETS)_2TlHg(SeCN)_4$,[93] α-$(BEDT\text{-}TTF)_2NH_4Hg(SCN)_4$,[94] and pressurized (to normal metallic state) α-$(BEDT\text{-}TTF)_2KHg(SCN)_4$.[95] An extremely strong LMA-like effect is observed in the anomalous low-temperature state of α-$(BEDT\text{-}TTF)_2MHg(SCN)_4$ with M = Tl,[96,97] K,[98−101] and Rb.[102]

At present there exist plenty of theoretical models associating the LMA effect in q1D conductors with the field-induced density-wave instability,[79,103,104] electron−electron interaction,[105−110] and violations of the Fermi-liquid behavior.[77,111,112] Here, we will present only models based on the Fermi-liquid, one-particle approach within the relaxation time approximation, as they appear to be more relevant to the case of normal metallic q2D compounds.

Perhaps the most popular is the model proposed by Osada and co-workers,[113] who considered the electron orbital motion in a system with a spectrum (eq 29) modified to include higher-order interchain transfer terms:

$$[t_y \cos(p_y a_y/\hbar) + t_z \cos(p_z a_z/\hbar)] \rightarrow \sum_{m,n} t_{mn} \cos[(mp_y a_y + np_z a_z)/\hbar] \tag{33}$$

where t_{mn} describe the effective electron hopping along the corresponding lattice vectors $\mathbf{R}_{mn} = (0, ma_y, na_z)$. The velocity in the *y* and *z* directions was found to exhibit peaks at LMAs. This result has a simple physical meaning: For a general field orientation, all the (m, n)-th contributions to the velocity perpendicular to the chains, being proportional to $t_{mn} \sin[(ma_y p_y(t) + na_z p_z(t))/\hbar]$, oscillate due to the time-dependent momentum $p_{y,z}(t)$ (see eqs 30 and 31) and their averages vanish at high fields. However, when the field is directed along one of the lattice vectors, $\mathbf{R}_{pq}$, that is, satisfies the condition in eq 32, the contribution from the (p, q)-th hopping term is exactly parallel to **B**; hence, it is not affected by the Lorentz force. Therefore, the total velocity does not vanish at any field at this direction, provided the hopping amplitude $4t_{pq}$ is finite.

More explicitly, the solution of the Boltzmann kinetic equation yields the components of the conductivity tensor in the form[113]

$$\begin{pmatrix} \sigma_{yy} & \sigma_{yz} \\ \sigma_{zy} & \sigma_{zz} \end{pmatrix} = D(\epsilon_F) \sum_{m,n} \left(\frac{et_{mn}}{\hbar}\right)^2 \begin{pmatrix} m^2 a_y^2 & mna_y a_z \\ mna_y a_z & n^2 a_z^2 \end{pmatrix} \times \frac{\tau}{1 + [(\omega - v_F G_{mn})\tau]^2} \tag{34}$$

where $D(\epsilon_F)$ is the density of states per unit volume at the Fermi level, ω is the frequency at which the conductivity is measured, and

$$G_{mn} = eB(ma_y \cos\theta - na_z \sin\theta)/\hbar \tag{35}$$

In the dc limit ($\omega = 0$), all the conductivity components σ_{ij} with $i, j = y, z$ exhibit peaks when $G_{mn} = 0$. This exactly corresponds to the LMA condition in eq 32. For a material isotropic in the *yz* plane, the oscillations of the terms σ_{ij} which determine the resistivity ρ_{yy} and ρ_{zz} cancel each other, so that there are nearly no features in the angular dependence of the magnetoresistance. However, the compounds we are considering are strongly anisotropic in the *yz* plane: even in the q1D salts $(TMTSF)_2X$ the anisotropy ratio $t_y/t_z \simeq 30$.[1] In this case, $\rho_{zz} \approx 1/\sigma_{zz}$ should exhibit distinct dips at LMAs.[113]

Obviously, the existence of a magnetoresistance dip at the LMA with index p/q relies on the significance of the contribution of the corresponding term t_{pq} to

the electronic spectrum. Because of the strongly suppressed electron transfer in the z direction in our materials, the terms with $q > 1$ can usually be neglected. Therefore, one should expect the resonances to be pronounced only at integer values $p/q = N$,[113,114] in agreement with the experiment.[80−89,91−95,115] On the other hand, it seems unlikely that the observation of the high-index resonances (for example, in $(TMTSF)_2ReO_4$, the features with N up to 21 are observed[86]) can be attributed to the existence of such high-order interchain transfer terms.

An alternative model proposed by Maki[116] does not require high-order interchain transfer (eq 33) but takes into account the nonlinearity of the real electron spectrum in the chain direction, which leads to a dependence of the velocity component v_x on momentum p_y. The idea of the momentum-dependent velocity v_x has recently been further explored by Lebed and Naughton.[117] They considered the dispersion relation in the form

$$\epsilon(\mathbf{p}) = v_x(p_y)[|p_x| - p_X(p_y)] - 2t_z \cos(p_z a_z/\hbar) \quad (36)$$

where

$$p_X(p_y) = p_F + 2t_y \cos(p_y a_y/\hbar)/v_F \quad (37)$$

and v_F is the Fermi velocity at $t_y = t_z = 0$. The conductivity σ_{zz} derived on the basis of quantum mechanical analysis has been found to exhibit peaks at LMAs. The weight factors of the oscillating terms are determined by the coefficients of the Fourier expansion of the momentum-dependent velocity $v_x(p_y)$ multiplied by tan θ.

From the semiclassical point of view, one could interpret the result as follows. Electrons stay longer at the parts of their trajectories where $v_x(p_y)$ is lower. These "effective" parts dominate in the time-averaged velocity in the high-field limit. As discussed above, the interlayer velocity component v_z is averaged to zero at a general field orientation. However, at LMAs the trajectories in **p**-space become periodic and v_z is the same at the different effective parts. This leads to a finite value of $\overline{v_z}$ and, hence, to enhanced interlayer conductivity σ_{zz}. One should, however, be cautious with this semiclassical description. In fact, Lebed and Naughton emphasize that their model cannot be reduced to a semiclassical consideration of electron orbits on a nonharmonically warped FS: rather it is associated with quantum interference effects causing 1D−2D crossovers of electron wave functions, depending on the field direction.[117]

2.3.2. Danner–Kang–Chaikin Oscillations

Another kind of oscillatory phenomena was found by Danner, Kang, and Chaikin[118] on $(TMTSF)_2ClO_4$ when the field was rotated from the direction of the least conductivity toward the chain direction, that is, in the xz plane in our notation. Their results are reproduced in Figure 9. The interlayer magnetoresistance shows a series of peaks as the field is approaching the x axis (the crystallographic a axis). The effect has been consistently described in terms

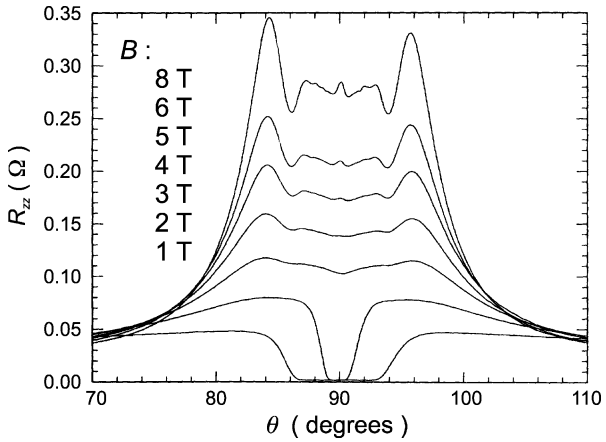

Figure 9. Angular dependence of the interlayer resistance of $(TMTSF)_2ClO_4$ at different fields between 1 and 8 T (from the bottom to the top), at $T = 0.5$ K. Data from ref 118. The 1 and 2 T curves show the superconducting transition as θ approaches 90°. At higher fields the superconductivity is suppressed and the DKC oscillations emerge.

of the semiclassical model.[118] We assume the linearized dispersion (eq 29) and consider the electron motion in the $p_y p_z$ plane under magnetic field $\mathbf{B} = (B \sin \theta, 0, B \cos \theta)$. The orbits are extended to infinity along p_y at θ not too close to $\pi/2$ (the region near $\theta = \pi/2$ will be briefly considered at the end of the paragraph). The frequency ω_y of crossing one Brillouin zone in the p_y direction is given by eq 30. At $\theta = 0$, electrons move parallel to p_y; their momentum in the z direction is conserved. Therefore, the interlayer velocity $v_z = d\epsilon/dp_z \propto \sin(p_z a_z/\hbar)$ is constant and the conductivity σ_{zz} does not differ much from its zero-field value. At a finite θ, p_z oscillates with time:

$$p_z(t) = p_z(0) + \frac{2t_y}{v_F} \tan \theta \sin(\omega_y t) \quad (38)$$

The amplitude of the oscillation, $4t_y \tan \theta/v_F$, increases with increasing θ. As long as the amplitude is smaller than the size of the Brillouin zone in the p_z direction, the velocity v_z takes only a part of the allowed values and its average over the periodic motion $\overline{v_z}$ is, in general, nonzero. However, when the amplitude becomes exactly equal to $2\pi\hbar/a_z$, the average becomes composed of equal positive and negative contributions over the path and, therefore, vanishes. The resistivity is maximum at this point. The next zero of $\overline{v_z}$ and peak in ρ_{zz} are expected when the orbit covers exactly two Brillouin zones in the p_z direction, then three, and so on. The corresponding orientations of the field are determined as

$$\tan \theta_N = N\frac{2\pi\hbar/a_z}{4t_y/v_F} = N\frac{\pi\hbar v_F}{2t_y a_z} \quad (39)$$

More explicitly (see ref 118), the condition for $\overline{v_z} = 0$ is determined by zeros of the Bessel function $J_0[2t_y a_z \tan \theta/(\hbar v_F)]$. However, since the argument of the Bessel function is bigger than 1 in the range of interest, eq 39 is a good expression for estimating the period of the Danner−Kang−Chaikin (DKC) oscilla-

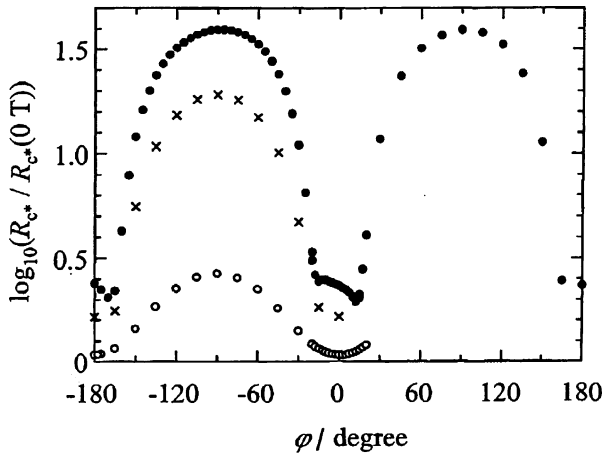

Figure 10. Interlayer resistance of $(DMET)_2I_3$ versus azimuthal angle φ, at magnetic field $B = 1$ T (open circles), 4 T (crosses), and 7 T (filled circles). The angle is measured from the 1D axis. At $\varphi \simeq \pm 15°$ a clear kink representing the third angular effect (TAE) is seen in the 7 T curve. (Reproduced with permission from ref 119. Copyright 1995 Physical Society of Japan.)

tions. From the positions of the resistivity peaks, one can evaluate the bandwidth in the y direction, provided the interchain period and Fermi velocity along the chains are known. For $(TMTSF)_2ClO_4$ in the anion-ordered state, the value $t_y = 0.012$ eV was obtained.[118] Above the ordering temperature, t_y should be doubled, yielding $4t_y = 0.096$ eV. A slightly larger value has been found for $(TMTSF)_2PF_6$ under a pressure of ≈10 kbar:[112] $4t_y = 0.13$ eV.

As the field direction becomes very close to the x axis, namely, when $\tan\theta$ reaches the critical value,

$$\tan\theta_c \simeq \frac{\hbar v_F}{2t_z a_z} \tag{40}$$

the geometry of electron orbits undergoes a remarkable change: Now the orbits become open along p_z rather than along p_y; in addition, there appear small closed orbits around maxima and minima of p_x on the FS. This is manifested by a narrow peak in the angular dependence of magnetoresistance around $\theta = \pi/2$ whose width provides an estimate of t_z.[118] The mechanism responsible for the peak is basically the same as that for the peak feature in the case of a cylindrical FS (see section 2.2.2) and for the "third angular effect" presented in the next paragraph.

2.3.3. Third Angular Effect

Figure 10 shows the interlayer magnetoresistance of the q1D metal $(DMET)_2I_3$ measured by Yoshino et al.[119] under a magnetic field rotating in the plane perpendicular to the least conducting direction. It has a maximum value when the field is perpendicular to the chains ($\varphi = \pm 90°$). Since the major component of the Fermi velocity points to the chain direction, such an orientation corresponds to the maximum Lorentz force (eq 1) and, thus, to the strongest damping of the average interlayer velocity. The Lorentz force gradually decreases when the field is turned toward the chain direction, leading to a decrease of the magnetoresistance. However, instead of smoothly coming to a minimum at $\varphi = 0°$, that is, at **B**|| chains, the high-field magnetoresistance (7-T curve in Figure 10) exhibits a sudden change in the slope at $\varphi \approx \pm 15°$.

Osada, Kagoshima, and Miura[120] have recognized this kink as a new topological effect characteristic of a q1D FS and called it "the third angular effect", TAE (after the LMA and DKC oscillations as the first two angular effects in q1D conductors). They reproduced the effect by numerical calculations of the interlayer resistivity ρ_{zz} based on the q1D spectrum (eq 28) and semiclassical Boltzmann equation. It was shown that a minimum of the resistivity occurs not at $\varphi = 0°$ but near the critical angle φ_c, at which the topology of electron orbits on the FS changes: all the orbits are open in the direction p_z at $\varphi > \varphi_c$ while small closed orbits exist around minima and maxima of p_x at $\varphi < \varphi_c$. For a quarter-filled band, as is, for example, the case of $(TMTSF)_2X$, the critical angle is[120]

$$\varphi_c = \arctan\left(\sqrt{2}\frac{t_y}{t_x}\frac{a_y}{a_x}\right) \tag{41}$$

The origin of the anomalous behavior at $\varphi \le \varphi_c$ was initially attributed to the appearance of the small closed orbits. However, Lebed and Bagmet[74] argued that the minimum of the resistivity can be explained without involving the closed orbits. They noticed that the critical angle (eq 41) corresponds to the field direction at which the orbits are tangent to the inflection point of the p_z = constant cross section of the FS. At this direction the number of electrons having their velocities almost parallel to **B** is maximum. The Lorentz force acting on such electrons is vanishingly small; therefore, their momentum is conserved and the interlayer velocity does not oscillate. As a result, these electrons are the most effective in the interlayer charge transport. As φ deviates from φ_c, the number of the effective electrons diminishes and ρ_{zz} grows. This explanation has been basically confirmed by a detailed numerical analysis of contributions of different orbits to the interlayer conductivity.[121,122] The calculations show that the conductivity in the vicinity of φ_c is dominated by electrons situating near the inflection line of the FS, no matter whether the corresponding orbits are closed or open: even electrons sitting on the closed orbit do not complete the whole circulation during the scattering time, since the Lorentz force acting on them is vanishingly small.

It should be noted that the mechanism involved in the TAE is essentially the same as that in the case of the peak structure near $\theta = \pi/2$ during the xz rotation of the field. The latter effect is observed both for cylindrical and sheetlike FSs (see sections 2.2.2 and 2.3.2), and the only difference is that the critical angle in those cases is determined by the *interlayer* transfer integral; thus, the warping of the FS in the p_z direction becomes crucially important.

From the above discussion it is clear that the TAE can be very useful in estimating the anisotropy of a q1D conductor in the xy plane. For example, it was applied to estimate the ratio t_y/t_x and its dependence on pressure in the $(DMET)_2X$ salts[123,124] in which the

DKC oscillations, giving similar information, are not observed. In principle, one can expect the TAE to be manifested also in q2D materials such as α- or κ-salts of BEDT-TTF which combine open and cylindrical FSs, provided the open sheets are not too strongly corrugated.

2.3.4. General Orientation of the Field Rotation Plane

We have considered separately rotations of the field in the planes yz ($\varphi = \pi/2$, θ varies), xz ($\varphi = 0$, θ varies), and xy ($\theta = \pi/2$, φ varies), which lead to the LMA, DKC, and TAE effects, respectively. Now, if both θ and φ are changed in an arbitrary manner, one could expect, in principle, a kind of superposition of these three effects. Indeed, the experiment[121] with the field rotating around the z axis and having a finite B_z component performed on $(TMTSF)_2ClO_4$ has revealed features which could be attributed to the three effects. In particular, periodic dips of the magnetoresistance have been observed at angles φ, θ such that

$$\tan\theta \sin\varphi = N\frac{a_y}{a_z} \qquad (42)$$

that is when the field projection on the yz plane satisfies the LMA condition. Numerical calculations[121] based on the semiclassical model have qualitatively reproduced the data. However, one unexpected result was noticed: clear LMA-like features at $|N| \geq 4$ could be observed at small φ whereas the pure yz rotation (i.e. at $\varphi = \pi/2$), for which the LMA effect was supposed to be the strongest, revealed resonances only at $|N| \leq 3$.

A detailed theoretical study of the angular effects in the case of arbitrary φ and θ based on the quantum mechanical analysis was performed by Osada[125,126] and by Lebed and Naughton.[127] The latter authors have also proposed an elegant interpretation in terms of semiclassical electron orbits on the FS.[127] In particular, it makes clear that tilting the field from the yz plane gives rise to a new mechanism of resonances at angles (eq 42) which cannot be reduced to the LMA effect observed in the case of the purely yz rotation. This is most likely the reason for the existence of high-N features found at small φ's in the experiment.[121] It should be noted that a similar result concerning LMA-like features in the case of a finite x-component of the magnetic field was obtained earlier by McKenzie and Moses.[128]

2.4. Resonances in the Frequency-Dependent Magnetotransport

So far we were dealing with magnetotransport properties in the dc limit, that is, at frequencies ω much smaller than the characteristic frequency, ω_c, of the periodic motion of electrons in **p**-space under a strong magnetic field. On the other hand, high-frequency ($\omega \sim \omega_c$) resonance methods are well-known to be very effective in studying the electronic system in conventional metals.[28] One should, therefore, expect them to be also useful in the case of organic conductors. Of course, the extreme anisotropy of these materials leads to important consequences in the high-frequency magnetotransport, which has recently become a subject of rather intensive theoretical[128−135] and experimental[135−144] studies (for a review of earlier works on this topic see, e.g., refs 26 and 129).

As in the dc case, we will focus here on the effects related to the interlayer conductivity, which will now essentially depend on the frequency of the electromagnetic excitation: $\sigma_{zz} = \sigma_{zz}(\omega)$. For the typical static magnetic fields used in the experiments, $B \sim 1-10$ T, the appropriate frequencies of the electromagnetic radiation are $\nu \equiv \omega/(2\pi) \lesssim 10^2$ GHz, that is, belong to the millimeter-wave (or very-far-infrared) range. The electrodynamic response from typical samples of organic conductors under realistic experimental conditions has been described in detail in refs 129, 132, 137, and 138. It was shown that the energy absorbed from the electromagnetic radiation is mostly determined by the interlayer conductivity when the sample is placed in the antinode of the oscillating magnetic field $\tilde{\mathbf{H}}$ polarized parallel to the plane of the highly conducting layers. In this (actually, most commonly used) geometry, the screening currents induced by $\tilde{\mathbf{H}}$ flow both perpendicular and parallel to the layers. However, due to the strong anisotropy, the skin (penetration) depth corresponding to the in-plane currents, $\delta_{\parallel} \sim 1\ \mu$m, is much smaller than that for the interlayer currents, $\delta_{\perp} \sim 10^2\ \mu$m. Given that the ratio between the sample dimensions along and across the layers is usually ≤ 10, the interlayer currents give the dominant contribution to the dissipation. Further, the skin depth $\delta_{\perp}$ greatly exceeds the mean free path in the cleanest samples as well as the Larmor radius, $r_L \lesssim 1\ \mu$m, for the static fields above 1 T. Thus, the electromagnetic response is determined by the bulk interlayer conductivity $\sigma_{zz}(\omega)$, and the classical approach corresponding to the normal skin effect regime[28] can be used.

We start with the consideration of a q2D metal with a cylindrical FS given by the dispersion relation (eq 20) (see section 2.2.1) placed in a high static magnetic field perpendicular to the layers ($\mathbf{B} \parallel z$ axis). The direction of the FS warping given by the effective hopping vector $\mathbf{h} = (u_x, u_y, d)$ is tilted from the cylinder axis. As a result, the interlayer velocity,

$$v_z = 2t_{\perp} \sin[(p_z d + p_x(t)u_x + p_y(t)u_y)/\hbar] \qquad (43)$$

oscillates with the cyclotron frequency $\omega_c = eB/m_c$, where m_c is the effective cyclotron mass (eq 6). It can be shown[129] that the interlayer conductivity $\sigma_{zz}(\omega)$ determined by v_z exhibits a resonance peak when the excitation frequency ω becomes equal to the cyclotron frequency, $\omega = \omega_c$. Thus, from the resonance frequency one can rather precisely determine the cyclotron mass m_c. It is, however, important to point out[129] that the origin of this effect is different from that of the conventional cyclotron resonance: the latter is directly related to the cyclotron (i.e. closed orbit) motion both in real space and in momentum space whereas the present, so-called *periodic orbit resonance* (POR), is caused by the cyclotron motion in momentum space, which results in periodic motion along the z direction in real space.

Another kind of POR emerges, according to ref 129, due to the fact that the warping of the FS of a real material is generally dependent on the azimuthal direction, that is, $t_\perp = t_\perp(p_x, p_y)$. For example, in the case of the twofold, $(d_{xx} + d_{yy})$ symmetry of the warping, it is easy to see that the z axis velocity experiences two cycles during the cyclotron period. This gives rise to the second harmonic resonance,[129] that is, at $\omega = 2\omega_c$.

If the static magnetic field **B** is parallel to the vector **h**, the fundamental POR vanishes but the second harmonic caused by the mechanism described above still persists. Attributing it, erroneously, to the fundamental resonance, one would obtain a apparent cyclotron mass 2 times lower than the actual one.

Further theoretical studies of multiple harmonics of the POR have been done by McKenzie and Moses[128] for the case of a tilted magnetic field **B**. They have generalized the dc formula (eq 17) for the conductivity by including the frequency dependence:

$$\sigma_{zz} = \sigma_{zz}^{\circ} \sum_{n=-\infty}^{\infty} \frac{J_n^{\,2}(p_F d \tan\theta/\hbar)}{1 + (\omega - n\omega_c)^2\tau^2} \qquad (44)$$

where $\omega_c = eB \cos \theta/m_c$ is the angle-dependent cyclotron frequency. One can readily see from eq 44 that the conductivity exhibits resonant peaks at the frequencies equal to an integer times the cyclotron frequency:

$$\omega = n\omega_c \qquad (45)$$

The magnitude of the peaks is modulated with changing the tilt angle θ due to the oscillating Bessel functions J_n. The latter effect is, of course, closely related to the AMRO phenomenon introduced in section 2.2.1. As a result, depending on the exact field orientation, one can obtain drastically different POR structures in the conductivity.[128]

A comprehensive verification of the theoretical predictions is still awaiting realization. Nevertheless, a good illustration of multiple resonances, which seems to be in qualitative agreement with the theory, has been obtained by Palassis et al.[139] on the q2D compound κ-(BEDT-TTF)$_2$I$_3$. Figure 11 reproduces the millimeter-wave absorption[139] plotted against the field strength B scaled by the excitation frequency ω, so that the x axis scale corresponds to cyclotron mass ($m_c = eB/\omega$). Different traces correspond to different frequencies and field orientations. The curves clearly demonstrate multiple harmonic PORs. The relative magnitude of the resonances strongly varies with θ; in particular, either the fundamental POR or the second harmonic becomes dominant depending on the angle.

Another interesting resonance effect occurs when the static field **B** is directed parallel to the conducting layers. In this case, the conductivity $\sigma_{zz}(\omega)$ is shown[134,135] to be mostly contributed by the carriers which have the extremal value of the in-plane velocity component perpendicular to the field, $v_\perp^{ext}$. The interlayer velocity $v_z(t)$ of such carriers oscillates with the frequency $\omega_c^{ext} = eBdv_\perp^{ext}/\hbar$, and the resonance

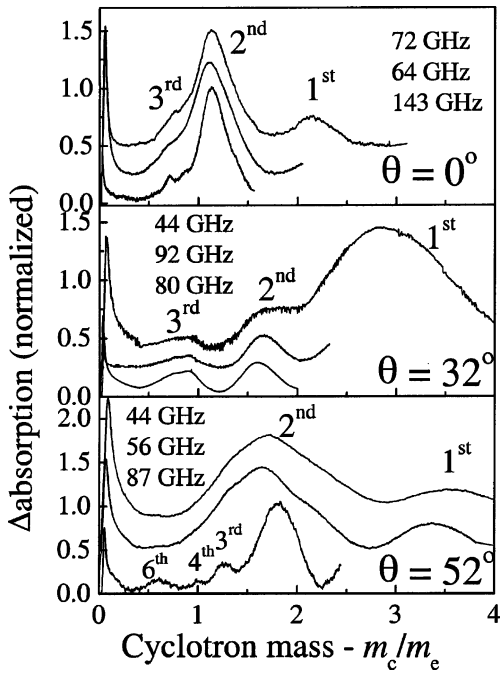

Figure 11. Millimeter-wave absorption in κ-(BEDT-TTF)$_2$I$_3$, versus cyclotron mass, for several frequencies $\nu = \omega/(2\pi)$ and tilt angles θ of the static magnetic field. The traces are offset for clarity. (Reproduced with permission from ref 139. Copyright 2001 Elsevier ScienceDirect.)

occurs when the frequency of the applied electromagnetic field matches ω_c^{ext}. This provides an elegant method of mapping the in-plane Fermi velocity as a function of the azimuthal angle φ, as has been demonstrated by Kovalev et al.[135] on κ-(BEDT-TTF)$_2$I$_3$.

Let us now consider a system with a FS open in the p_yp_z plane and a high magnetic field applied parallel to this plane: $\mathbf{B} = (0, B \sin \theta, B \cos \theta)$. In the case of multiple finite transfer integrals t_{mn} (see eq 33), the existence of a resonance effect directly follows from expression 34 for the conductivity:[113] the denominator of the (m, n)-th term of the sum in eq 34 reduces to unity when

$$\omega = ev_F B(ma_y \cos \theta - na_z \sin \theta)/\hbar \qquad (46)$$

that is when the measurement frequency matches the frequency of the (m, n)-th Fourier component of the oscillating interchain velocity.

Experimentally, such resonances, called Fermi-surface traversal resonances (FTRs), have been observed for the first time by Ardavan et al.[136] in α-(BEDT-TTF)$_2$KHg(SCN)$_4$. Later, Kovalev et al.,[144] using a very highly sensitive millimeter-wave technique,[137] carried out a detailed study on the same compound and found multiple (up to the fifth order) FTRs at different radiation frequencies and field orientations. For example, Figure 12 shows traces of the absorption recorded, with fixed ratios ω/B, while varying the tilt angle θ.[144] The curves strongly resemble the angle-dependent dc magnetoresistance observed on this material at low temperatures (see, e.g., refs 98 and 99), albeit inverted: the absorption displays a series of peaks corresponding to the peaks in the conductivity whereas the dc magnetoresis-

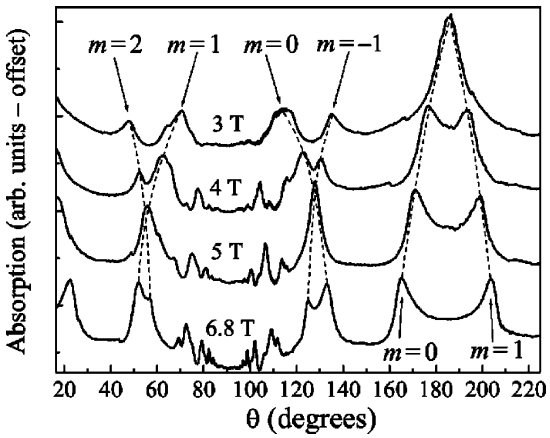

Figure 12. Angular sweeps of the millimeter-wave absorption in α-(BEDT-TTF)$_2$KHg(SCN)$_4$, at different fixed values of the static magnetic field B (offset for clarity), at $T = 2.2$ K. The measurement frequency, $\nu \equiv \omega/(2\pi) = 53.9$, is common for all the curves. The positions of the peaks, corresponding to the FTR effect, are clearly dependent on B, as indicated by dashed lines for the low-index peaks (with $m = -1, 0, 1, 2$; $n = 1$). (Reproduced with permission from ref 144. Copyright 2002 American Physical Society.)

tance, $\propto 1/\sigma_{zz}$, is characterized by sharp dips. However, in remarkable contrast to the dc case, the peak positions are now clearly dependent on the strength of the magnetic field B. This is exactly the fingerprint of the FTR effect. Based on the FTR condition generalized for the realistic case of a low symmetry of the Brillouin zone and an arbitrary orientation of the static magnetic field, $\mathbf{B} = B(\sin\theta\sin\varphi, \sin\theta\cos\varphi, \cos\theta)$

$$\frac{\omega}{B_{\rm res}\cos\theta} = \frac{ev_{\rm F}}{\hbar} d\cos\theta|\tan\theta_{mn} - \tan\theta| \quad (47)$$

where $B_{\rm res}$ is the magnetic field at which the resonance occurs at the given fixed millimeter-wave frequency, and θ_{mn} is the tilt angle corresponding to the (m, n)-th LMA peak in the dc conductivity (see section 2.3.1), Kovalev et al.[144] determined the in-plane Fermi velocity: $v_{\rm F} = 6.5 \times 10^4$ m/s.

Similar studies have been performed by Oshima et al.[142] on another compound characterized by the open FS, (DMET)$_2$I$_3$. A number of features in the millimeter-wave transmission attributed to high-order FTRs have been observed. Based on the experimental data, the authors have evaluated the Fermi velocity, $v_{\rm F} = 2.7 \times 10^4$ m/s, and the anisotropic transfer integral ratio, $t_x/t_y/t_z \approx 80{:}25{:}1$.

McKenzie and Moses[128] have argued that the existence of finite high-order transfer integrals t_{mn} is not a necessary condition for the FTR effect. According to these authors, the resonances may take place even if all t_{mn} with $n, m > 1$ are zero, provided the magnetic field **B** has an appreciable component perpendicular to the open FS plane. In fact, this effect is similar to that discussed in section 2.3.4 for the dc conductivity.

On the other hand, it seems that a generalization of the quantum mechanical analysis of the LMA effect performed by Lebed et al.[117] (see section 2.3.1) to the case of frequency-dependent conductivity should lead to FTR resonances associated with the Fourier components of the velocity $v_x(p_y)$ rather than with the multiple transfer integrals.

2.5. Problem of the Interlayer Coherence

The basic concept of the semiclassical theory of the charge transport in metals is the coherent motion of electron wave packets with well-defined wave vectors through the crystal.[28,31] This necessarily implies that the size of the wave packet Δr must be smaller than the mean free path l. On the other hand, the requirement of a well-defined wave vector **k** and, hence, (quasi)momentum $\mathbf{p} = \hbar\mathbf{k}$ sets the lower limit to Δr, due to the uncertainty principle: $\Delta r \sim \hbar/\Delta p$. The uncertainty in the momentum Δp should be, of course, much smaller than the maximum momentum in the first Brillouin zone, $\sim\hbar/a$, where a is a crystal lattice period. Therefore, the wave packet is supposed to be spread over many lattice periods. Thus, we come to the condition

$$a \ll \Delta r \ll l \quad (48)$$

which should be satisfied for the semiclassical model to be applicable.

In strongly anisotropic organic conductors, the interlayer transport is limited due to very low values of the interlayer transfer integral $t_\perp$. If the latter is small enough or if the scattering rate τ is too high so that the inequality

$$t_\perp \ll \hbar/\tau \quad (49)$$

holds, an electron scatters before it is able to penetrate from one highly conducting layer to the next one. Since $l < a$ in that case, the condition in eq 48 cannot be fulfilled and the semiclassical model becomes inappropriate for description of the interlayer transport. One may, therefore, expect some new effects in that case. In particular, in low-dimensional strongly correlated systems such as q1D organic conductors, prominent features associated with deviations from the Fermi liquid behavior emerge.[77]

One can, in principle, distinguish two different regimes of the interlayer charge transfer in this situation. In the strongly incoherent regime, the electron hopping between adjacent layers is entirely caused by interaction (say, with phonons or impurities), that is, scattering processes. The electron states before and after hopping are uncorrelated; the interlayer transport is essentially nonmetallic in this case.

It is possible, however, to imagine a *weakly incoherent* situation when an electron coherently tunnels between the nearest neighboring layers, due to a finite $t_\perp$, but scatters many times within the layer before tunneling to the next layer. Thus, even though the phase of the electron wave function conserves during a single tunneling process, a sequence of tunneling events becomes uncorrelated and the system loses coherence in the direction perpendicular to the layers when the condition in eq 49 is satisfied. As a result, no well-defined momentum in the interlayer direction can be prescribed to the electron and the FS is supposed to become purely 2D.[145] Nevertheless, at zero magnetic field, the conductivity σ_{zz} is predicted[146−148] to preserve the metallic temperature

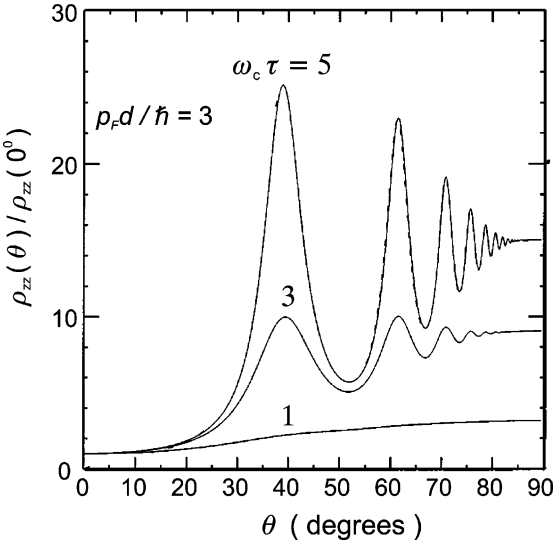

Figure 13. Angular dependence of the interlayer magnetoresistance of a q2D metal in the weakly incoherent regime calculated[145] for different values of the parameter $\omega_c\tau$. The curves are identical to those obtained for the fully coherent regime at all angles θ except those very close to 90°.

dependence. It is simply proportional to the intralayer mean scattering time τ and, hence, to the intralayer conductivity $\sigma_{||}$:

$$\sigma_{zz} \sim \sigma_{||}\left(\frac{t_\perp}{t_{||}}\right)^2\left(\frac{d}{a}\right)^2 \qquad (50)$$

where $t_{||}$ and a are, respectively, the intralayer transfer integral and lattice period, and d is the interlayer spacing. Thus, it is difficult to distinguish between the weakly incoherent and the coherent interlayer transport regimes in the absence of magnetic field.

A detailed theoretical comparison of the high-field ($\omega_c\tau \gg 1$) magnetotransport in the coherent and weakly incoherent regimes was performed by McKenzie and Moses.[145] For the latter case, the conductivity σ_{zz} was obtained by calculating the tunneling rate between two adjacent layers on the basis of the metal−insulator−metal junction model. It has been found that, as long as the magnetic field direction is not close to the 2D plane, the conductivity displays the same behavior as in the fully coherent case. In particular, the AMRO effect and the DKC oscillations have been reproduced for the cylindrical and open FSs, respectively. The angular dependence of the background magnetoresistance has also been obtained identical to that in the coherent regime: it increases at tilting the field from the z axis and saturates at high tilt angles θ. Figure 13 shows the interlayer magnetoresistance calculated[145] as a function of the field orientation for the case of a cylindrical FS. Both the oscillatory part and the monotonic background closely resemble the calculations[62] based on the coherent 2D model (cf. Figure 5). The only difference in the angular dependence develops at θ very close to 90°: no peak feature is found in the weakly incoherent regime, by contrast to the coherent one. As discussed in section 2.2.2, the narrow peak around 90° appears as a result of qualitative topological changes of the cyclotron orbits on the 3D warped FS cylinder (the same effect takes place in the case of the open Fermi sheets corrugated in the z direction; see section 2.3.2). It is, therefore, natural that the effect is absent in the case of a purely 2D FS associated with the incoherent interlayer transport. Recently Osada et al.[149] have confirmed, by independent quantum mechanical calculations, the existence of all the angular effects except the peak feature in the weakly incoherent regime.

The work of McKenzie and Moses[145] has stimulated a number of experimental studies aimed to check the theory and to clarify the mechanism of the interlayer transport in various q2D conductors. Of particular interest are experiments on the most anisotropic of the known q2D organic compounds, such as κ-(BEDT-TTF)$_2$I$_3$,[150] κ-(BEDT-TTF)$_2$Cu(NCS)$_2$,[151] α-(BEDT-TTF)$_2$MHg(SCN)$_4$,[94] and β''-(BEDT-TTF)$_2$SF$_5$CH$_2$CF$_2$SO$_3$.[150] In the former two salts, the peak feature has been found, thus confirming the 3D coherent transport and providing an estimate of the interlayer transfer integral (see eq 27). The width of the peak was found to be ≈0.4° for κ-(BEDT-TTF)$_2$I$_3$ and 0.5 ± 0.2° for κ-(BEDT-TTF)$_2$Cu(NCS)$_2$, leading to similar values of $t_\perp \simeq 0.05$ meV. This is considerably smaller than the values $\hbar/\tau \approx 0.14$ and 0.24 meV, respectively, obtained from the Dingle factor of the magnetic quantum oscillations (see section 3). The obtained relationship between $t_\perp$ and $\hbar/\tau$ apparently contradicts the condition in eq 48. Thus, the validity of this condition as a prerequisite of the coherent transport was questioned.[151] However, recent studies of quantum oscillations of the interlayer resistivity[67] have shown that the conventional Dingle factor is mainly determined by macroscopic inhomogeneities of the sample rather than pointlike defects. Similar suggestions were made on the basis of comparison between the behavior of the quantum oscillations and other properties sensitive to the sample quality.[129,152] Unlike microscopic defects (e.g., impurities and vacancies), the large-scale spatial inhomogeneities do not affect the mechanism of the interlayer charge transfer. Therefore, the effective relaxation rate entering the condition in eq 48 is likely much lower than that determined from the quantum oscillations in organic conductors.

By contrast to the case of the above two compounds, no peak feature has been found in β''-(BEDT-TTF)$_2$SF$_5$CH$_2$CF$_2$SO$_3$ within the angular resolution of 0.01°, suggesting the absence of the interlayer coherence in this salt.[150] The angular dependence of the magnetoresistance measured[150] at $T = 0.5$ K at different fields is presented in Figure 14. The superposition of the AMRO and giant SdH oscillations makes the whole picture rather complicated, but we now focus on the behavior at high tilt angles, around $\theta = 90°$ (and $-90°$). At low fields, the resistance sharply drops down as θ approaches 90 °, due to the superconducting transition. The superconductivity is suppressed at $B > 20$ T. Nevertheless, the peak feature is completely absent; instead, the magnetoresistance exhibits a broad ($\Delta\theta \geq 20°$) depression. Such a considerable decrease of the magnetoresistance

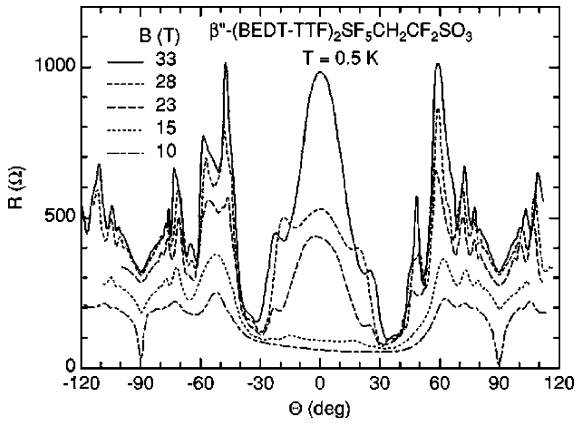

Figure 14. Angular dependence of the interlayer magnetoresistance of β''-(BEDT-TTF)$_2$SF$_5$CH$_2$CF$_2$SO$_3$ at T = 0.5 K for different fields up to 33 T. (Reproduced with permission from ref 150. Copyright 2002 American Physical Society.)

near the parallel field orientation is not consistent with either the coherent or weakly incoherent transport scenario.[145]

A comparative experimental study of the coherent versus incoherent interlayer transport has been done by Kuraguchi et al.[153] on artificial q2D GaAs/AlGaAs superlatices with different interlayer barriers. On the narrow-barrier sample, the usual angular dependence of the interlayer magnetoresistance was found: ρ_{zz} increased with tilting the field toward the 2D plane, showing the peak feature around $\pm 90°$. By contrast, no peak and the opposite angular dependence (maximum at low θ; minimum at $\theta = 90°$) were observed on the sample with the larger barrier. Actually, the difference between the behaviors of the two samples looks quite similar to the difference between the q1D salts (TMTSF)$_2$X with X = ClO_4 and PF_6 (the latter under pressure).[112] In the latter salt the uncoventional angular dependence of the magnetoresistance has been associated[77] with field-induced dimensional crossovers and non-Fermi liquid effects. It would be very interesting to further study whether the behavior of the q1D and q2D compounds in the incoherent-coupling regime has a common nature.

3. Magnetic Quantum Oscillations

If conduction electrons move on closed orbits in a strong magnetic field, their electron spectrum becomes quantized. The quantization was first suggested by Landau,[154] who derived the spectrum of a free electron gas in a magnetic field in the form

$$\epsilon(n,p_B) = (n + {}^1/_2)\hbar\omega_c + \frac{p_B^2}{2m_e} \qquad (51)$$

where $n = 0, 1, 2,...$, $\omega_c = eB/m_e$ is the cyclotron frequency of a free electron (see eq 5), and p_B is the momentum component parallel to the field **B**. This result is of course a direct consequence of the wave property of electrons. Intuitively, magnetic field confines, via the Lorentz force (eq 1), the electron motion to a circle with the radius $r_B = p/eB$, in the plane perpendicular to **B**. The boundary condition of this periodic motion is that the circumference of the orbit be an integer times the electron's wavelength. In quantum mechanics, this should lead to a discrete set of eigenenergies of the system. Therefore, the spectrum in the plane perpendicular to **B** (i.e. at a fixed p_B) becomes degenerate, including only a discrete set of allowed energies (eq 51). In **p**-space, the only allowed states for electrons lie on coaxial tubes, so-called *Landau tubes*, with areas of cross sections perpendicular to **B** satisfying the *Onsager relation*:[155]

$$S_n(\epsilon,p_B) = (n + \gamma)2\pi\hbar eB \qquad (52)$$

where $\gamma = {}^1/_2$ in the free electron model. The expression in eq 52 turns out to be valid for real metals with arbitrary dispersion relations. The only modification is that γ can, in general, slightly deviate from $^1/_2$, being weakly dependent on ϵ and p_B.[22] In most cases, the deviation is insignificant, and it will be neglected in the following.

At $T = 0$ electrons occupy the states on the Landau tubes up to the Fermi level ζ. (The chemical potential ζ may, strictly speaking, deviate from the constant Fermi energy ϵ_F. This is particularly important in the extremely 2D case, as will be discussed in section 3.3. However, for 3D metals the deviations are usually negligibly small.[22]) When magnetic field increases, the number of occupied states on the largest Landau tube, which is still inside the FS, decreases and vanishes infinitely rapidly when the tube touches the extreme cross section of the FS, S_{extr}. With a continuous change of B, the Landau tubes subsequently cross S_{extr}, with a period in the inverse-field scale:

$$\Delta\left(\frac{1}{B}\right) = 2\pi e\hbar/S_{extr} \qquad (53)$$

This leads to a periodic variation of the free energy of the electronic system and the density of states and, consequently, to oscillations of various physical properties such as magnetization, heat capacity, elastic constants, conductivity, thermoelectric power, and so forth. From the period of oscillations (eq 53) one can immediately determine the corresponding cross-sectional area of the FS. In addition, as will be shown below, the oscillation amplitude gives information on some other important properties of the electronic system.

The quantum oscillations of resistivity and magnetization, that is, the Shubnikov−de Haas (SdH) and de Haas−van Alphen (dHvA) effects, were historically the first experimental methods of probing the FS and, thus, were most extensively used in Fermiology of conventional metals.[21] A brilliant comprehensive review on the standard 3D model of magnetic quantum oscillations and on its applications has been done by Shoenberg.[22] In the next section we will summarize the main results of the theory and illustrate how they can be used to study the conducting system of organic metals. In section 3.2 some examples will be presented, showing that the extremely high anisotropy of our materials may lead to substantial deviations of the oscillations from the standard theory, requiring its modification. The

theoretical models of the dHvA effect in extremely anisotropic materials and their applications to organic conductors will be considered in sections 3.3 and 3.4, respectively. Finally, some remarkable manifestations of the q2D character of the SdH effect in organic conductors will be discussed in section 3.5.

3.1. Standard Theory and Applications to Organic Conductors

3.1.1. Lifshitz–Kosevich Formula for the de Haas–van Alphen (DHvA) Effect

Oscillations of the energy of the electronic system with changing magnetic field give rise to oscillating magnetization, which can be obtained as the field derivative of the Gibbs thermodynamic potential Ω at constant temperature and chemical potential: $M = -(\partial\Omega/\partial B)_{T,\xi}$. The general formula for the dHvA oscillations in 3D metals has been derived by Lifshitz and Kosevich.[156] Here we will only present the results of the theory. The principles of the derivation can be found in the textbooks on the metal theory, see, for example, refs 27−29; a thorough analysis is given in Shoenberg's monograph.[22]

If the FS contains only one extremal cross section perpendicular to the field, the oscillatory part of the magnetization along **B** can be written as a sum of harmonics periodic in the $1/B$ scale

$$\tilde{M} = -\sum_{r=1}^{\infty} \frac{1}{r^{3/2}} M_r \sin\left[2\pi r\left(\frac{F}{B} - \frac{1}{2}\right) \pm \frac{\pi}{4}\right] \quad (54)$$

with the fundamental frequency

$$F = \frac{S_{\mathrm{extr}}}{2\pi e\hbar} \quad (55)$$

The sign "+" or "−" in the argument of the sine function is chosen for the minimum or the maximum cross-sectional area, respectively. The harmonic amplitudes are expressed as

$$M_r = \left(\frac{e}{2\pi\hbar}\right)^{3/2} \frac{S_{\mathrm{extr}} B^{1/2}}{\pi^2 m_{\mathrm{c}} |S''|_{\mathrm{extr}}^{1/2}} R_{\mathrm{T}}(r)\, R_{\mathrm{D}}(r)\, R_{\mathrm{S}}(r) \quad (56)$$

where m_{c} is the cyclotron mass (eq 6); $(S'')_{\mathrm{extr}} = (\partial^2 S/\partial p_B^2)_{\mathrm{extr}}$ characterizes the FS curvature along **B** around the extremal cross section; and the damping factors R_{T}, R_{D}, and R_{S} caused by finite temperature, scattering effects, and Zeeman splitting, respectively, will be described in the next subsection. The expression for magnetization oscillations (eq 54) with frequency (eq 55), amplitudes (eq 56), and the damping factors defined in section 3.1.3 is called the *Lifshitz−Kosevich (LK) formula*.

As will be shown below, $R_{\mathrm{T}}(r)$ and $R_{\mathrm{D}}(r)$ decrease exponentially fast with increasing the harmonic index; in addition, the harmonic contributions are decreased by the prefactor $r^{-3/2}$. Therefore, it is often enough to consider the behavior of the fundamental harmonic, $r = 1$.

If the FS contains multiple extremal cross sections, they additively contribute to the oscillations. In the case of a weakly warped cylindrical FS, the oscillations are caused by two extremal cross sections, maximum $S_{\max}$ and minimum $S_{\min}$. Since the difference $\Delta S = S_{\max} - S_{\min}$ is small, one can suggest the electron parameters entering eq 56 are approximately the same. Then, considering only the first harmonic, the dHvA signal is

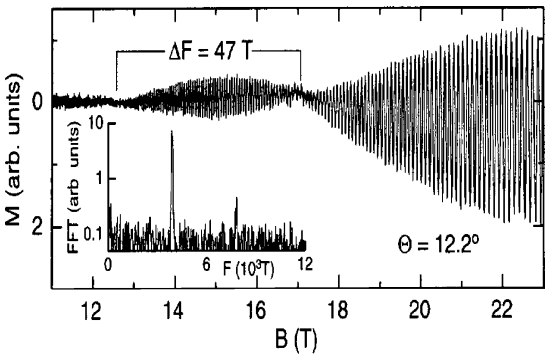

Figure 15. dHvA oscillations in β-(BEDT-TTF)$_2$IBr$_2$ at $T = 0.4$ K, at the field slightly tilted from the direction normal to the layers. The oscillations exhibit the beating behavior owing to the slight warping of the FS cylinder. The inset shows the fast Fourier transformation of the data. (Reproduced with permission from ref 70. Copyright 1996 EDP Sciences.)

$$\tilde{M} \approx M_1\left[\sin\left(2\pi\frac{F_{\max}}{B} - \pi - \frac{\pi}{4}\right) + \sin\left(2\pi\frac{F_{\min}}{B} - \pi + \frac{\pi}{4}\right)\right] = 2M_1 \sin\left[2\pi\left(\frac{F}{B} - \frac{1}{2}\right)\right] \cos\left(2\pi\frac{\Delta F}{2B} - \frac{\pi}{4}\right) \quad (57)$$

where $F = (S_{\max} + S_{\min})/(4\pi e\hbar)$ is the average of the frequencies $F_{\max}$ and $F_{\min}$ corresponding to the maximum and minimum cross sections, respectively, and

$$\Delta F = F_{\max} - F_{\min} = \Delta S/(2\pi e\hbar) \quad (58)$$

Figure 15 shows an example of the dHvA signal from β-(BEDT-TTF)$_2$IBr$_2$.[70] The fundamental frequency $F \approx 3840$ T yields the average cross section of the FS cylinder $\approx 4.05 \times 10^{-49}$ m^2 kg^2/s^2 that corresponds to ≈53% of the 2D Brillouin zone area, in good agreement with the results of the AMRO analysis[3] (see section 2.2). In line with eq 57, the amplitude of the fundamental harmonic is modulated with a low frequency determined by the warping of the FS: two nodes are clearly seen at about 12.5 and 17 T, respectively. For the model q2D zero-field spectrum (eq 13), one has $F/B = \epsilon_{\mathrm{F}}/(\hbar\omega_{\mathrm{c}})$ and $\Delta F/B = 4t_\perp/(\hbar\omega_{\mathrm{c}})$, and the frequency of the beats provides an evaluation of the anisotropy ratio:

$$\frac{2t_\perp}{\epsilon_{\mathrm{F}}} = \frac{\Delta F}{2F} \quad (59)$$

Taking $\Delta F = 50-55$ T from the experiments,[67,70] this ratio is estimated to be in the range 1/155 to 1/140 for β-(BEDT-TTF)$_2$IBr$_2$. It is consistent with what is obtained from the peak feature in the angle-dependent semiclassical magnetoresistance (see section 2.2.2).

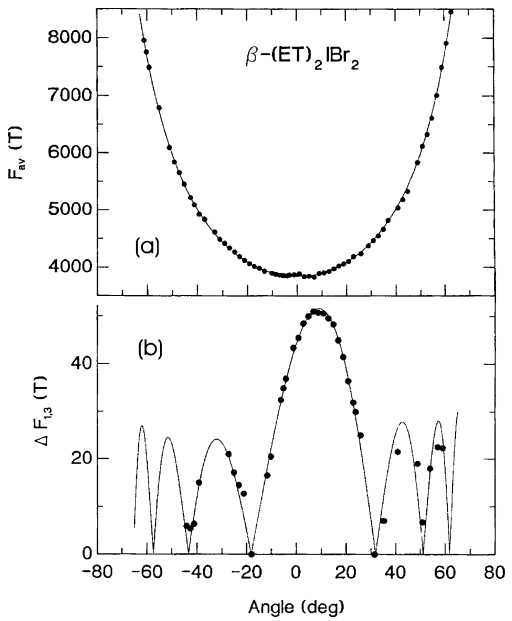

Figure 16. Angular dependence of the fundamental dHvA frequency F (a) and of the difference frequency ΔF (b) in β-(BEDT-TTF)$_2$IBr$_2$. (Reproduced with permission from ref 61. Copyright 1993 Elsevier ScienceDirect.)

It is instructive to trace the oscillation behavior while changing the magnetic field orientation. The cross-sectional area and, hence, the frequency F are obviously the smallest when the field is parallel to the axis of the FS, that is, perpendicular to the highly conducting plane, $\theta = 0$ in Figure 16. With tilting the field, the areas of both the largest and the smallest orbits increase so that $F \propto 1/\cos\theta$, as shown in Figure 16a.[61] By contrast, the frequency difference ΔF presented in Figure 16b displays highly nonmonotonic behavior,[61] going to zero at certain θ's. This phenomenon is closely related to the AMRO effect discussed in section 2.2.1: the beat frequency vanishes at the angles defined by eq 21 at which all the orbits on the FS have the same area and the semiclassical magnetoresistance is maximum. Indeed, the data in Figure 16b are nicely fitted using eq 14 modified to include the asymmetry of the FS warping in the way it was done in eq 21.

As was already mentioned in section 2.2.1, the amplitude of the quantum oscillations is strongly enhanced at the AMRO peaks, that is, at the same angles at which $\Delta F = 0$. This is naturally because *all the orbits* on the FS are extremal and contribute to the oscillations at these angles. Strictly speaking, this statement is valid only when the modulation of the FS is perfectly harmonic. If more than one harmonic appreciably contribute to the modulation, the positions of the peaks of the quantum oscillation amplitude are predicted to shift from the AMRO peaks.[157] A careful inspection of the angle dependence of the SdH amplitude in β-(BEDT-TTF)$_2$IBr$_2$ reveals that its maximum is shifted by $\approx 1°$ with respect to the first AMRO peak.[158] A detailed study of this shift might be useful for determination of the exact form of the FS warping.

Finally, it should be noted that the beating behavior as a signature of the 3D warped FS can only be observed when the warping is bigger than the distance between subsequent Landau tubes near the Fermi level. For the model q2D dispersion (eq 13), this condition can be expressed as

$$W_\perp \equiv 4t_\perp > \hbar\omega_c \tag{60}$$

where $W_\perp$ is the conduction bandwidth in the interlayer direction. As will be seen from the following (sections 3.2 and 3.4), this requirement is often not fulfilled in organic metals.

3.1.2. Shubnikov–de Haas (SdH) Oscillations

The theory of the SdH oscillations is more complex than that of the dHvA effect, since the former are entirely caused by deviations from the τ-approximation and one should, in principle, consider a detailed problem of scattering processes modified by a quantizing magnetic field.[159] Fortunately, it is usually possible to obtain a satisfactory description by following Pippard's idea[23,160] that the scattering probability and, hence, the resistivity are proportional to the density of states around the Fermi level, $D(\zeta)$. The latter can be shown (see, e.g., ref 22) to be proportional to the field-derivative of magnetization:

$$\tilde{D}(\zeta) \propto \left(\frac{m_c B}{S_{extr}}\right)^2 \frac{\partial \tilde{M}}{\partial B} \tag{61}$$

As a result, the oscillatory part of the conductivity can be expressed in the form

$$\tilde{\sigma}/\sigma_0 = \sum_{r=1}^{\infty} \frac{1}{r^{1/2}} a_r \cos\left[2\pi\left(\frac{F}{B} - \frac{1}{2}\right) \pm \frac{\pi}{4}\right] \tag{62}$$

where

$$a_r \propto \frac{m_c B^{1/2}}{(S'')_{extr}^{1/2}} R_T(r) R_D(r) R_S(r) \tag{63}$$

and σ_0 is the background conductivity.

Equations 54−56, 62, and 63 with the damping factors R_T, R_D, and R_S introduced below are the basic formulas for a quantitative analysis of the dHvA and SdH oscillations in 3D metals.

3.1.3. Damping Factors

The first damping factor in eqs 56 and 63, R_T, originates from the temperature induced smearing of the Fermi distribution function. Roughly speaking, a metal with the Fermi energy ϵ_F° and $T > 0$ can be considered as a superposition of metals with $T = 0$, having Fermi energies distributed around ϵ_F°. The oscillation frequencies associated with such metals, $F \propto S_{extr}$, would slightly differ from each other. This should lead to smearing the phase of the resulting oscillations and, hence, to a decrease of the amplitude. The exact expression for R_T is[156]

$$R_T(r) = \frac{2\pi^2 r k_B T/(\hbar\omega_c)}{\sinh[2\pi^2 r k_B T/(\hbar\omega_c)]} = \frac{Kr\mu T/B}{\sinh(Kr\mu T/B)} \tag{64}$$

where

$$\mu = m_c/m_e \quad (65)$$

is the cyclotron mass normalized to the free electron mass m_e, and $K \equiv 2\pi^2 k_B m_e/(\hbar e) \approx 14.7$ T/K. Equation 64 determines the temperature dependence of the oscillation amplitudes in eqs 56 and 63. By fitting eq 64 to the experimental data, one obtains the effective cyclotron mass. At large arguments x, $\sinh(x) \approx \exp(x)/2$, so that the temperature dependence (eq 64) is reduced, at high enough T, to

$$R_T(r) \propto \frac{T}{B}\exp(-Kr\mu T/B) \quad (66)$$

so that μ is directly extracted from the slope of the linear plot $\ln(M_r/T)$ or $\ln(a_r/T)$ versus T.

The values m_c determined for organic metals usually range between $\simeq 2m_e$ and $7m_e$; that is, they significantly exceed the free electron mass.[25] The highest, to date, value, $\mu = 12.4 \pm 1.1$, has been recently reported for β-(BDA-TTP)$_2$SbF$_6$.[49] A comparison between m_c and the so-called band mass, which is obtained from usual band structure calculations in neglect of electron−electron and electron−phonon interactions, gives information about the role of many-body interactions in the material.[22] For example, such a comparison performed by Merino and McKenzie[161] for several organic metals reveals appreciable renormalization of μ due to many-body effects. This is in line with a number of other independent evidences for the importance of electron−electron and electron−phonon interactions in these compounds discussed, for example, in refs 1, 11, 12, and 162.

In a perfect crystal (the scattering rate $1/\tau = 0$), the quantized Landau subbands given by eq 51 are infinitely sharp in the plane perpendicular to the magnetic field. According to the uncertainty principle, a finite relaxation time broadens the subbands. Usually the broadening is described by the Lorentz distribution function with the half-width $\Gamma = \hbar/2\tau$.[22] The corresponding, so-called Dingle damping factor to the oscillation amplitude is[163,164]

$$R_D(r) = \exp\left(-\frac{\pi r}{\omega_c \tau}\right) = \exp(-Kr\mu T_D/B) \quad (67)$$

where $T_D = \hbar/(2\pi k_B \tau)$ is called the Dingle temperature. Provided μ is known from the temperature damping factor, the relaxation time can be estimated from the field dependence of the oscillation amplitude by fitting it to eq 56 or 63 with the Dingle factor (eq 67).

Typical values of T_D obtained for organic metals are of the order of 1 K, that corresponds to $\tau \sim 10^{-12}$ s. A rough estimate for the mean free path in the highly conducting plane, $l \sim 10^2-10^3$ Å, can be made using typical Fermi velocities[1] of $\sim 10^4-10^5$ m/s. The upper limit for T_D is set by experimental conditions for observation of the oscillations; usually at $T_D >$ 3−4 K they become vanishingly small in fields $\leq$ 30 T. The lowest, to the best of our knowledge, Dingle temperature, $T_D \approx 0.25$ K, was reported for clean samples of α-(BEDT-TTF)$_2$KHg(SCN)$_4$ (in the high-field state),[165] κ-(BEDT-TTF)$_2$I$_3$,[166] and β''-(BEDT-TTF)$_2$SF$_5$CH$_2$CF$_2$SO$_3$.[167] It should be noted that all three materials are extremely highly anisotropic. As will be discussed below, the standard Lifshitz−Kosevich (LK) formalism presented here cannot be applied to such systems. The values T_D for the former two salts were obtained from a numerical model treatment suggested for 2D metals.[165] In the case of the latter salt, the data were taken in the low-field region where deviations from the LK model are supposed to be insignificant. An upper limit of 0.1 K was more recently suggested for T_D in a crystal of κ-(BEDT-TTF)$_2$I$_3$[168] on the basis of a low-field SdH experiment. However, this estimation should be taken with caution, since the experimental conditions corresponded to the region where the material exhibits highly unusual, far from being understood, properties (see refs 168−170 and references therein).

Another important point to be kept in mind is that τ derived from the Dingle factor is usually considerably lower than the normal transport relaxation time τ_{tr}.[67,129,171] The reason is that the amplitude of quantum oscillations is highly sensitive to long-range scattering defects, such as dislocations, and macroscopic spatial inhomogeneities,[22] which are unimportant for the normal classical transport. A special case in which the relaxation time close to τ_{tr} can be extracted from quantum oscillations will be presented in section 3.5.1.

The third damping factor, R_S, describes the effect of the Zeeman spin splitting: each Landau subband (eq 51) is, in fact, split into two with the energy difference

$$\Delta\epsilon = g\beta_0 B \quad (68)$$

where g is the Landé factor and $\beta_0 = e\hbar/(2m_e)$ is the Bohr magneton. For free electrons, $g \approx 2$ and $\Delta\epsilon \approx \hbar eB/m_e$ is equal to the Landau subband spacing $\hbar\omega_c$. Therefore, at a fixed p_B, the n-th Landau subband with spin parallel to **B** and the $(n-1)$-th Landau subband with spin antiparallel to **B** cross the Fermi level at the same field, so that the oscillations are contributed in-phase by both spin subbands. However, in real metals generally $\Delta\epsilon \neq \hbar\omega_c$ and there is a phase shift between contributions from subbands with opposite spins. This leads to a reduction of the oscillation amplitude by the factor

$$R_S(r) = \cos\left(\frac{\pi}{2} rg\mu\right) \quad (69)$$

Both the g-factor and the effective cyclotron mass in eq 69 are renormalized by electron−electron and electron−phonon interactions. In particular, g may significantly differ from the value g_s measured in electron-spin-resonance experiments, which is not affected by many-body correlations. If μ is known from $M_r(T)$, R_S provides evaluation of the g-factor. Comparing the latter with g_s, one obtains information on the influence of many-body interactions on spin splitting.

As mentioned above, the area of cyclotron orbits in a q2D metal increases proportional to $1/\cos\theta$ with

tilting the field. This leads to a decreasing cyclotron frequency, $\omega_c \propto \cos\theta$ or, equivalently, increasing cyclotron mass, $\mu(\theta) = \mu(0)/\cos\theta$. Substitution of this θ-dependence in eq 69 yields a periodic vanishing of R_S: it becomes zero every time when $rg\mu(0)/\cos\theta$ is an odd integer. Thus, by finding the angles at which the amplitude of the r-th harmonic goes to zero, one can rather precisely determine the product $g\mu(0)$. This *spin-zero* method has been frequently used in dHvA and SdH studies of organic metals; see refs 25 and 172 for a review.

A remarkable manifestation of the spin-splitting effect has been found in λ-$(BETS)_2FeCl_4$. This material is of particularly high interest since the recent discovery of high-magnetic-field-induced superconductivity.[14] At zero field it is in an antiferromagnetic insulating state below 9 K,[173] which is, however, completely suppressed by magnetic fields above 10 T,[174,175] and, eventually, the superconducting state is stabilized in the field between 17 and 42 T directed parallel to conducting layers.[14,176] Two scenarios were originally proposed to explain this field-induced superconductivity.[14] According to one of them, a high magnetic field confines the electron motion to a single layer, thus causing a dimensional crossover from q2D to purely 2D transport and consequent stabilization of superconductivity as predicted by a number of theoretical models.[177−182] Another possible mechanism is the Jaccarino−Peter compensation effect:[183] due to the exchange interaction J with magnetic moments localized on Fe^{3+} ions in the anion layers, conduction electrons experience an exchange field B_J directed against the external field B. The material becomes superconducting when $|B_{eff}| = |B - B_J|$ is smaller than the paramagnetic Chandrasekhar−Clogston limit, provided the orbital pair-breaking is suppressed.[176]

Figure 17 shows the oscillating part of magnetoresistance in λ-$(BETS)_2FeCl_4$ as a function of inverse field.[184] The amplitude of the fundamental harmonic is clearly modulated, yielding the split peak, $F_1 = 608$ T and $F_2 = 738$ T, in the Fourier transform shown in the inset in Figure 17. At first sight, this beating behavior is a signature of a warped FS, as was discussed above (see eqs 57 and 58). However, the angular dependence of both frequencies, which is presented in Figure 18, reveals a monotonic change of the difference $F_2 - F_1$, $\propto 1/\cos\theta$, in sharp contrast to the expected oscillating behavior, as, for example, shown in Figure 16b. An alternative explanation proposed by Cépas et al.[185] invokes the spin-splitting effect. In the presence of an internal field, the spin-splitting factor (eq 69) is modified and becomes field-dependent:[22]

$$R_S = \cos\left[\frac{\pi}{2}g\left(1 - \frac{B_J}{B}\right)\mu\right] \qquad (70)$$

(here we set $r = 1$ to analyze the fundamental harmonic). Now R_S is modulating the oscillation amplitude (eqs 56 and 63) periodically in $1/B$, similarly to the effect of the FS warping (eq 57). However, the angular dependence of the beat frequency, $F_{beat} = g\mu B_J/4$, being determined by that of the cyclotron mass μ, is simply proportional to $1/\cos\theta$, in agreement with the experimental observation. The exchange field, $B_J = 32$ T, evaluated from F_{beat} is in excellent agreement with the value expected from the phase diagram, assuming the Jaccarino−Peter scenario,[176] thus providing a solid argument in favor of the latter. Similar estimations have been performed on a few compounds of the λ-$(BETS)_2Fe_xGa_{1-x}Cl_4$ series,[186] and a reasonable correlation between the internal field and the concentration, x, of the magnetic ions Fe^{3+} was found.

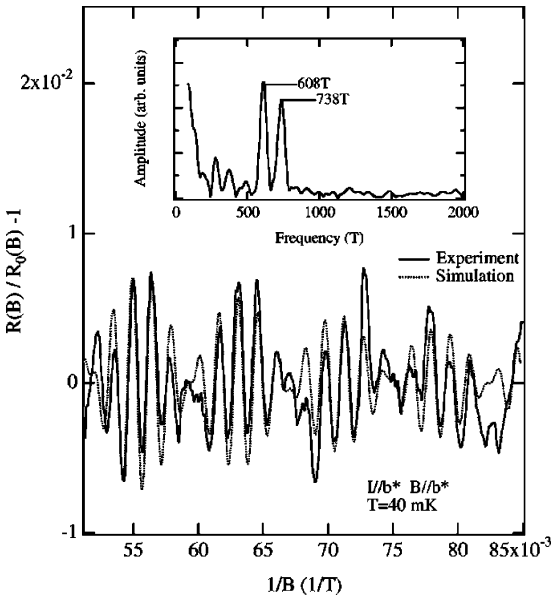

Figure 17. Oscillatory part of the magnetoresistance of λ-$(BETS)_2FeCl_4$ as a function of inverse magnetic field. The dotted line is the result of a numerical simulation based on the LK formula with the parameters $\mu = 1.4$ and $T_D = 0.5$ K. The amplitude of the oscillations is modulated, revealing two frequencies close to each other, as shown by the Fourier transformation in the inset. (Reproduced with permission from ref 184. Copyright 2001 American Physical Society.)

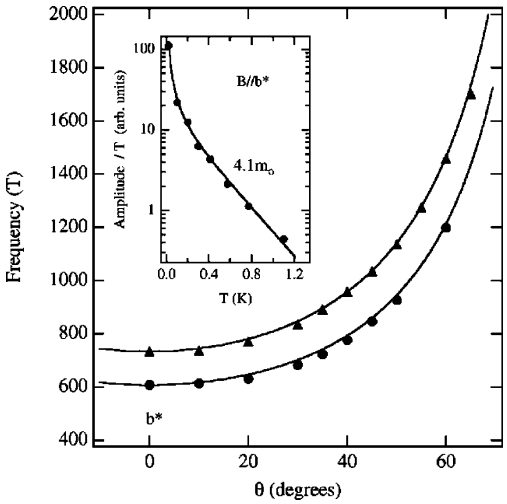

Figure 18. Angular dependence of the SdH oscillation frequencies in λ-$(BETS)_2FeCl_4$. Both frequencies as well as the difference between them follow the $1/(\cos\theta)$ law. The inset shows the LK fit to the temperature dependence of the oscillation amplitude (see eq 64), yielding the cyclotron effective mass $m_c = 4.1m_e$. (Reproduced with permission from ref 184. Copyright 2001 American Physical Society.)

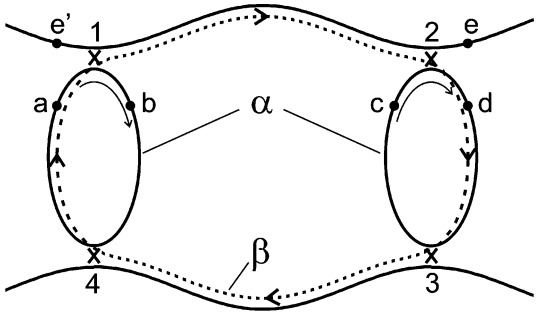

Figure 19. Schematic view of a linear-chain MB network. The MB junctions are indicated by crosses labeled as 1, 2, 3, and 4, respectively. At low magnetic fields an electron moves, in a perpendicular magnetic field, on the classical orbits, e.g., on the closed orbits α. Arrows indicate the allowed direction of the cyclotron motion at the given field direction. At high fields the electron can tunnel through the MB junctions, producing, for example, the closed orbit a−1−2−d−3−4−a labeled as β.

The same effect has very likely been observed in κ-$(BETS)_2FeBr_4$.[187,188] This compound is the first ambient-pressure antiferromagnetic organic superconductor.[189−192] SdH oscillations exhibit pronounced beats with the frequency of ≈100 T[187,188] originally attributed to the FS warping. Cépas et al.[185] have proposed that the beats have the same nature as in λ-$(BETS)_2FeCl_4$. They have estimated the internal field and predicted field-induced superconductivity in the range 11−13 T. Indeed, recent experiments on the resistivity and thermal conductivity[193−195] have provided convincing evidence of the field-induced superconductivity in the field range centered at ≈12.5 T, in remarkable agreement with the theoretical prediction.

3.1.4. Magnetic Breakdown

The described above scheme of the Landau level quantization and the LK theory have been derived under the basic assumption that the effect of magnetic field is reduced to a coherent cyclotron motion of electron wave packets along well-defined trajectories, both in real space and **p**-space. This *quasiclassical approximation* is valid when the characteristic cyclotron energy $\hbar\omega_c$ is much smaller than the relevant band energies $\sim\epsilon_F$. However, if two conducting bands come close to each other at the Fermi level, an electron can tunnel through the small gap between the bands in a high enough field.[196] This phenomenon, called *magnetic breakdown* (MB), can be represented in **p**-space as switching between orbits corresponding to different parts of the FS, as illustrated in Figure 19. The FS shown in Figure 19 consists of closed pockets and open sheets coming close to each other at the MB junctions 1, 2, 3, and 4. In a magnetic field applied perpendicular to the p_xp_y plane, electrons move on the FS in the direction shown by the arrows. When an electron starting, say, from point a approaches MB junction 1, it can either keep staying on the same closed orbit α or tunnel through the gap, switching to the open sheet. The tunneling probability Y exponentially increases with field:[197]

$$Y = \exp(-B_{MB}/B) \tag{71}$$

where

$$B_{MB} \simeq \frac{m}{e\hbar}\frac{\Delta_g^{\,2}}{\epsilon_F} \tag{72}$$

is a characteristic breakdown field and Δ_g is the interband gap at the MB junction. It follows from eqs 71 and 72 that the MB becomes significantly pronounced when the cyclotron energy is $\hbar\omega_c \sim \Delta_g(\Delta_g/\epsilon_F)$, which may be much lower than the interband gap.

At very low ($B \ll B_{MB}$) and very high ($B \gg B_{MB}$) fields, one can use the quasiclassical approach, since the electron trajectories are well defined: in the former case, the electrons always stay on the same semiclassical orbits; in the latter case they freely pass through the MB junctions, producing the large closed trajectory β shown by the dotted line in Figure 19. However, if $B \sim B_{MB}$, the trajectories are no longer well defined and one has, in principle, to solve explicitly a very sophisticated quantum-mechanical problem of the electron spectrum in the presence of competing incommensurate lattice and magnetic field potentials.[198]

On the other hand, Falicov and Stachowiak[199] have shown that the dHvA effect can still be satisfactorily described by considering quasiclassical electron wave packets that move on all possible closed orbits, that is, return back to a starting point using all possible paths in the MB network. In this approach, the initial wave of unit amplitude entering a MB junction is separated into a transmitted wave with amplitude υ and a reflected wave with amplitude ξ, such that[200,201]

$$\upsilon = \sqrt{Y}; \quad \xi = \sqrt{1 - Y} \tag{73}$$

The conservation of particles leads to the phase difference of $\pi/2$ between the transmitted and reflected waves. While the absolute phases are not defined, it is conventionally assumed[199−201] that the reflected phase preserves the initial phase and the transmitted one changes by $\pi/2$. It is therefore convenient to rewrite the tunneling amplitude as $i\upsilon$.

Further on, as the wave packet traverses the quasiclassical (i.e. away from MB junctions) path λ in **p**-space in time t_λ, its phase acquires an additional change:

$$\phi_\lambda = \frac{1}{\hbar eB}\int_\lambda p_x \, dp_y \tag{74}$$

while its amplitude is being damped due to the finite scattering rate $1/\tau$ by the factor $\exp(-t_\lambda/2\tau)$. It follows from eq 74 that in the absence of MB the phase change over a complete closed orbit is equal to $S/(\hbar eB)$, where S is the corresponding enclosed area, so that the boundary condition for the phase exactly coincides with Onsager's quantization rule (eq 52).

Considering the described evolution of the phases and amplitudes, Falicov and Stachowiak[199] arrived at the expression for the oscillatory part of the free energy and, therefore, magnetization reproducing the LK formulation in which all possible closed orbits

additively contribute but each contribution is multiplied by the MB reduction factor:

$$R_{\mathrm{MB},j} = (\mathrm{i}\upsilon)^{l_{1,j}}\xi^{l_{2,j}} \tag{75}$$

where $l_{1,j}$ and $l_{2,j}$ are the numbers of points at which the electron encircling the j-th orbit must tunnel through and be reflected from a MB junction, respectively. Equation 75 suggests that the MB probabilities are the same for all the MB junctions. Otherwise, one should of course substitute different probability amplitudes corresponding to relevant junctions.

Turning to the practical realization of the MB phenomenon, organic metals provide a unique laboratory for it. Since the Fermi energies of these materials are quite low, typically from few tens to one hundred millielectronvolts, even gaps which are not very small compared to ϵ_F can give rise to MB effects at accessible magnetic fields. For example, Honold et al.[202] have reported on a MB in the high-field state of α-(BEDT-TTF)$_2$KHg(SCN)$_4$ through the gap of ≃23 meV that is of the same order as ϵ_F for this compound. Further, the characteristic Brillouin zone dimensions are considerably smaller than those of conventional metals. Therefore, the electron phase coherence can be preserved on the entire FS in clean samples and coherent MB effects can be clearly observed. Finally, due to the extremely weak dependence of the FSs on the interlayer momentum, the MB junctions are represented in **p**-space by lines (perpendicular to the conducting layers) rather than points, as is the case in usual 3D metals. Therefore, the condition of the exact orientation of the plane of a cyclotron orbit with respect to the crystal axes is not as crucial as it is for 3D materials. For example, quantum oscillations corresponding to an orbit passing through four MB junctions were observed by Meyer et al.[203] on κ-(BEDT-TTF)$_2$Cu(NCS)$_2$ at tilt angles of the magnetic field ranging from 0° up to 55°. Even at higher tilt angles, the coherent MB has been reported for another q2D organic conductor, (BEDT-TTF)$_8$Hg$_4$Cl$_{12}$(C$_6$H$_5$Br)$_2$, by Vignolles et al.[204,205] This contrasts with the behavior in 3D materials: for example, in magnesium the phase coherence on orbits containing more than 2 MB junctions is broken already at tilt angles less than 0.1°.[206]

The best studied organic compound showing the MB behavior is κ-(BEDT-TTF)$_2$Cu(NCS)$_2$ (see refs 25 and 26 for a detailed review). The topology of its FS[5] is actually identical to the textbook linear-chain MB network shown in Figure 19 (cf. Figure 1c). The MB effect in this compound was discovered by Heidmann et al.[207] They have observed SdH oscillations with the frequency $F_\beta = 3840$ T corresponding to a phase-coherent motion over orbit β in Figure 19 including tunneling through four MB junctions. This was actually the first experimental confirmation of the existence of the open FS sheets predicted by the band structure calculations.[5] Besides F_β, the SdH spectrum[207] contained a strong contribution from the semiclassical α-orbit, $F_\alpha \approx 600$ T and its higher harmonics, $2F_\alpha$ and $3F_\alpha$, as well as combination frequencies $F_\beta + nF_\alpha$ with $n = -2, -1$, and $+1$. These results were soon confirmed by Sasaki et al.[208] The MB field of about 16 T has been estimated from the magnetoresistance oscillations[208,209] that would correspond to the breakdown gap $\Delta_g \simeq 5$ meV. Later measurements of the dHvA effect[203,210] have given about twice as large an MB field, $B_{MB} = (30.5 \pm 2)$ T, yielding $\Delta_g \simeq 7$ meV $\simeq 0.1\epsilon_F$.

Similarly to F_β, the frequency $F_\beta + F_\alpha$ is readily explained in terms of the described Falicov−Stachowiak theory:[199] it can be attributed to the closed orbits $a-1-2-d-3-c-2-d-3-4-a$ and $a-1-b-4-a-1-2-d-3-4-a$ in Figure 19, both enclosing the area equal to the sum of α- and β-orbit areas. On the other hand, to generate the difference frequency such as $F_\beta - F_\alpha$, one has to consider a closed orbit like $a-1-2-c-3-4-a$. However, the motion along the path $2-c-3$ is only allowed in the opposite direction, as indicated by the arrow in Figure 19. Therefore, such a closed orbit is forbidden and the frequency $F_\beta - F_\alpha$ (as well as $F_\beta - 2F_\alpha$) should not exist according to the Falicov−Stachowiak model.

To understand the occurrence of such "forbidden" frequencies in the SdH spectrum, one has to take into account the effect of *quantum interference* (QI) between the electron wave packets traveling from one point of the MB network to another via different paths. This effect, in its simplest realization of two open orbits connecting two MB junctions (so-called Stark interferometer), has been discovered in magnesium and thoroughly analyzed by Stark and coworkers.[206] A generalized theory of the QI in a common case of a coherent MB network was developed by Kaganov and Slutskin.[198] This theory predicts complicated spectra of oscillations of kinetic properties, such as conductivity, including various linear combinations of fundamental harmonics.

The QI effect as a possible origin of the difference frequencies in κ-(BEDT-TTF)$_2$Cu(NCS)$_2$ was suggested by Caulfield et al.[209] and investigated in detail by Kartsovnik et al.[211] and Harrison et al.[212] To illustrate how it works in this case, let us turn again to the MB network in Figure 19. Imagine only two of various ways that an electron wave packet starting, with unit amplitude, from point e' propagates to point e can be realized: path $\lambda_1 \sim e'-1-2-d-3-4-a-1-2-e$ and path $\lambda_2 \sim e'-1-2-d-3-c-2-e$. (Of course, in reality there are other ways, the most probable being $e'-1-2-e$, but we omit them for the moment, for the sake of simplicity.) Taking into account the changes of the amplitude and phase at the MB junctions as well as the phase change (eq 74) occurring upon traversing the quasiclassical parts of the orbit, one can express the resulting wave functions as

$$\gamma_1 = \xi^2\upsilon^4 \exp[\mathrm{i}(\varphi_{e'e} + \varphi_\beta)] \tag{76}$$

and

$$\gamma_2 = -\xi^2\upsilon^2 \exp[\mathrm{i}(\varphi_{e'e} + \varphi_\alpha)] \tag{77}$$

for the electrons moving along the paths λ_1 and λ_2, respectively. Here $\varphi_{e'e}$ is the phase change (eq 74) acquired on the quasiclassical path $e'-1-2-e$, $\varphi_\alpha = S_\alpha/(\hbar eB)$, and $\varphi_\beta = S_\beta/(\hbar eB)$. Then, the total prob-

ability for an electron to pass from point e' to point e is[198,206]

$$P_{e'e} = \sum_{i,j} \gamma_i \gamma_j^* = \gamma_1^2 + \gamma_2^2 + \gamma_1 \gamma_2^* + \gamma_2 \gamma_1^* \quad (78)$$

The two last terms in eq 78 describe the interference between the wave packets propagating via different paths and are equal, respectively, to $-\xi^4 v^6 \exp[i(\varphi_\beta - \varphi_\alpha)]$ and $-\xi^4 v^6 \exp[-i(\varphi_\beta - \varphi_\alpha)]$. Therefore, their sum is

$$\gamma_1 \gamma_2^* + \gamma_2 \gamma_1^* \propto \cos(\varphi_\beta - \varphi_\alpha) = \cos\left(2\pi \frac{F_\beta - F_\alpha}{B}\right) \quad (79)$$

The probability of propagating between points e' and e obviously affects the open orbit contribution to the magnetoresistance. Thus, one should expect the oscillating term with frequency $F_\beta - F_\alpha$ to contribute to the SdH spectrum. Taking into account other possible paths between points e' and e, one obtains the other "forbidden" frequencies such as $F_\beta - 2F_\alpha$, $2F_\beta - 2F_\alpha$, and so forth observed in the experiment.

As mentioned above, the amplitude of the electron wave packet is damped on the quasiclassical orbit due to scattering. This leads to the usual Dingle damping factor like in the LK theory (eq 67). It is easy to see that the normalized cyclotron mass μ in eq 67 should be equal to the sum of the cyclotron masses corresponding to the interfering paths: for example, $\mu = \mu_\beta + \mu_\alpha$ for the oscillations with $F = F_\beta + F_\alpha$. More interesting is the temperature dependence of the oscillation amplitude. Like in the LK theory, it is determined by the energy dependence of the oscillation phase;[198,206] however, now it is the *difference* between the phases of the interfering trajectories:

$$\left(\frac{\partial \varphi_{\lambda_1}}{\partial \epsilon}\right)_{p_B} - \left(\frac{\partial \varphi_{\lambda_2}}{\partial \epsilon}\right)_{p_B} = \frac{2\pi m_e}{\hbar e B}(\mu_{\lambda_1} - \mu_{\lambda_2}) \quad (80)$$

Therefore, the corresponding thermal damping factor, having the same form as in eq 64, contains the mass equal to the *difference* between the cyclotron masses on paths λ_1 and λ_2. In particular, the mass corresponding to the oscillations $F_\beta - 2F_\alpha$ was estimated[211] as $\mu_{\beta-2\alpha} = 0.9 \pm 0.1$, that is, 4 and 7 times smaller than the masses of the pure F_α and F_β oscillations, respectively. It was further reduced to ≤ 0.3 by applying the pressure of $\simeq 8$ kbar,[211] allowing the direct observation of the oscillations at temperatures as high as 9 K at which all the other quantum oscillations were completely suppressed. Of course, even with the zero effective mass, quantum oscillations should eventually be killed by rising temperature. On one hand, this is caused by the scattering rate increasing with temperature.[211,213,214] On the other hand, the LK theory may be violated in the case of the zero mass.[215] These questions have only marginally been investigated thus far (see, e.g., ref 216). It would be therefore very interesting to perform further experimental and theoretical studies of the QI oscillations with the zero effective mass.

According to the theory,[198] the QI phenomenon is manifested solely in the kinetic properties of the electronic system; the energy spectrum remains unaffected. Since magnetization is an inherently thermodynamic quantity, it should be insensitive to the QI. However, significant contributions of the "forbidden" frequencies have been also found in the dHvA signal from κ-(BEDT-TTF)$_2$Cu(NCS)$_2$.[203,210] The possible origin of the "forbidden" frequencies in magnetization oscillations will be discussed in section 3.4.3.

One can compare the manifestations of the MB in κ-(BEDT-TTF)$_2$Cu(NCS)$_2$ with those in other κ-type salts. The closest analogues of this compound, in the sense of physical properties, are the superconductors κ-(BEDT-TTF)$_2$Cu[N(CN)$_2$]Br and κ-(BEDT-TTF)$_2$Cu[N(CN)$_2$]Cl (the latter is a Mott insulator at ambient pressure but becomes metallic and superconducting at pressures $\geq$ 300 bar).[1,11,17] According to the band structure calculations,[17,34] the major features of the FS are predicted to be the same for all three compounds. However, due to the presence of the inversion symmetry in the crystal structure of the latter two salts, the conducting bands are degenerate at the Brillouin zone boundary, so that the interband gap is predicted to be zero. Therefore, the quantum oscillations should correspond to the complete MB regime; that is, only the big β-orbit should be realized. Indeed, the frequency F_β dominates the ambient-pressure oscillation spectrum in the salt with the anion Cu[N(CN)$_2$]Br.[217−221] However, the frequency F_α has also been detected in both the SdH and dHvA signals.[221] This means that the interband gap Δ_g does exist in this compound though it is much smaller than in the Cu(NCS)$_2$ salt. In principle, the existence of a tiny gap, <1 meV, may be caused by a finite spin−orbit interaction[28] which is not taken into account in the band structure calculations.[17,34] Under pressure the oscillation spectrum considerably changes: the α-orbit disappears and instead a frequency $F_\alpha' \approx F_\alpha/4$ is observed.[218,220,222] This result has been interpreted[220] in terms of the FS reconstruction caused by a structural transition.[223] In κ-(BEDT-TTF)$_2$Cu[N(CN)$_2$]Cl both F_β and F_α have been found under pressures above 3 kbar,[224,225] which also indicates the presence of a sizable interband gap. No combination frequencies corresponding to the QI effect have been reported so far.

While the FS of the κ-type salts can be represented by the simple linear chain MB network, more complicated geometries can be found in other organic conductors. An illustrative example is the salts with polymeric halomercurate anions: (BEDT-TTF)$_8$Hg$_4$Cl$_{12}$(C$_6$H$_5$X)$_2$ with X = Cl, Br.[204,205,214,226] The FS of these compounds shown in Figure 20 originates from hybridization of two pairs of q1D sheets open in directions (0,1) and (1,1) in the conducting plane.[227] As a result, it contains a holelike cylinder and an electronlike cylinder having equal cross-sectional areas. The gaps E_1 and E_2 between the cylinders are small enough to allow strong MB effects in fields above 10 T. Now, by contrast to the *linear* chain of coupled orbits as in Figure 19, we obtain a sophisticated *two-dimensional* network giving rise to a vast variety of different frequencies in the SdH and dHvA spectra.[204,214]

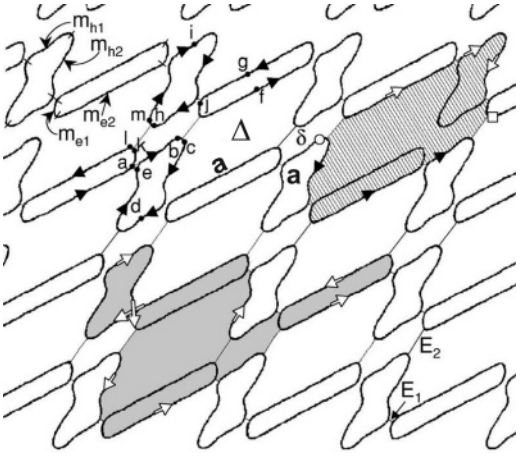

Figure 20. FS of $(BEDT\text{-}TTF)_8Hg_4Cl_{12}(C_6H_5X)_2$ with X = Cl and Br according to the band structure calculations.[227] Bold labels "**a**" denote the equal areas of the small semiclassical closed orbits on the q2D holelike and (elongated) electronlike FS pockets; the labels "Δ" and "δ" denote, respectively, the big and the small areas between the FS pockets; E_1 and E_2 are the MB gaps separating the FS pockets in **p**-space. Shaded and hatched areas depict examples of a closed and of a QI orbit, respectively, which would yield the oscillation frequency corresponding to 100% of the Brillouin zone area. (Reproduced with permission from ref 214. Copyright 2002 American Physical Society.)

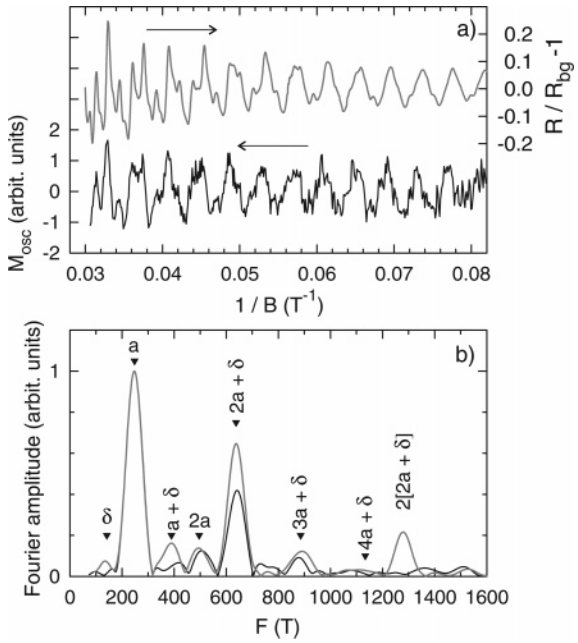

Figure 21. (a) Oscillatory part of the magnetoresistance (gray curve, right scale) and magnetization (black curve, left scale) of $(BEDT\text{-}TTF)_8Hg_4Cl_{12}(C_6H_5Br)_2$ at $T = 1.8$ K. (b) Corresponding Fourier spectra. (Reproduced with permission from ref 204. Copyright 2003 Springer.)

Figure 21 shows an example of SdH and dHvA oscillations measured on the X = Br salt[204] at T = 1.8 K along with the corresponding Fourier spectra. While the main contribution comes from the classical orbits α around the single holelike and electronlike parts of the FS, several combination frequencies labeled as $n\alpha + \delta$ are clearly pronounced. There is also a marginally resolved peak δ in the spectrum of the SdH oscillations which, however, is only very weakly temperature-dependent, so that it becomes

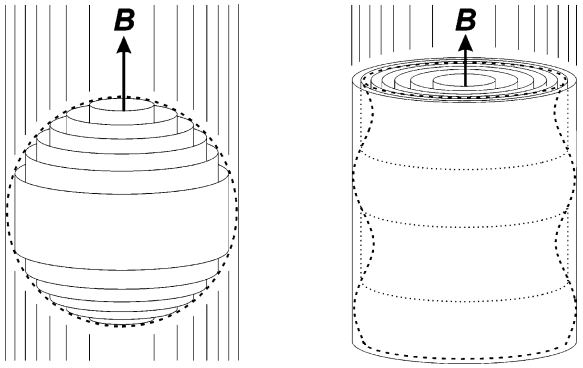

Figure 22. Schematic representation of the Landau tubes (thin lines) crossing a 3D isotropic FS and a q2D FS (thick dotted lines). The 3D FS is crossed by many Landau tubes. By contrast, only few Landau tubes cross the q2D FS at a given field. The number of tubes crossing the FS in the latter case depends on the FS warping and on the strength of the magnetic field.

dominating at higher temperatures, $T \geq 6$ K.[204,205] In addition, frequency F_b, corresponding to the whole Brillouin zone area, and its numerous combinations with F_α and F_δ are observed in magnetoresistance in fields above 20 T.[214] According to the FS topology, there are various, rather complicated, orbits to which the observed frequencies can be assigned. For example, the shaded and hatched areas in Figure 20 would correspond, respectively, to the closed (Landau quantized) MB orbit and QI pattern, both yielding the frequency equal to F_b. The actual origin of F_b has been established via the temperature dependence of its amplitude. By fitting it to the LK temperature damping factor, the effective cyclotron mass of $\leq 0.4m_\alpha$ has been obtained (m_α is the mass corresponding to the fundamental oscillations). This is an order of magnitude lower than expected for the closed MB orbit but perfectly agrees with the zero mass value expected for the QI loop. On the other hand, the effective cyclotron masses corresponding to the low frequency F_δ and some other combination frequencies have been found[204,205,214] to be significantly lower than those calculated for any relevant closed MB orbits or QI paths. This suggests that the standard theory of magnetic quantum oscillations is not thoroughly valid for this material. One of the possible reasons for that is the extremely high anisotropy of the electronic system.

3.2. Violations of the Three-Dimensionality

The presented above formulas for the dHvA and SdH effects are generally valid when the FS is intersected by many Landau tubes, as shown in the left part of Figure 22. This obviously requires that (i) the spacing between the adjacent Landau subbands is much smaller than the Fermi energy, $\hbar\omega_c \ll \epsilon_F$, and (ii) the energy dispersion in the direction parallel to **B** is sufficiently large. Under these conditions, the oscillations are relatively small, being contributed by only a small fraction of charge carriers situated in the vicinity of the extremal cross section of the FS. The first assumption is usually valid for organic metals: the Fermi energy is typically of the order of 0.1 eV[1] whereas the cyclotron energy $\hbar\omega_c$

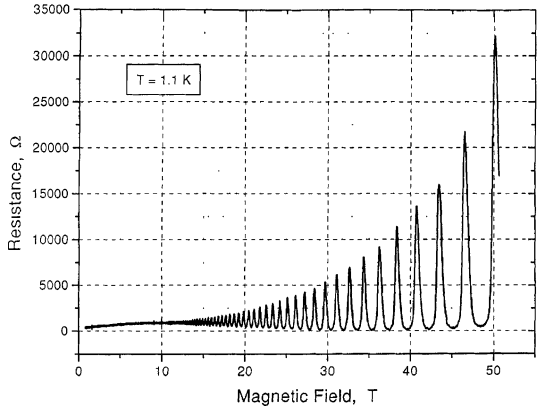

Figure 23. Giant SdH oscillations in a high-quality sample of α-(BEDT-TTF)$_2$TlHg(SeCN)$_2$ in pulsed magnetic fields perpendicular to the layers, at $T = 1.1$ K. (Reproduced with permission from ref 47. Copyright 1996 EDP Sciences.)

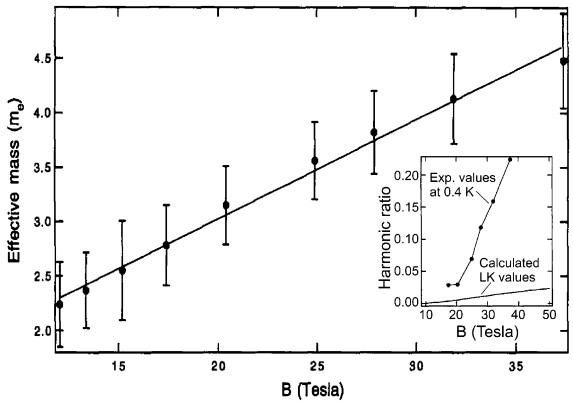

Figure 24. Illustration of the violation of the 3D LK model in α-(BEDT-TTF)$_2$NH$_4$Hg(SCN)$_2$. Main panel: field-dependent values of the effective cyclotron mass parameter obtained by the LK fitting to the temperature dependence of the SdH amplitude. Inset: comparison of the experimentally determined field-dependent ratio between the first and second harmonic amplitudes of the SdH signal with that predicted by the LK model. (Reproduced with permission from ref 229. Copyright 1996 Elsevier Science-Direct.)

does not exceed 2−3 meV even in pulsed magnetic fields up to 50−60 T. However, condition (ii) is often broken in these highly anisotropic materials.

The right panel of Figure 22 shows schematically a warped Fermi cylinder determined by the q2D dispersion (eq 13) and Landau tubes in the magnetic field parallel to the cylinder axis (i.e. normal to the highly conducting layers). The number of tubes intersecting the FS can be estimated from the ratio of the interlayer bandwidth $W_\perp$ to the distance $\hbar\omega_c$ between the Landau subbands (eq 51), $W_\perp/\hbar\omega_c \simeq \Delta F/B$ (see eqs 57−59). For β-(BEDT-TTF)$_2$IBr$_2$ this ratio is less than 4 in the field of 15 T, so at most four Landau tubes at a time can intersect the FS at this field. As a result, oscillations of the electronic energy are enhanced and one may expect deviations from the standard 3D theory. Indeed, magnetoresistance measurements performed on the β_H-(BEDT-TTF)$_2$I$_3$ salt, which is very similar to β-(BEDT-TTF)$_2$IBr$_2$ in its anisotropic electronic structure (see section 2.2.2), have revealed SdH oscillations with the amplitude exceeding the background resistance by an order of magnitude.[65] So strong an amplitude and high harmonic content cannot be described within the 3D model.

Even a stronger SdH effect has been observed[47,228] on α-(BEDT-TTF)$_2$TlHg(SeCN)$_4$: the amplitude of the oscillations shown in Figure 23 for $T = 1.1$ K amounts to ∼100 times the background at the field of 50 T. Using eqs 63 and 64 for the cyclotron mass determination leads to a surprisingly field-dependent result: $\mu \approx 1.8$, 2.7, and 4.2 at fields about 10, 30, and 45 T, respectively. A similar field-dependent mass was reported for the isostructural compound α-(BEDT-TTF)$_2$NH$_4$Hg(SCN)$_4$.[229] As shown in Figure 24, the cyclotron mass evaluated according to the LK formula (eq 64) increases approximately linearly with the field, with the slope of ≃0.1 T^{-1}. The inset in Figure 24 displays the experimentally measured[229] ratio between the amplitudes of the second and first harmonics of the SdH oscillations in the same compound. For comparison, the prediction of the LK theory is shown in the same figure by the solid continuous line. The discrepancy between the theory and experiment rapidly grows with increasing the field, reaching an order of magnitude at $B \geq 30$ T. Highly anomalous behavior has also been observed for magnetoresistance oscillations in κ-(BEDT-TTF)$_2$I$_3$.[166,168−170] Besides the high harmonic content and field-dependent effective cyclotron mass, it was found that the total oscillation amplitude decreased instead of growing, as the sample was cooled below 1 K in high magnetic fields directed exactly perpendicular to the layers.

It should be noted that no signs of beating of the oscillations have been found in the latter three compounds in the field range between 5 and 50 T. This sets the upper limit of the ratio $W_\perp/\hbar\omega_c \leq 0.5$ at the field of 10 T. Therefore, already at this moderate field the FS can be crossed by not more than one Landau tube at a time, which clearly contradicts the basic assumption of the standard 3D model.

The dHvA oscillations have also been found to violate the 3D theory. Strong oscillations of magnetization with anomalously high harmonic content have been observed, for example, in θ-(BEDT-TTF)$_2$I$_3$,[230] κ-(BEDT-TTF)$_2$I$_3$,[166] the high-field state of α-(BEDT-TTF)$_2$KHg(SCN)$_4$,[230,231] and β″-(BEDT-TTF)$_2$SF$_5$CH$_2$CF$_2$SO$_3$.[232] The effective cyclotron mass estimated according to the LK expression (eq 64) from the temperature dependence of the amplitude of the second harmonic of the dHvA signal has been found to be significantly smaller than that obtained from the analysis of the fundamental harmonic in α-(BEDT-TTF)$_2$KHg(SCN)$_4$[231] and in κ-(BEDT-TTF)$_2$Cu(NCS)$_2$.[203] As mentioned in section 3.1.4, the dHvA spectrum in the latter compound reveals "forbidden" frequencies which cannot be explained by the standard MB theories.

3.3. Two-Dimensional Models of the DHvA Effect

3.3.1. Lifshitz–Kosevich–Shoenberg Formula

Obviously, an appropriate description of the magnetic quantum oscillations in the materials mentioned above must involve their highly 2D character.

In particular, one should take into account an increase of the number of electrons contributing to the oscillations. In the limiting, perfectly 2D case the interlayer bandwidth $W_\perp$ is zero, Landau subbands are degenerate into sharp levels, and *all electrons on the FS* provide in-phase contributions. A modification of the LK formula for the ideally 2D case with a constant, that is, field-independent chemical potential, $\zeta = \epsilon_F$, was proposed by Shoenberg[233] and confirmed later by a more rigorous theoretical analysis.[234,235] The *Lifshitz−Kosevich−Shoenberg* (LKS) formula (also known in the literature as the 2D LK formula) represents the magnetization oscillations in the harmonic expansion form similar to eq 54:

$$\tilde{M} = -\sum_{r=1}^{\infty} \frac{1}{r} M_r \sin\left[2\pi r\left(\frac{F}{B} - \frac{1}{2}\right)\right] = \sum_{r=1}^{\infty} \frac{(-1)^{r+1}}{r} M_r \sin\left(2\pi r \frac{F}{B}\right) \quad (81)$$

where F is defined by eq 55 with S_{extr} being simply the area of the FS cross section S, which is constant in the 2D case, and the harmonic amplitudes are

$$M_r = \frac{e}{2\pi\hbar} \frac{S}{\pi^2 m_c d} R_T(r)\, R_D(r)\, R_S(r) \quad (82)$$

with the damping factors defined by eqs 64, 67, and 69. Here **B** is supposed to be applied perpendicular to the 2D plane. Since the cyclotron orbits in two dimensions are determined solely by the perpendicular field component $B_\perp$, the generalization for an arbitrary field direction is obvious: one should simply substitute $B_\perp = B \cos\theta$ for B in the argument of sine in eq 81, as well as in the damping factors R_T and R_D, and add the factor $1/\cos\theta$ to the argument of the cosine in the spin-splitting factor R_S (eq 69) (θ is, as before, the tilt angle with respect to the normal to the 2D plane).

Comparing expressions 56 and 82 for the dHvA amplitude, we notice the following three points:

(i) The 2D amplitude is enhanced in comparison to the 3D one by a factor of the order of $(\epsilon_F/\hbar\omega_c)^{1/2}$. For our materials this gives roughly an order of magnitude in fields of ~10 T.

(ii) The harmonic ratio is enhanced by the factor $r^{1/2}$. This is the main reason for the "anomalously" high harmonic contents obtained in the magnetization experiments mentioned above.[166,230,232] When the damping factors are close to unity, that is, in a very clean material and at low enough temperatures, dHvA oscillations take the so-called *inverse-sawtooth* form: at increasing field the magnetization steeply increases as a Landau level crosses the Fermi energy and then decreases approximately linearly until the next Landau level comes close to ϵ_F. This behavior is schematically shown in Figure 25.

(iii) The field dependence of M_r is slightly different in the 2D case due to the absence of the factor $B^{1/2}$ in eq 82. This should be taken into account in the determination of the Dingle temperature T_D. On the other hand, the temperature dependence is completely determined by the same factor R_T as in the 3D case. Therefore, the LKS formula is equivalent to the 3D LK formula with respect to the cyclotron mass analysis.

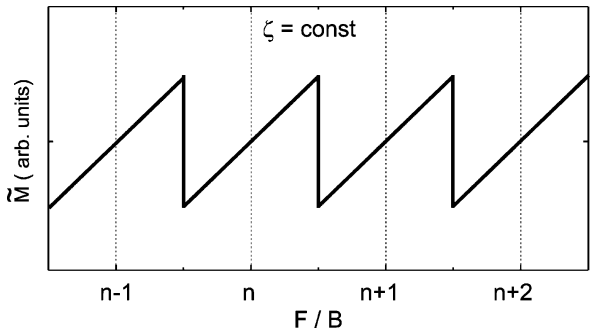

Figure 25. Dependence of the oscillating magnetization of an ideal 2D metal on inverse magnetic field predicted by the Lifshitz−Kosevich−Shoenberg formula (eq 81) for zero temperature, in the absence of scattering. The model implies the constant chemical potential, $\zeta = \epsilon_F$. The oscillations have the inverse sawtooth shape: $\tilde{M}$ linearly decreases at increasing field and discontinuously jumps up every time when a Landau level coincides with the 2D FS, i.e., when the ratio $F/B = \epsilon_F/\hbar\omega_c$ is an odd half-integer number.

While the LKS formula successfully describes dHvA oscillations in some cases, as will be shown below, there are several strong restrictions as to its general applicability. First of all, it assumes the chemical potential ζ to be independent of field. This assumption may turn inappropriate in highly 2D materials. Indeed, considering, for simplicity, the case $T = 0$, the requirement of the constant chemical potential, $\zeta = \epsilon_F$, implies that the lowest unoccupied state remains always at ϵ_F, independent of B. When the Landau levels are sharp ($\hbar/\tau \ll \hbar\omega_c$), this condition can be fulfilled only if there are additional, field-independent states (e.g. impurity states or another conduction band with a sufficiently high density of states) or the total carrier concentration is allowed to change (high magnetostriction). Otherwise, the chemical potential must be, at least partially, pinned to the nearest Landau level and hence oscillate with changing B. This problem has been extensively studied in recent years, and the results will be reviewed below.

The next problem of the 2D LKS model is that it completely neglects dispersion in the third direction, which is always present in real bulk materials. In section 3.3.5 it will be shown how to take into account a finite interlayer charge transfer.

Finally, the LKS formula suggests that scattering processes are described by the 3D Dingle factor, which is not obvious in an extremely 2D case, as will be briefly discussed in section 3.3.6.

3.3.2. Role of Chemical Potential Oscillations

To illustrate the role of the chemical potential oscillations in the dHvA effect, we consider first an ideal 2D metal with a constant concentration of charge carriers, N = constant, and a parabolic in-plane dispersion. The xy plane is conventionally associated with the 2D plane, and the field is applied in the perpendicular direction: $\mathbf{B} = (0, 0, B)$.

For a qualitative consideration, we make further simplifications, assuming zero temperature and scattering rate and neglecting the electron spin. Let us start with the field $B^*_{n_F}$ at which the Landau levels with $n = 0, 1, 2, ..., n_F$ are completely filled and the level with $n = n_F + 1$ is empty. This corresponds to the condition

$$(n_F + 1)\hbar\omega_c = \epsilon_F \tag{83}$$

The chemical potential coincides with the Fermi energy, $\zeta = \epsilon_F$, situating exactly in the middle of the gap between levels n_F and $(n_F + 1)$. Taking into account that the carrier concentration is

$$N = \frac{\pi p_F^{\,2}}{(2\pi\hbar)^2 d} = \frac{\epsilon_F m_c}{2\pi\hbar^2 d} \tag{84}$$

where d is the unit cell period in the z direction, and the condition in eq 83, we obtain the number of the carriers (per unit volume) on each degenerate Landau level up to $n = n_F$:

$$\nu = \frac{N}{n_F + 1} = \frac{eB}{2\pi\hbar d} \tag{85}$$

With increasing the field, the Landau levels shift up in the energy scale and their degeneracy (eq 85) grows, so that free states appear on level n_F. Therefore, the chemical potential jumps down to this level and stays pinned to it, rising linearly with B until the level becomes completely empty, at the field $B^*_{n_F-1}$, such that $n_F\hbar\omega_c = \epsilon_F$. At this point ζ jumps to level $(n_F - 1)$ and so on. Thus, the chemical potential ζ exhibits sawtooth oscillations around ϵ_F, with the amplitude equal to half the distance between the Landau levels, $\hbar\omega_c/2$, as shown in Figure 26a.

Now, to obtain the magnetization oscillations, one has to express the total electron energy as a function of magnetic field and take the derivative with respect to B. The energy E in the unit volume is

$$E_{n_F}(B) = \nu \sum_{n=0}^{n_F-1} \hbar\omega_c\left(n + \frac{1}{2}\right) + (N - n_F\nu)\hbar\omega_c\left(n_F + \frac{1}{2}\right) \tag{86}$$

The second term on the left-hand side of eq 86 reflects the fact that the n_F-th level is, generally speaking, only partially filled. Equation 86 can be rewritten in the form

$$E_{n_F}(B) = -\nu\hbar\omega_c\frac{n_F(n_F + 1)}{2} + N\hbar\omega_c\left(n_F + \frac{1}{2}\right) \tag{87}$$

Since both ν and ω_c are linear functions of B, the energy depends quadratically on the field when n_F is fixed. This dependence holds in the field interval at which $\epsilon_F/(n_F + 1) < \hbar\omega_c < \epsilon_F/n_F$, where the filling of level n_F is changing between 0 and ν. When, with increasing field, the energy of level n_F rises above $\epsilon_F + \hbar\omega_c/2$; that is, when $n_F\hbar\omega_c > \epsilon_F$, this level becomes empty, the chemical potential jumps to the next highest level, $(n_F - 1)$, and the energy of the system switches from $E_{n_F}(B)$ to $E_{n_F-1}(B)$. As a result, the total field dependence $E(B)$ consists of a series of parabolas, as shown in Figure 26b. Correspondingly, the magnetization $M = -dE/dB$ exhibits the sawtooth oscillations displayed in Figure 26c: it increases linearly with field everywhere except the points $n\hbar\omega_c = \epsilon_F$, at which exactly an integer number of Landau levels is filled. Note that the oscillations of magnetization $\tilde{M}$ reproduce the form of the chemical potential oscillations in Figure 26a. On the other hand, comparing them with the LKS oscillations corresponding to the condition ζ = constant, we see that the latter can be obtained by inverting the present "sawtooth" and shifting it by half the period.

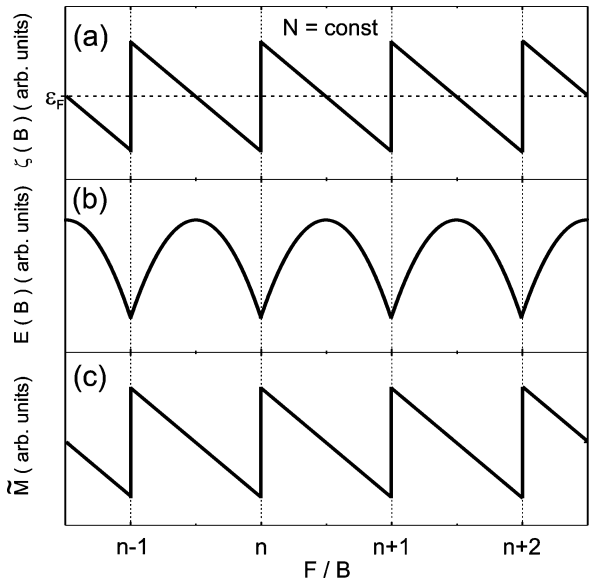

Figure 26. Oscillations of the chemical potential (a), free energy (b), and magnetization (c) at a constant number of charge carriers. The temperature and scattering rate are assumed to be zero. $\tilde{M}$ reproduces the sawtooth shape of the chemical potential oscillations: it linearly grows with increasing field (decreasing F/B) and drops down whenever the Fermi level is situated in the middle between adjacent Landau levels, i.e., at integer filling factors $F/B = \epsilon_F/\hbar\omega_c = 0, 1, ..., n - 1, n, n + 1, ...$

The described sawtoothlike behavior of the oscillatory magnetization in a 2D system with a constant number of carriers has been qualitatively predicted by Peierls[236] as early as in 1933. However, he considered the 2D case as "physically meaningless" at that time. It was only in the 1980s, when 2D and q2D conducting materials attracted substantial interest, that the quantitative theory of the 2D dHvA effect started to develop. It was pioneered by Vagner and co-workers, who were the first to derive analytical expressions for oscillatory magnetization[237] and magnetic susceptibility[238] of a 2D metal with a constant carrier concentration at a finite temperature.

Unlike in the LK or LKS model, where the oscillations of the chemical potential are neglected, in the present case $\tilde{M}$ cannot be generally represented in a simple harmonic form, as will be seen below. In particular, effects of finite temperature and scattering cannot be straightforwardly separated from each other. On the other hand, as was noted in ref 237, the problem is considerably simplified in high fields,

when the temperature induced smearing of the Fermi edge, k_BT, and the Landau level width, $\Gamma = \hbar/(2\tau)$, are much smaller than the spacing $\hbar\omega_c$ between the levels. Under these conditions, the oscillatory behavior is dominated by the field-dependent filling of the two Landau levels nearest (at a given field) to ϵ_F; all the lower levels are completely filled, and all the higher levels are empty. With these simplifications, Vagner et al. have obtained an explicit dependence of magnetization on magnetic field and temperature[237] and proposed a simple expression for the envelope of the oscillations in the high-field limit:[239]

$$M_{extr} \simeq \pm \frac{e\epsilon_F}{2\pi\hbar d}\left(1 - \frac{1}{\alpha}\ln(2\alpha) - \frac{1}{\alpha}\right) \qquad (88)$$

where M_{extr} are the minimum and maximum values of the oscillating magnetization, and $\alpha \equiv \hbar\omega_c/k_BT \gg 1$ should be taken at integer filling factors, $\epsilon_F/\hbar\omega_c = n$, that is, at the fields at which the chemical potential is situated in the middle between the adjacent Landau levels. Formula 88 is valid when $\Gamma \ll k_BT \ll \hbar\omega_c$ or, more strictly,[235] when $(\hbar\omega_c\Gamma)^{1/2} \ll k_BT \ll \hbar\omega_c$.

Another limit, $k_BT \ll \Gamma$, was considered by Grigoriev.[240] It was shown that if the Landau level broadening due to scattering can be described by a Lorentzian and is independent of B (like in the 3D case), the magnetization at N = constant can be reduced to the form similar to the LKS expression with the only but important difference being (cf. the wave forms of the oscillations in Figures 25 and 26c) that all the even harmonics change the sign in eq 82. Such a simple relation to the LKS formula is, however, broken if the effect of finite temperature cannot be neglected or the concentration of the carriers responsible for the oscillations is allowed to change to a certain extent with magnetic field.[240]

The temperature effect on the oscillation amplitude at N = constant is quite different from that at ζ = constant. This is already seen from the asymptotic high-field expression (eq 88), which cannot be reduced to the temperature damping factor of harmonic amplitudes (eq 64) staying in the LKS formula. Numerical analysis[241] shows that the sawtoothlike wave form at N = constant smoothes, with increasing temperature, slower than in the case ζ = constant.

3.3.3. Systems with a Finite Electron Reservoir

Now let us consider the situation intermediate between N = constant and ζ = constant, which is actually typical of many organic conductors. Indeed, a simple cylindrical FS, like in β-type salts, is rather an exception than a rule among these materials. The FSs of the most extensively studied κ-, α-, and λ-salts of BEDT-TTF and BETS combine holelike cylinders with electronlike sheets open in the 2D plane. The thermodynamic equilibrium implies that the charge carriers can be transferred between the corresponding conduction bands with changing the field, to maintain the same chemical potential throughout the sample. The field-independent states on the open Fermi sheets serve as a reservoir of carriers, reducing oscillations of ζ.

Intuitively, this can be understood through the same qualitative consideration as was made above for the pure case of N = constant. However, by contrast to the latter case, we should take into account that the position of the chemical potential is now ultimately determined by the energy ϵ_R of the highest occupied state in the second reservoir band. Again, we associate the beginning of the period with the field $B^*_{n_F}$, defined by condition 83, at which level n_F is fully occupied and level $(n_F + 1)$ is empty. The chemical potential is situated in the middle of the gap between these levels, coinciding with the Fermi energy: $\zeta = \epsilon_R = \epsilon_F$. As the field starts to increase, the Landau level degeneracy ν determined by eq 85 increases. Therefore, the carriers are transferred from the highest occupied states of the reservoir band to level n_F, whose energy $\epsilon^{2D}_{n_F}(B)$ is lower than ϵ_F. As a result, the chemical potential starts to decrease until it reaches $\epsilon^{2D}_{n_F}(B)$. Starting from that point, the carrier exchange between level n_F and the reservoir changes to the opposite direction, so that ϵ_R increases, remaining equal to $\epsilon^{2D}_{n_F}(B)$ until the Landau level becomes completely empty. This happens, obviously, at a lower field than $B^*_{n_F-1}$. In the rest of the period, carriers are transferred from the reservoir to level $(n_F - 1)$ and $\zeta = \epsilon_R$ gradually decreases, reaching the Fermi energy ϵ_F at the end of the period, $B = B^*_{n_F-1}$.

As a result, the amplitude of the chemical potential oscillations is reduced in comparison to the case without a reservoir. The reduction factor is obviously determined by the ratio between the densities of states in the relevant bands near the Fermi level:

$$n_R = \frac{D^R(\epsilon_F)}{D_0^{2D}(\epsilon_F)} \qquad (89)$$

where $D^R(\epsilon_F)$ and $D_0^{2D}(\epsilon_F)$ are respectively the densities of states of the reservoir band and of the 2D band at zero field. [Hereinafter, it is assumed that $D^R(\epsilon)$ does not change in the small interval $\epsilon_F \pm \hbar\omega_c/2$ and equals $D^R(\epsilon_F)$.] For example, in the limiting case, $n_R \gg 1$, the carriers can be transferred to and from the reservoir without a significant change of ϵ_R, so that the oscillations of the chemical potential become negligible.

Turning now to the oscillating behavior of magnetization, of course it must be influenced by the behavior of the chemical potential and, therefore, by the presence of a reservoir. This was for the first time noted by Vagner et al.,[242] who considered theoretically the effect of reservoir states on the dHvA oscillations in layered AsF_6-intercalated graphite. A detailed numerical study of the chemical potential and magnetization oscillations in a system with a field-independent reservoir has been performed by Harrison et al.[165] Figure 27 illustrates the influence of the reservoir strength n_R on the wave form and amplitude of the oscillating chemical potential $\tilde{\zeta}(B) = \zeta(B) - \epsilon_F$ and magnetization $\tilde{M}(B)$ at T, $1/\tau = 0$. The fraction γ of the period over which $\tilde{\zeta}$ increases, following the highest occupied Landau

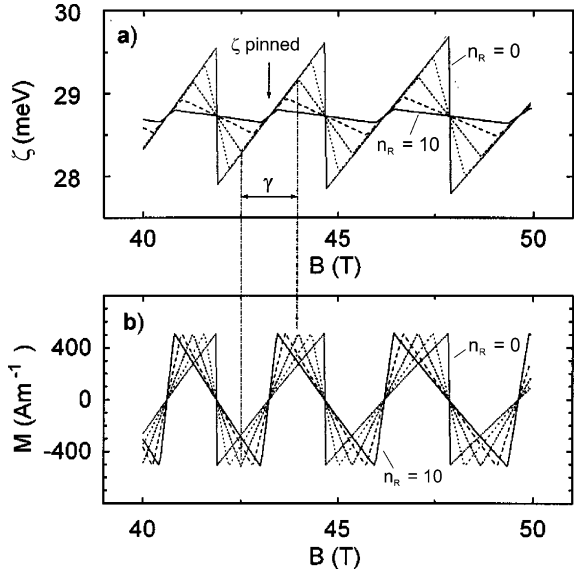

Figure 27. Oscillations of the chemical potential (a) and of the magnetization (b) calculated for different values of the reservoir strength: $n_R = 0$, $1/3$, 1, 3, and 10. The temperature and scattering rate are assumed to be zero. The parameter γ, see eq 90, corresponds to the part of the oscillation period during which the chemical potential ζ is pinned to a Landau level. With increasing n_R the oscillations of ζ diminish. The magnetization oscillations repeat the shape of the chemical potential oscillations, retaining, however, the amplitude independent of n_R. (Reproduced with permission from ref 165. Copyright 1996 American Physical Society.)

level, decreases as the strength of the reservoir, n_R, increases:[165]

$$\gamma = \frac{1}{1 + n_R} \tag{90}$$

The wave form of the magnetization oscillations repeats that of $\tilde{\zeta}$; at the same time their amplitude remains independent of n_R. This suggests an empirical relationship:[165]

$$\tilde{M} = \frac{N}{B}(1 + n_R)\tilde{\zeta} \tag{91}$$

Effects of finite temperature and scattering have also been studied in ref 165, demonstrating substantial deviations from the LK model. On the other hand, the relationship (eq 91) between $\tilde{M}$ and $\tilde{\zeta}$ has been found to hold at any reasonable T and τ. Later it was confirmed on the basis of a more rigorous analysis; see, for example, refs 240 and 241.

The dependence of the wave form of the dHvA oscillations on the reservoir states means that the latter affect the relative amplitudes of the oscillation harmonics. As was already mentioned, at zero temperature all the even harmonics change the sign at $n_R = 0$ in comparison to the LKS case, $n_R = \infty$. In the intermediate case, $n_R = 1$, the even harmonics are absent at $T = 0$ and, since the total dHvA amplitude remains constant, the odd harmonics exceed the LKS values: for example, the first harmonic is ~30% higher than its LKS value.[243] The harmonic content is significantly modified by temperature: numerical calculations[243] show that the second harmonic depends nonmonotonically on T at $n_R > 0.5$ and may even change sign as T is varied.

The most general description of the dHvA effect in a 2D metal with a field-independent reservoir of carriers has been proposed by Grigoriev[240] and Champel and Mineev.[234,244] It was shown that the magnetization can be generally expressed in the form

$$\tilde{M} = \sum_{r=1}^{\infty} \frac{(-1)^{r+1}}{r} M_r \sin\left[2\pi r\left(\frac{F}{B} + \frac{\tilde{\zeta}(B)}{\hbar\omega_c}\right)\right] \tag{92}$$

with the harmonic amplitudes M_r determined by eq 82. In comparison with the LKS formula (eq 81), the present expression includes the oscillations of the chemical potential, $\tilde{\zeta}$, in the argument of the sine. Although the term $\tilde{\zeta}/(\hbar\omega_c) \leq 1/2$ is normally much smaller than the ratio F/B, which determines the oscillation frequency, it may significantly change the phase within a given oscillation period.

The explicit equation for $\tilde{\zeta}$ reads[240,244]

$$\tilde{\zeta}(B) = \frac{\hbar\omega_c}{\pi(1 + n_R)} \sum_{r=1}^{\infty} \frac{(-1)^{r+1}}{r} R_T(r)\, R_D(r)\, R_S(r) \times \sin\left[2\pi r\left(\frac{F}{B} + \frac{\tilde{\zeta}(B)}{\hbar\omega_c}\right)\right] \tag{93}$$

At low temperatures and high fields, the damping factors R_T and R_D are close to unity and, if the reservoir strength n_R is not too high, the oscillations $\tilde{\zeta}$ drastically affect the wave form and, hence, the harmonic content of the oscillating magnetization.

In general, the transcendental equation (eq 93) cannot be solved analytically. However, if the number of significant harmonics in the experimentally measured dHvA signal is not very big, eqs 92, 93, and 82 can be used for fitting the data and extracting the electronic parameters.

An alternative method of analyzing experimental data has been proposed by Harrison et al.[165] These authors notice that the oscillating Helmholtz free energy H takes its extremum (minimum and maximum) values when the chemical potential is equal to ϵ_F. This happens always at the fields corresponding to integer ($n\hbar\omega_c = \epsilon_F$; H is minimum) and odd half-integer [$(n + 1/2)\hbar\omega_c = \epsilon_F$; H is maximum] fillings of Landau levels, irrespectively of the presence of a reservoir. Therefore, it is suggested that the peak-to-peak amplitude H_{p-p} is independent of the reservoir states and can be calculated at any value of n_R. Then, the easiest way is to use the LKS model assuming $\tilde{\zeta} = 0$, that is, $n_R = \infty$. In this model H_{p-p} is given by[22,233]

$$H_{p-p} = 2\frac{B^2}{F}\sum_{r_{odd}} \frac{M_r}{2\pi r} = 2a\frac{B^2}{F}\sum_{r_{odd}} \frac{1}{4\pi^2 r^2} R_T(r)\, R_D(r)\, R_S(r) \tag{94}$$

where M_r are the LKS harmonic amplitudes, $a = eS/(\pi^2\hbar m_c d)$, and the summation is performed over

all significant odd-harmonic amplitudes. The second equality in eq 94 can be used for fitting to the experimental data. For example, if only the first three harmonics are significant, one obtains[165]

$$M_1 + \frac{M_3}{3} \propto \frac{K\mu T/B}{\sinh(K\mu T/B)} \exp(-K\mu T_D/B) + \frac{1}{9}\frac{3K\mu T/B}{\sinh(3K\mu T/B)} \exp(-3K\mu T_D/B) \quad (95)$$

where expressions 64 and 67 are substituted for R_T and R_D, respectively, and the spin-splitting effect is neglected. This formula can be iteratively fitted to the experimentally measured field- and temperature-dependent amplitudes M_1 and M_3, and the electronic parameters μ and T_D can be extracted. After that, the parameter γ (eq 90) can be adjusted so as to place the minima and maxima of the magnetization at the same positions as those in the experimental data (recall that γ determines the fraction of the dHvA period at which the magnetization rises with the field; see Figure 27).

3.3.4. Systems with Multiple Quantized Bands

Another interesting case to consider is a multiband system in which more than one band is subject to the Landau quantization. Originally, the interest in such systems was triggered by the observation of the difference frequency, $F_\beta - F_\alpha$, in the dHvA signal from κ-(BEDT-TTF)$_2$Cu(NCS)$_2$[203] which is not allowed within the standard MB (magnetic breakdown) theory (see section 3.1.4). Later, similar "forbidden" frequencies were found in α-(BEDT-TTF)$_2$KHg(SCN)$_4$[202] and in other inorganic materials: an InGaAs quantum-well system[245] and Sr_2RuO_4.[246] In the organic metals, the effect has been observed, so far, only in the MB regime, that is, when the existence of two fundamental frequencies, F_α and F_β, is caused by the small semiclassical orbit α and big MB orbit β. Therefore, it was initially supposed[247,248] that the MB is a necessary condition for the manifestation of the "forbidden" frequencies. However, subsequent extensive theoretical studies[212,249−259] have shown that the effect can be explained purely by the chemical potential oscillations, without invoking the MB and can be realized as well in systems containing several independent (i.e. not connected through the MB) 2D bands.[249−251,254,−259] While the exact theoretical description of the combination frequencies is still a matter of debate (see, e.g., refs 259−261), their physical origin can be understood based on the discussion above. Indeed, in the case when more than one 2D band contribute to the dHvA effect, the equations for the oscillatory magnetization (eq 92) and chemical potential (eq 93) should be generalized to sum up the corresponding contributions.[256−258] Then, the presence of more than one fundamental frequency in the oscillating chemical potential should lead to frequency mixing effects in the resulting magnetization. In particular, the "forbidden" difference frequencies such as $F_\beta - F_\alpha$, $F_\beta - 2F_\alpha$, and so forth are expected to emerge in the oscillation spectrum. On a qualitative level, such frequencies are a result of a communication between two Landau-quantized 2D bands via the chemical potential: if, for example, the chemical potential is pinned to a Landau level of the α-band and moves up with the latter (at increasing field), the frequency $F_{\beta'}$ with which it is crossed by the Landau levels of the β-band is shifted by an amount close to the α-frequency, that is, $F_{\beta'} \simeq F_\beta - F_\alpha$.

3.3.5. Influence of the Interlayer Coupling

Up to now we considered dHvA oscillations in the ideally 2D case, that is, completely neglected the coupling between the conducting layers. The latter is, however, always present in real bulk materials. A finite interlayer dispersion turns sharp (in the absence of scattering) Landau levels into subbands with the width given by the interlayer bandwidth $W_\perp$. This obviously leads to a reduction of the chemical potential oscillations and to a modification of the wave form of the dHvA oscillations.

The influence of the finite $W_\perp$ on the 2D dHvA effect has been theoretically studied by Grigoriev and Vagner.[262,263] In particular, an analytical expression for the envelope of the magnetization oscillations valid in a wide range, $0 < W_\perp < \hbar\omega_c$, was derived.

Assuming the interlayer coupling is described by the usual dispersion relation $\epsilon(p_z) = -2t_\perp \cos(p_z d/\hbar)$, one can incorporate it into the general expressions for $\tilde{M}$ (eq 92) and $\tilde{\zeta}$ (eq 93) by multiplying each harmonic term by the factor[240,244,255,264,265]

$$R_W = J_0\left(2\pi r \frac{2t_\perp}{\hbar\omega_c}\right) \quad (96)$$

where J_0 is the 0-th order Bessel function. In the limit $2t_\perp \ll \hbar\omega_c$, the Bessel function is close to unity and one returns back to the purely 2D case. On the other hand, when $2t_\perp > \hbar\omega_c$, one can use the large argument approximation (eq 15) for the Bessel function, arriving at the conventional 3D result with the oscillation amplitude periodically modulated according to eq 57.

As was shown in section 3.1.1, the modulation, that is, the beating behavior of the oscillations, depends in a nonmonotonic manner on the tilt angle of the magnetic field. The beat frequency vanishes at angles (eq 21) in line with the AMRO phenomenon (see section 2.2.1). One should therefore expect an enhancement of the 2D character of the quantum oscillations at these angles. For example, numerical simulations performed by Nakano[264] for the case of two q2D Landau-quantized bands yield a strong enhancement of the amplitude of the "forbidden" frequencies due to the chemical potential oscillations at the field directions satisfying condition 21 for both bands. This effect has indeed been observed by Ohmichi et al.[266] on the q2D compound Sr_2RuO_4. It would be very interesting to look for similar or other manifestations of the enhancement of two-dimensionality with changing the field orientation in organic conductors displaying the AMRO effect. Probably it is this mechanism that caused the considerable increase of the harmonic content of the dHvA signal from β-(BEDT-TTF)$_2$X with X = IBr_2

and I_3 at certain field orientations observed by Wosnitza et al.[70]

3.3.6. Comment on the Dingle Factor

In the models presented above, the finite scattering is taken into account by introducing the Dingle factor (eq 67). This is correct in the case when the Landau level broadening caused by the scattering is independent of magnetic field and has the Lorentzian shape. While it is generally true for conventional 3D metals,[22,164] it is still not clear whether the same rule holds as well for 2D systems (see, e.g., ref 267 and references therein for a discussion). This question is quite important, since not only the field but also the temperature dependence of the 2D dHvA signal is sensitive to the exact shape of the Landau levels.[235]

The situation may become even more complicated in the intermediate, q2D case. As pointed out by Maniv and Vagner,[268] the effect of impurity scattering should depend on the interlayer tunneling probability or, in other words, on the interlayer transfer integral $t_\perp$. The physical reason for that is the following:[268] A strictly 2D electron moving, in a strong magnetic field, along a planar cyclotron orbit can pass several times in the vicinity of one and the same impurity, with the number of times increasing with $\omega_c\tau$. The scattering rate for such an electron is therefore enhanced by the magnetic field.[269] However, in a *quasi*-2D material, the electron can avoid the impurity by tunneling to another layer. This leads to a modification of the scattering rate and, hence, of the Landau level broadening, depending on the interplay between three characteristic energies: $\hbar\omega_c$, $\hbar/\tau$, and $t_\perp$. A further complication comes from the fact that not only pointlike impurities but also long-range imperfections are important in the 2D case. In particular, they strongly contribute to damping of the oscillations in organic metals.[67]

Usually the shape of the Landau levels is studied by comparing experimental data with theoretical models assuming various shapes and choosing the one which provides a better fit (see, e.g., ref 267). A direct way of determination of the density-of-states distribution, including the shape of the Landau levels, from the form of a single dHvA oscillation has been recently proposed by Grigoriev.[235,263] This information would be very important not only for describing the quantum oscillations but also for a general understanding of different scattering mechanisms in q2D organic conductors. One should, however, note that the proposed method requires extremely accurate measurements of the oscillation wave form.

3.4. Models versus Experiment

From what was presented above, it is clear that the behavior of the dHvA oscillations becomes essentially 2D when the Landau level spacing $\hbar\omega_c$ is larger than the interlayer bandwidth $W_\perp$.

At high temperatures, when the temperature-induced smearing of the Fermi edge, k_BT, exceeds the value $\hbar\omega_c$, one can universally use the LKS formula (eq 81). As a matter of fact, only the fundamental harmonic is significant in the dHvA effect at $k_BT/(\hbar\omega_c) > \sim 0.2$, even for extremely 2D materials (see, e.g., refs 241 and 243). In this case the temperature dependence of the oscillation amplitude is expected to be identical to that of the 3D LK model while the field dependence is slightly modified. At lower temperatures the higher harmonics start to significantly contribute to the dHvA effect. The 2D character may then be manifested by a nontrivial wave form of the oscillations and substantial deviations from the LK field and temperature dependence. Typically, the Landau level separation in organic conductors is $\hbar\omega_c < \sim 1$ meV in accessible steady magnetic fields. Therefore, the 2D features become particularly important at temperatures below 1.0−1.5 K. Additionally, the broadening of the Landau levels due to scattering, $\sim\hbar/\tau$, should of course be smaller than $\hbar\omega_c$. This sets the necessary requirement to the sample quality.

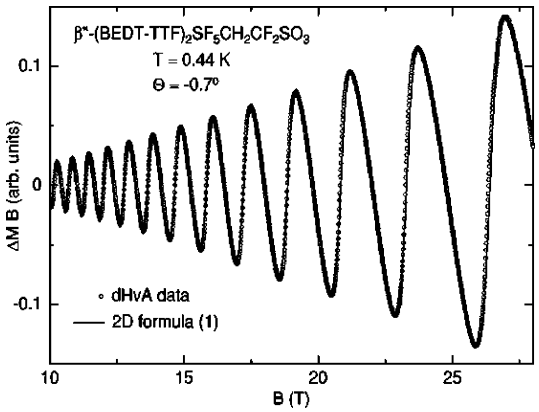

Figure 28. dHvA effect in β''-(BEDT-TTF)$_2$SF$_5$CH$_2$CF$_2$SO$_3$ measured experimentally (circles) along with that obtained within the LKS formula (solid line), using the damping factors determined from low-field, high-temperature measurements. (Reproduced with permission from ref 232. Copyright 2000 American Physical Society.)

In this section we will consider three examples of the organic compounds in which the above conditions can obviously be satisfied, leading to different manifestations of the 2D nature of the dHvA effect.

3.4.1. β''-(BEDT-TTF)$_2$SF$_5$CH$_2$CF$_2$SO$_3$

This compound is a prominent example of a highly 2D electronic system in a bulk material. Despite the fact that the packing of the BEDT-TTF molecules in the conducting layers is quite different from that in the κ-type salts, the FS topology predicted by extended-Hückel band structure calculations[270,271] is similar: it contains holelike cylinders and electronlike open sheets. The cylindrical part of the FS is manifested under magnetic fields by pronounced AMROs[150,272] and magnetic quantum oscillations.[167,232,271−274] As mentioned in section 2.4, the extremely high electronic anisotropy is already reflected in the behavior of the semiclassical magnetoresistance as a function of the field orientation. The quantum oscillations also display features characteristic of a highly 2D system.

Figure 28 shows an example of the oscillatory magnetization[232] recorded at $T = 0.44$ K in the field nearly perpendicular to the layers. The oscillation frequency, $F = (198 \pm 1)$ T, reveals the FS cross

section equal to 5% of the Brillouin zone area. This value is a factor of 3 smaller than predicted by the refined band structure calculations[271] but perfectly agrees with the results of the AMRO experiment.[272] The oscillations in Figure 28 have a clear inverse-sawtooth wave form typical of a q2D metal with a constant chemical potential. Indeed, the solid curve, representing the 2D LKS formula (eq 81), is virtually indistinguishable from the experimental data. The values of the cyclotron mass $\mu = 1.9$, spin-splitting factor $g\mu = 3.9$, and Dingle temperature $T_D = 0.4$ K used for calculating the LKS curve have been taken from measurements[232,271] performed at higher temperatures and lower fields, at which the dHvA signal is perfectly harmonic. Thus, the wave form of the magnetization oscillations appears to be fully consistent with that expected from a 2D metal with negligibly small oscillations of the chemical potential.

The reason for such a perfect stabilization of the chemical potential ζ in this highly 2D material is not quite clear at present. Of course, ζ may be pinned, to a certain extent, by the q1D electron reservoir associated with the open sheets of the FS that are predicted by the band structure calculations[270,271] (although no direct experimental evidences for the existence of such sheets have been reported as yet). The possible influence of the field-independent electron reservoir in this compound has been studied[232] in the framework of the numerical model proposed by Harrison et al.[165] (see section 3.3.3). The simulations have shown that the density of states of the reservoir band must be at least 5 times higher than that of the 2D band in order to account for the observed wave form. It is not clear whether one can expect such a high density of states on the open Fermi sheets. Besides, it was noted[275] that the numerical model[165] reproduces the experimental data less accurately than the LKS formula.

An incommensurate charge- or spin-density wave associated with the nesting of the open Fermi sheets was proposed by Nam et al.[274] as a possible reason for the stabilization of the chemical potential. A density wave was indeed predicted to play a stabilizing role for the chemical potential in a system combining a nested q1D and Landau-quantized q2D bands.[276] However, even though an incommensurate density wave can be more efficient than a commensurate one,[274] it must still have an infinitely high density of states in order to completely suppress oscillations of ζ. Furthermore, no clear evidence of a density wave has been found in the present compound thus far.

An alternative mechanism for stabilizing the chemical potential may be, in principle, the magnetostriction effect as noted by Champel and Mineev.[277] Indeed, if the low-temperature compressibility is dominated by the conduction electrons, the sample volume and, hence, the carrier concentration can change in a magnetic field so as to cancel the oscillations of the chemical potential.[278]

Another unsolved question concerning the dHvA effect in β''-(BEDT-TTF)$_2$SF$_5$CH$_2$CF$_2$SO$_3$ is the temperature dependence of the oscillation amplitude. As follows from the LKS model, this dependence must be described by the conventional LK temperature damping factor R_T (eq 64). However, the LK fit to the experimental data obtained at low temperature, $T = 0.4$ K, yields a field-dependent cyclotron mass value:[232] at $B < 12$ T the mass is equal to $1.9m_e$, agreeing with the higher temperature result, whereas a lower value of $1.6m_e$ is found to better fit the high-field (around $B = 20$ T) data. Moreover, the temperature dependence of the second and third harmonic amplitudes gives $\mu = 1.4$ and 1.0, respectively,[172] that is, considerably lower than what is determined from the fundamental harmonic. Such an apparently field- and harmonic-dependent cyclotron mass could be explained by the models involving an oscillating chemical potential. However, this would contradict the above conclusion, that $\zeta =$ constant, based on the wave form of the dHvA signal. Thus, further studies are necessary for developing a consistent quantitative description of the dHvA in this compound.

3.4.2. α-(BEDT-TTF)$_2$KHg(SCN)$_4$

This compound is a member of the isostructural family α-(BEDT-TTF)$_2$MHg(XCN)$_4$, where M = K, Tl, Rb, or NH_4 and X = S, Se. An example of the FS typical of these salts, combining the q2D cylinder and a pair of open q1D sheets, is shown in Figure 1d. Three of these compounds, with M = K, Tl, and Rb and with X = S, have been of particular interest over the past decade due to their highly unusual behavior under magnetic fields. Numerous anomalies displayed by these compounds are presently associated with the nesting instability of the q1D band resulting in a charge-density wave (CDW), characterized by a very low energy gap, and its interaction with the coexisting metallic q2D band. The basic properties of α-(BEDT-TTF)$_2$MHg(XCN)$_4$ are reviewed in refs 25, 26, and 47; for recent progress, see refs 279−281 and references therein. Here we will restrict ourselves to the high-field, low-temperature dHvA effect, illustrating the role of the two-dimensionality.

The high-field regime is defined by the so-called kink field B_k ($B_k \simeq 24$ T in our compound) at which the zero-field state CDW$_0$ is transformed into the CDW$_x$ state with a field-dependent wave vector (see, e.g., ref 280). The energy gap is strongly reduced in the CDW$_x$ state in comparison to that in the CDW$_0$, so that the cyclotron orbits on the cylindrical part of the FS are considered to be the same as in the normal metallic state.

The lower curve in Figure 29 taken from ref 165 represents the low-temperature magnetization in α-(BEDT-TTF)$_2$KHg(SCN)$_4$ obtained in the pulsed-field experiment.[231] The oscillation frequency, $F_\alpha \approx 670$ T, corresponds to the cyclotron orbit on the cylindrical part of the FS, in agreement with the band structure predictions. The rapid damping of the dHvA signal at fields below ≃24 T is associated with the kink transition. The strong oscillations observed in the high-field state are characterized by only a weakly asymmetric wave form. Nevertheless, the Fourier analysis[231] reveals a high harmonic content inconsistent with the 3D LK model. Moreover, the cyclotron mass estimated from the temperature dependence of the amplitude of the second harmonic

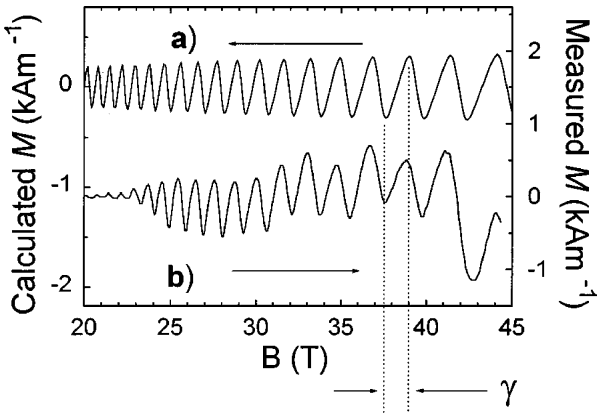

Figure 29. (a) Numerically calculated magnetization for the high-field state of α-(BEDT-TTF)$_2$KHg(SCN)$_2$ using the parameters μ, τ, and n_R determined experimentally.[165,231] (b) Corresponding measured magnetization. The arrows point to the appropriate axes. (Reproduced with permission from ref 165. Copyright 1996 American Physical Society.)

using eq 64 is almost two times lower than that obtained from the fundamental harmonic, thus indicating a strong violation of the conventional LK behavior. On the other hand, the wave form and the field dependence of the oscillation amplitude can be fairly well reproduced by the numerical model[165] using the parameters $\mu = 2.6$, $\tau = 5$ ps (i.e. $T_D = 0.24$ K), and $n_R = 0.4 \pm 0.2$. The calculated curve is shown in the upper part of Figure 29.

The presented data imply an appreciable effect of reservoir states attenuating oscillations of the chemical potential. At first sight, the role of the reservoir could be taken by the q1D band predicted by the band structure calculations. However, the q1D band should be at least partially closed by the CDW gap even in the high-field state. Alternatively, as mentioned in section 3.4.1, the chemical potential can be stabilized by the CDW itself. In the limit of a completely depinned incommensurate CDW, the latter would act in the same way as the normal metallic band.[279] In fact, there is a rather delicate interplay between the high-field CDW$_x$ state and the Landau quantization effect on the metallic q2D band reflected, for example, in a hysteretic behavior of the magnetization and anomalous features in oscillating magnetoresistance.[279] Nevertheless, the amplitude and the wave form of the dHvA oscillations appear to be well described by the above model in which the CDW plays the role of a reservoir damping the chemical potential oscillations.

Honold et al.[202] have reported on the observation of the MB frequency $F_\beta \approx 4250$ T in the dHvA spectrum obtained in pulsed fields of up to 60 T. This would correspond to the orbit involving both the cylindrical and planar parts of the FS. The situation resembles that with κ-(BEDT-TTF)$_2$Cu(NCS)$_2$ (see section 3.1.4), only the estimated MB field, $B_{MB} = (70 \pm 10)$ T, is much higher in the present case. Minor contributions from the combination frequencies, $F_\beta \pm F_\alpha$, have also been detected and attributed tentatively to the effect of the chemical potential oscillations in this highly 2D compound.[202] However, no details have been reported on these combination

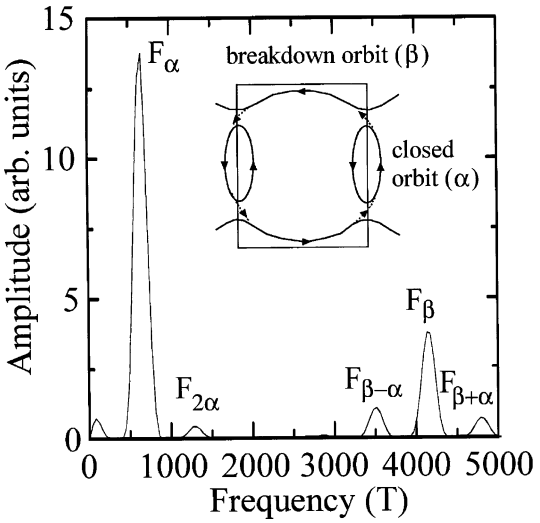

Figure 30. Fast Fourier transformation of the dHvA signal from κ-(BEDT-TTF)$_2$Cu(NCS)$_2$ measured at $T = 0.4$ K in the field range from 20 to 27 T. A prominent peak at the frequency $F_{\beta-\alpha} = F_\beta - F_\alpha$ is seen. (Reproduced with permission from ref 282. Copyright 1999 Elsevier Science-Direct.)

frequencies probably because of their very low amplitudes.

3.4.3. κ-(BEDT-TTF)$_2$Cu(NCS)$_2$

As discussed in section 3.1.4, κ-(BEDT-TTF)$_2$Cu(NCS)$_2$ displays a variety of features associated with the MB. Among them are the difference combination frequencies $F_\beta - nF_\alpha$ which are not allowed in the framework of the standard MB theory.[22,198−201] Figure 30 demonstrates an example of the Fourier spectrum of the dHvA oscillations in κ-(BEDT-TTF)$_2$Cu(NCS)$_2$ recorded at $T = 0.4$ K in the field window between 20 and 27 T.[282] The spectrum is dominated by the contributions from the classical orbit α and from the main MB orbit β. The peak at $F_\beta + F_\alpha$ can also be attributed to the MB orbit consisting of the MB β-loop plus classical α-loop. Besides, the peak at the "forbidden" frequency $F_\beta - F_\alpha$ even exceeding the one at $F_\beta + F_\alpha$ is present.

The straightforward fitting of the temperature-dependent amplitude of the "$\beta - \alpha$" oscillation by the LK damping factor (eq 64) yields the cyclotron mass parameter, $\mu_{\beta-\alpha} = 8.5$, which is heavier than the mass at the β-orbit, $\mu_\beta \approx 7$.[210,282] This is in notable contrast to the behavior of the difference frequency contribution in the oscillating magnetoresistance: in that case the relation $\mu_{\beta-n\alpha} \approx \mu_\beta - n\mu_\alpha$ was observed, in accordance with the QI scenario[211,212] (see eq 80 and the discussion in section 3.1.4). On the other hand, the temperature dependence of the magnetization oscillations with the combination frequencies seems to be consistent with the predictions for the dHvA effect in multiple-band 2D systems as presented in section 3.3.4. For example, the calculations carried out by Nakano[264] for two independent (i.e. not coupled via MB) 2D bands, α and β, predict that the amplitude of the $\beta - \alpha$ oscillations decreases, with increasing temperature, faster than those of the individual α and β oscillations. If, in analogy with the 3D LK formula, one characterizes the temperature depen-

dence of the amplitude by some "effective mass" m^* (which of course must not coincide with the real cyclotron mass in the 2D case), Nakano's calculations[264] yield m^*_β, $m^*_\alpha < m^*_{\beta\pm\alpha} < m^*_\beta + m^*_\alpha$. This result agrees with the experimental data reported by Uji et al.[210] and Steep et al.[282]

While the multiple-independent-band models[249−251,254,256−259] succeed in explaining the presence of the "forbidden" frequencies, one has to take into account the MB phenomenon in order to adequately describe the oscillations in κ-(BEDT-TTF)$_2$Cu(NCS)$_2$. The comparison between the models with and without the MB was performed by Kishigi et al.[254,257] In particular, it was argued that two independent mechanisms, namely, the MB and chemical potential oscillations, provide out-of-phase contributions to the $(\beta + \alpha)$-frequency that lead to a decrease of the amplitude with increasing the MB probability. At the same time, the $(\beta - \alpha)$-frequency is not explicitly affected by the MB. As a result, the amplitude of the $(\beta + \alpha)$ oscillations, dominating in the multiple-independent-band model, may become smaller than that of the "forbidden" frequency, $(\beta - \alpha)$, in the actual case of the MB network. This relationship between the two amplitudes is indeed found in the experiment.[282]

With increasing temperature, the oscillations of the chemical potential are rapidly suppressed, which causes the rapid decrease of the $(\beta - \alpha)$ amplitude. On the other hand, the MB mechanism is not sensitive to temperature; therefore, the temperature damping of the $(\beta + \alpha)$ oscillations should be considerably slower than that of the $(\beta - \alpha)$ oscillations.This explains the experimentally obtained relationship between the "effective masses": $m^*_{\beta+\alpha} < m^*_{\beta-\alpha}$.[210,282]

A further qualitative test of the validity of the above models can be made by studying the dependence of the oscillation amplitude on the field orientation. As was mentioned in section 3.1.3, the Zeeman spin-splitting effect leads to a periodic dependence of the amplitude on the tilt angle. By tuning the angle-dependent spin-splitting parameter, $g\mu(\theta) = g\mu(0)/\cos\theta$, to an odd integer value, $2n + 1$, one reaches the spin-zero condition for the fundamental harmonic (see eq 69). If, in our case, the field direction is set to a spin zero of one of the fundamental harmonics, F_α or F_β, the contribution of this harmonic to the chemical potential oscillations vanishes. This should lead to the disappearance of the "forbidden" $(\beta - \alpha)$-frequency. However, the $(\beta + \alpha)$-frequency should persist, being still contributed by the standard MB mechanism. Moreover, its amplitude may even become enhanced due to the absence of the out-of-phase contribution from the chemical potential oscillations. In the present compound, the spin zero for the harmonic F_β corresponds to the tilt angle $\theta \approx 34°$.[203,283] Indeed, at this orientation the "forbidden" frequencies $F_\beta - F_\alpha$ and $F_\beta - 2F_\alpha$ were found to vanish whereas the combination $F_\beta + F_\alpha$ persisted and probably even had a small local maximum.[283]

The contributions of the higher harmonics of the fundamental frequency F_α to the Fourier spectrum in Figure 30 are quite small: the height of the peak at $2F_\alpha$ is less than 5% of that at F_α; the third harmonic is even not resolved in the present scale. This, however, is not an argument for the validity of the 3D LK model. As shown by Itskovsky,[258] the presence of more than one Landau-quantized band leads to a suppression of the higher harmonics even in strongly 2D systems. In fact, one band in the multiple-band system plays the role of the electron reservoir for the other, thus damping the chemical potential oscillations, in a way similar to that discussed in section 3.3.3 for the case of coexisting 2D and q1D bands. Of course, now one has to take into account the Landau quantization of both bands.

The 2D character of the dHvA effect in the present compound is also reflected in the temperature dependence of the second harmonic amplitudes. Like it was for the two compounds described above, the "effective masses" derived from the LK analysis of the second harmonic amplitudes, $A_{2\alpha}$ and $A_{2\beta}$, are much lower than those found from the fundamental harmonics.[203,210,283] At fields above 24 T, the amplitude of the harmonic $A_{2\alpha}$ has even been found to decrease with decreasing temperature.[283] Such a behavior drastically contrasts the LK predictions but is consistent with the 2D models taking into account the chemical potential oscillations (see, e.g., ref 258).

It should be noted that besides the above-mentioned models there are a few other theories proposing the existence of the "forbidden" frequencies. Kim, Brooks, and co-workers[284−286] have suggested these frequencies to be a consequence of a nonlinear field dependence of the quantized magnetic subbands due to nonparabolicity of the realistic band structure. They argued[285] that the difference frequencies even persist (though become smaller) in the case of a fixed chemical potential. However, the field range used by those authors for the numerical simulations ($\geq$400 T for the present compound) is comparable to the quantum limit for at least one of the bands and by far exceeds the fields used in the described experiments.

Another explanation of the "forbidden" frequencies in κ-(BEDT-TTF)$_2$Cu(NCS)$_2$ has been proposed by Gvozdikov et al.,[287] who calculated the field-induced modification of the energy spectrum of a 2D system in a linear-chain MB network configuration like that shown in Figure 19. The width and positions of the Landau subbands originating from the main MB orbit β have been shown to oscillate with the frequency F_α, leading to the combination frequencies such as $F_\beta \pm F_\alpha$. As a physical reason, it is suggested that the small classical orbits α play the role of "switches" for the interconnected MB orbits β, acting in a way analogous to the Stark quantum interferometer. The model[287] was demonstrated to fit quite well to the dHvA oscillations observed in experiments at two temperatures, 1.3 and 0.4 K. A further, more systematic comparison between the theory and the experimentally obtained field and temperature dependence of different harmonics is highly desirable. In particular, it would be interesting to check the prediction of the model[287] about the existence of a weak field-dependent shift of the MB frequencies. Of course, it is possible that more than one of the

mentioned mechanisms are actually responsible for the "forbidden" frequencies observed in κ-(BEDT-TTF)$_2$Cu(NCS)$_2$.

3.5. SdH Effect in Layered Metals

The examples presented in section 3.2 indicate strong deviations of the SdH oscillations in organic conductors from the predictions of the standard 3D theory. Unfortunately, by contrast to the dHvA effect, a comprehensive theory of the SdH effect in q2D metals is still lacking. The main problem is that the quantum oscillations of magnetoresistance crucially depend on details of the charge transfer and scattering processes, whose nature in the organic conductors is far from being well understood. Nevertheless, a number of recent theoretical works[67,145,165,288−293] have provided a basis for at least a qualitative understanding of some prominent anomalies of the SdH oscillations observed in the experiment.

Here we will restrict our consideration to the magnetoresistance measured perpendicular to the highly conducting plane, which is the usual configuration in experiments on the layered organic conductors (see, e.g., section 2). Of course, to describe the metallic conductivity across the layers, one has to take into account the finite interlayer coupling. Therefore, we will introduce, as usual, the interlayer transfer integral $t_\perp$ and assume the electron spectrum in a high magnetic field to have the form

$$\epsilon(n,p_z) = \hbar\omega_c(n + 1/2) - 2t_\perp \cos(p_z d/\hbar) \quad (97)$$

We will consider two different cases characterized by different scales of the ratio between the interlayer bandwidth $W_\perp = 4t_\perp$ and the cyclotron energy $\hbar\omega_c$. First, the case of a relatively strong interlayer coupling, when the ratio $W_\perp/(\hbar\omega_c)$ is bigger (though not much bigger!) than unity, will be discussed. Then, the highly-2D limit, $W_\perp/(\hbar\omega_c) \ll 1$, will be briefly considered.

3.5.1. Relatively Strong Interlayer Coupling

Figure 31 shows an example of the oscillating interlayer resistance of β-(BEDT-TTF)$_2$IBr$_2$.[67] At the lowest temperature, rapid SdH oscillations, $F \simeq 3900$ T, of a rather small amplitude ($\sim$1% of the background resistance at $B \simeq 14$ T) are observed, basically resembling the behavior of the dHvA oscillations presented in section 3.1.1. In particular, one can see clear beats with the frequency $F_{beat} = \Delta F/2 \simeq 20$ T (where ΔF is defined by eq 58), in accordance with the significant warping of the FS: $\Delta S/S \simeq 10^{-2}$. In the given field range, the ratio between the interlayer bandwidth and the cyclotron energy, $W_\perp/(\hbar\omega_c) = \Delta F/B$, varies between approximately 6 and 3. Hence, the FS is intersected by several Landau levels at a fixed field. The dHvA effect is still quite well described by the 3D LK model under this condition. By contrast, the SdH effect already displays some distinct anomalies.

The most prominent anomaly is the slow oscillations which are clearly seen in Figure 31. The frequency of these oscillations, $F_{slow} \approx 42$ T, is about

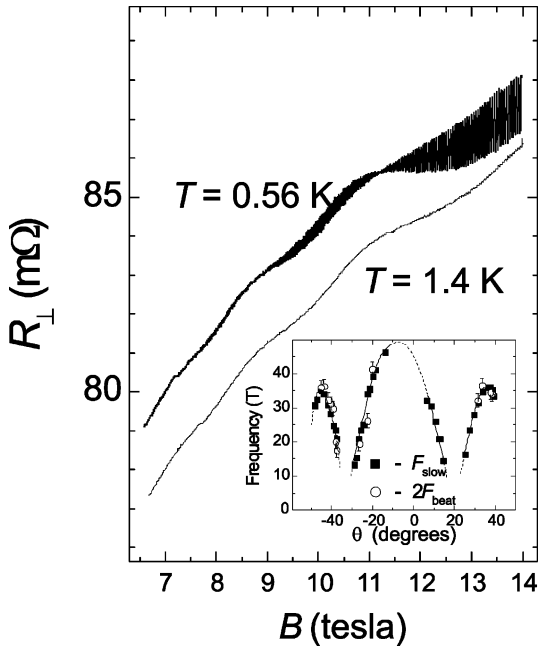

Figure 31. Interlayer resistance of β-(BEDT-TTF)$_2$IBr$_2$ as a function of magnetic field, at different temperatures.[67] The fundamental SdH oscillations exhibit beats and are superposed by slow oscillations. Inset: Angular dependence of the slow oscillation frequency[67] (solid squares) and of the doubled beat frequency, $2F_{beat} = \Delta F$ (open circles).

100 times smaller than the fundamental frequency. Their amplitude is virtually independent of temperature: it is almost the same at $T = 0.56$ and 1.4 K whereas the fundamental oscillations are greatly suppressed at 1.4 K.

While the existence of the slow oscillations in the present compound has been established already in the first works on the SdH effect,[24,38] their nature remained unsolved till very recently. No small FS pockets which could give rise to the low-frequency SdH oscillations have been revealed by the band structure calculations.[20,294,295] Similar slow oscillations of unclear origin have been reported for a number of other organic conductors, for example, β-(BEDT-TTF)$_2$I$_3$,[296,297] κ-(BEDT-TTF)$_2$Cu$_2$(CN)$_3$,[298] κ-(BETS)$_2$C(CN)$_3$,[299] and κ-(BETS)$_2$FeBr$_4$.[187,188]

A clue for solving the problem is given by the angular dependence of the frequency $F_{slow}(\theta)$ shown in the inset in Figure 31. By contrast to the fundamental frequency having the usual 1/cos θ dependence, the low frequency displays a highly nonmonotonic behavior which is practically identical to that of the beat frequency (see Figure 16b in section 3.1.1): it vanishes at the angles corresponding to the AMRO peaks.[67] Indeed, the comparison between the frequencies of the slow oscillations and of the beats given in the inset in Figure 31 reveals the relationship $F_{slow}(\theta) \approx 2F_{beat}(\theta)$. Thus, one can conclude that, like the beats of the rapid SdH oscillations, the slow oscillations originate from the warping of the FS cylinder.

The mechanism responsible for the slow oscillations can be clarified by analyzing the semiclassical Boltzmann transport equation for the conductivity:[67]

$$\sigma_{zz} = -e^2 \int \tau(\epsilon)\, I(\epsilon)\, \frac{\mathrm{d}f_0}{\mathrm{d}\epsilon}\, \mathrm{d}\epsilon \qquad (98)$$

where $I(\epsilon) = \sum|v_z(\epsilon)|^2$ is the square of the interlayer velocity summed over all states at the energy ϵ. The only difference of this expression from eq 3 used for calculating the classical conductivity consists of putting the relaxation time τ to the integrand, since its dependence on energy becomes essential due to the Landau quantization. As mentioned in section 3.1.2, the scattering probability and, hence, the scattering rate, $1/\tau$, are proportional to the density of states, which oscillates in magnetic field. On the other hand, in the q2D case, when the cyclotron energy is comparable to the interlayer transfer integral, oscillations of the interlayer velocity and therefore of the quantity $I(\epsilon)$ become important.[165,291] It is the interference between the two oscillating factors, $\tau(\epsilon)$ and $I(\epsilon)$, which gives rise to the slow oscillations.

This can be illustrated by the following simplified consideration. Keeping only the fundamental harmonic, one can express the oscillating factors as[234,300]

$$\tau(\epsilon) \propto 1 + \tilde{a}\, \cos\left(2\pi \frac{\epsilon}{\hbar\omega_c}\right) \qquad (99)$$

and[291]

$$I(\epsilon) \propto 1 - \tilde{b}\, \cos\left(2\pi \frac{\epsilon}{\hbar\omega_c}\right) \qquad (100)$$

where the amplitudes of the fundamental oscillations, $\tilde{a}$ and $\tilde{b}$, are slowly modulated due to the weak warping of the FS. In our case, when the ratio $W_\perp/(\hbar\omega_c)$ is bigger than unity, the amplitudes $\tilde{a}$ and $\tilde{b}$ are proportional to $\cos[(2\pi F_{beat}/B) - (\pi/4)]$ and to $\sin[(2\pi F_{beat}/B) - (\pi/4)]$, respectively. Then the product of τ and I is

$$\tau(\epsilon)\, I(\epsilon) \propto 1 + (\tilde{a} - \tilde{b})\, \cos\left(2\pi \frac{\epsilon}{\hbar\omega_c}\right) - \frac{\tilde{a}\tilde{b}}{2} \qquad (101)$$

Here we used the identity $\cos^2 x = (1 + \cos 2x)/2$ and neglected the second harmonic term (at the experimental conditions[67] it is eventually suppressed by the temperature and Dingle damping factors). The second term in eq 101 is responsible for the fundamental frequency of the SdH oscillations. It is the product $\tilde{a}\tilde{b}$ in the last term in eq 101 which gives the slow oscillations with the frequency $F_{slow} = 2F_{beat}$, in agreement with the experiment.

Since the product $\tilde{a}\tilde{b}$ does not contain the electron energy, its contribution to the conductivity (eq 98) is insensitive to the temperature smearing of the Fermi distribution function $f_0(\epsilon,T)$. Therefore, the amplitude of the slow oscillations is not suppressed by the temperature damping factor R_T, by contrast to the amplitude of the fundamental SdH harmonic. Indeed, as shown in Figure 31, the amplitude of the slow oscillations at $T = 1.4$ K is about the same as at 0.56 K whereas the fundamental harmonic has almost completely vanished at 1.4 K.

Further, the Dingle factor entering the amplitude of the slow oscillations is different from the Dingle factor of the fundamental harmonic. Since the slow oscillations are independent of the electron energy (hence, of the exact position of the chemical potential), the corresponding Dingle factor does not include the effects of macroscopic spatial inhomogeneities of the sample.[67,292] It was found[67] that the Dingle temperature extracted from the field dependence of the slow oscillation amplitude, $T_D^* \approx 0.15$ K, is about 5 times smaller than the conventional Dingle temperature T_D determined from the fundamental harmonic in β-(BEDT-TTF)$_2$IBr$_2$. This leads to the conclusion that macroscopic spatial inhomogeneities, such as internal strains or/and mosaic structures, play a dominant role in damping the fundamental quantum oscillations in the sample. By contrast, the semiclassical transport relaxation time τ_{tr} is mostly determined by pointlike scatterers and can be extracted from the slow oscillations: $\tau_{tr} \approx \hbar/(2\pi k_B T_D^*) \approx 8 \times 10^{-12}$ s. This estimate is, in fact, close to that obtained from the angular-dependent semiclassical magnetoresistance (see section 2.2.2).

Another important result of the interference between the oscillations of the relaxation time and interlayer velocity is a phase shift of the beats of the fundamental SdH oscillations. As seen from eq 101, the modulation of the fundamental amplitude is determined by the difference $(\tilde{a} - \tilde{b})$. The oscillations of $\tilde{a}$ and $\tilde{b}$ are of the same frequency but shifted by the phase factor $\simeq\pi/2$.[291] Consequently, the phase factor of the resulting beats should have an intermediate value, depending on the relative strength of the contributions from the oscillating relaxation time and velocity. The latter is determined by the ratio $\hbar\omega_c/t_\perp$.[291] The explicit solution of the Boltzmann transport equation (eq 98) yields the expression for the first harmonic in the interlayer conductivity in the form:[291]

$$\tilde{\sigma}_{zz}^{(1)} \propto \cos\left[2\pi\left(\frac{F}{B} - \frac{1}{2}\right)\right] \cos\left(2\pi\frac{\Delta F}{2B} - \frac{\pi}{4} + \phi\right) \qquad (102)$$

where

$$\phi = \arctan\left(\frac{\hbar\omega_c}{2\pi t_\perp}\right) = \arctan\left(\frac{\hbar e B}{2\pi m_c t_\perp}\right) \qquad (103)$$

Comparing this expression with eq 57 describing the beating dHvA oscillations, we see that the beats of the SdH oscillations are shifted by the phase, $0 < \phi < \pi/2$, which depends on the FS warping and on the magnetic field strength.

Figure 32 presents an example of the oscillating magnetization and magnetoresistance of β-(BEDT-TTF)$_2$IBr$_2$[291] (the slowly oscillating background has been subtracted from the magnetoresistance data). The beat nodes of the SdH oscillations are clearly shifted from those of the dHvA oscillations. It should be noted that similar and even larger shifts were observed on other layered compounds, κ-(BEDT-TTF)$_2$Cu[N(CN)$_2$]Br[221] and (BEDT-TTF)$_4$[Ni(dto)$_2$].[301] For the latter salt, a phase shift as large as $\pi/2$ was reported. Certainly, so large a shift and, in particular, its dependence on magnetic field must be taken into account when one attempts to evaluate the FS warping from the beating behavior.

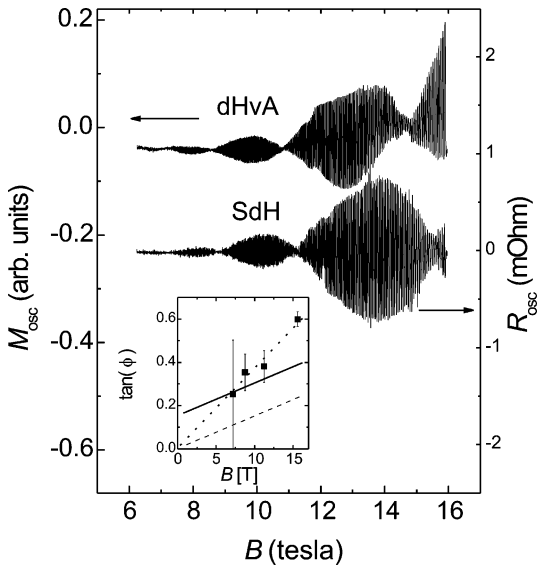

Figure 32. Oscillating magnetization (left scale) and interlayer magnetoresistance (right scale) of β-(BEDT-TTF)$_2$IBr$_2$ at $T = 0.4$ K and $\theta \approx 14.8°$. Data from ref 291. Inset: Tangent of the phase shift between the node positions in the SdH and dHvA signals as a function of magnetic field.[291] The dotted line is the linear fit to the data. The dashed and solid lines represent the expected field dependence obtained with the semiclassical transport equation[291] and with the quantum mechanical Kubo formula,[292] respectively.

The inset in Figure 32 shows that the phase shift increases with increasing the field, as would be expected from eq 103. The slope of the linear fit to the data (dotted line) gives, according to eq 103, the interlayer transfer integral: $t_\perp \simeq 0.12$ meV. This is, however, more than 2 times lower than the estimation based on the beat frequency, $t_\perp = e\hbar F_{beat}/(2m_c) \simeq 0.28$ meV. The substitution of the latter value into eq 103 leads to the dashed line in Figure 32, which lies considerably below the experimental points.

The discrepancy has been partially eliminated by the quantum mechanical calculations[292] based on the Kubo formula. This technique yields an additional, quantum correction to the oscillating conductivity which leads to an increase of the argument of arctan in eq 103 by a constant value depending on the ratio between $t_\perp$ and the Dingle temperature. With this correction, the theoretical phase shift, represented by the solid line in the inset to Figure 32, is in reasonable agreement with the data at fields around 10 T. However, it is still too low, comparing to the experiment at higher fields.

The theory[291,292] predicts the phase shift to increase toward the maximum value of $\pi/2$ with decreasing the interlayer transfer integral. The latter can be effectively diminished by setting the field orientation to an AMRO maximum.[41,46] Indeed, an increase of the phase shift was experimentally observed at changing the field direction toward an AMRO peak in β-(BEDT-TTF)$_2$IBr$_2$.[73] However, the value ϕ was found to strongly exceed the theoretical maximum of $\pi/2$.

The presented results illustrate that, by contrast to the dHvA effect, the SdH effect exhibits substantial deviations from the conventional 3D behavior even

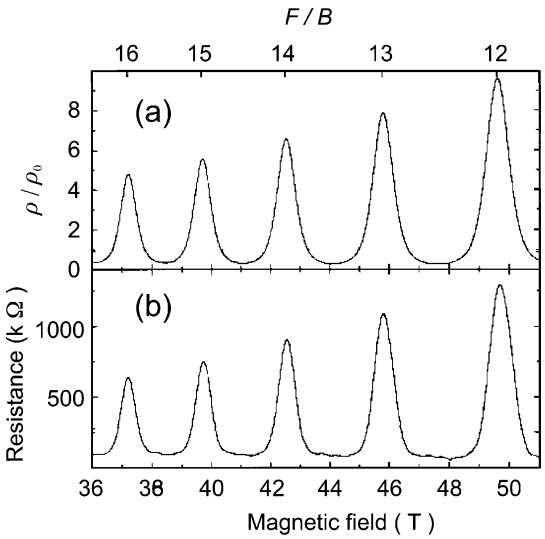

Figure 33. (a) Numerical simulations[165] of the SdH oscillations in α-(BEDT-TTF)$_2$NH$_4$Hg(SCN)$_2$ at $T = 0.4$ K based on the Boltzmann transport equation with the parameters $F = 595$ T, $m_c = 3m_e$, $\tau = 1.2 \times 10^{-12}$ s, $n_R = 0.4$. (b) SdH effect in the interlayer resistance of the same compound measured[229] at $T = 0.4$ K. Note that the resistance peaks at integer filling factors $F/B = \epsilon_F/\hbar\omega_c = n$.

at a relatively strong interlayer coupling, when $W_\perp/(\hbar\omega_c) > 1$. In particular, slow oscillations arise as a result of the interference between the oscillations of the relaxation time and of the interlayer velocity. These slow oscillations are not affected by the temperature smearing of the Fermi edge and by spatial variations of the chemical potential caused by the sample inhomogeneity. As a result, they survive at higher temperatures and lower fields, at which the main SdH oscillations are completely suppressed.

Incidentally, besides the FS warping, any other mechanism leading to a modulation of the amplitude of the fundamental SdH harmonic is expected to give rise to the slow oscillations due to the same interference effect. For example, the slow oscillations observed in κ-(BETS)$_2$FeBr$_4$[187,188] are most likely caused by the field-dependent spin-splitting effect, leading to a modulation of the main SdH oscillations as discussed in section 3.1.3.

The existing theoretical models[67,291,292] successfully describe the new features, at least, on the qualitative level. However, quantitative disagreements arise as the ratio $W_\perp/(\hbar\omega_c)$ decreases, approaching unity.

3.5.2. Highly Two-Dimensional Limit

Despite the considerable amount of experimental data on the SdH effect in the strongly 2D limit, $W_\perp \ll \hbar\omega_c$ (see section 3.2), only few attempts at their theoretical description have been done so far. Here we will present two examples of the comparison between the experimentally observed SdH oscillations in highly 2D organic conductors and the existing models.

The lower panel of Figure 33 shows the oscillatory magnetoresistance in α-(BEDT-TTF)$_2$NH$_4$(SCN)$_4$ measured at $T = 0.4$ K by Sandhu et al.[229] This compound is isostructural to the discussed above α-(BEDT-TTF)$_2$KHg(SCN)$_4$ salt and presents the same FS

topology: a cylindrical FS plus a pair of open sheets (Figure 1d). By contrast to the latter, it does not undergo the density-wave transition, so that its FS remains unchanged at all temperatures. The SdH oscillations originate from the FS cylinder occupying ≈14% of the Brillouin zone. No beats have been observed down to at least 6 T.[25,302] Thus, the warping of the FS is smaller than the spacing between the Landau tubes above 6 T. The field range of Figure 33, therefore, corresponds to the highly 2D limit. Indeed, the oscillations here are characterized by a very high amplitude and a strongly unharmonic wave form.

To model these oscillations, Harrison et al.[165] have performed a numerical simulation based on the Boltzmann transport equation. Oscillations of the chemical potential in the presence of the electron reservoir provided by the nonquantized q1D band were taken into account in the way described in section 3.3.3. The results are shown in the upper panel of Figure 33. One can see that, in agreement with the experiment, the magnetoresistance exhibits sharp peaks at integer filling numbers, $\epsilon_F/(\hbar\omega_c) = n$, that is, when the chemical potential is situated in the middle between the Landau levels. The amplitude of the oscillations and its field dependence are also quite well reproduced by the calculations. Moreover, the model[165] successfully describes the experimentally observed (see Figure 24, section 3.2) dramatic increase of the apparent cyclotron mass with increasing the field.

One can notice, however, that the calculated curve has a considerably more rounded shape near the minima of the magnetoresistance. Furthermore, the reservoir strength used for the calculations, $n_R = D^{1D}/D_0^{2D} = 0.4$, is significantly lower than the value obtained more recently from the dHvA data,[303] $n_R \approx 2.0$. As discussed in section 3.3.3, the reservoir states play an important role in stabilizing the chemical potential and thus strongly affect the wave form of the quantum oscillations. A substitution of the higher n_R in the model[165] would lead to a further broadening of the resistance peaks and, hence, to a stronger disagreement with the experiment.

To achieve a better agreement, one should likely apply the quantum transport theory instead of the semiclassical Boltzmann equation. The quantum correction to the conductivity was argued[292] to be significant already in the case of a relatively strong interlayer coupling. In the highly 2D limit it becomes even more important, as will be demonstrated in the following example.

Figure 34 shows the interlayer magnetoresistance of β''-(BEDT-TTF)$_2$SF$_5$CH$_2$CF$_2$SO$_3$ measured[274] as a function of magnetic field at different temperatures ranging from 4.0 K down to 0.59 K. The SdH oscillations here definitely correspond to the highly 2D regime. Indeed, the interlayer bandwidth $W_\perp$ in this compound is estimated[150] to be lower than 10^{-2} meV. This is much smaller than the Landau level separation in fields above 20 T ($\hbar\omega_c \approx 1.2$ meV at $B = 20$ T). Furthermore, the scattering induced broadening of Landau levels, $\hbar/\tau = 0.44$ meV,[274] strongly exceeds the interlayer bandwidth, making the influence of the latter on the shape of the levels negligible. As a result, the oscillations of the interlayer conductivity are entirely governed by the quantized motion within the 2D plane;[165,293] the interlayer coupling only determines the zero-field conductivity $\sigma_{zz}(B = 0)$, which is simply a constant scaling factor for $\sigma_{zz}(B) = 1/\rho_{zz}(B)$.

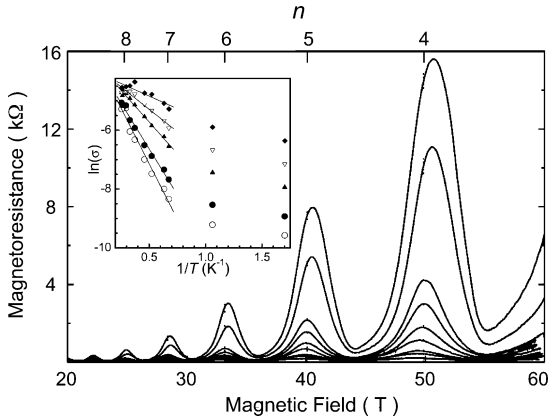

Figure 34. Strong SdH effect in the interlayer resistance of β''-(BEDT-TTF)$_2$SF$_5$CH$_2$CF$_2$SO$_3$ measured at the following temperatures, from the top: 0.59, 0.94, 1.48, 1.58, 1.91, 2.18, 2.68, 3.03, 3.38, 3.80, and 4.00 K. Inset: Logarithmic plot of the conductivity against inverse temperature at the magnetoresistance peaks close to the following integer filling numbers n, from the bottom: $n = 4$, 5, 6, 7, and 8. The data reveal the activation behavior (eq 104) at temperatures between 1.4 and 4.0 K. Data from ref 274.

The oscillations shown in Figure 34 are characterized by a very high amplitude rapidly growing with the field. Remarkably, the resistance at the maxima of the oscillations increases exponentially with decreasing the temperature. The inset in Figure 34 shows $\ln(\sigma_{zz}) = -\ln(\rho_{zz})$ at these points versus $1/T$. The data are well described by the thermal activation law[274]

$$\sigma_{zz} \propto \exp\left(-\frac{\Delta}{k_B T}\right) \qquad (104)$$

at temperatures between 1.4 and 4.0 K.

The activation behavior has been initially attributed to a gap in the density of states developing due to the Landau quantization in this highly 2D material. This interpretation, however, has not been supported by quantitative arguments. A more rigorous analysis has been done by Champel and Mineev,[277,293] who performed the quantum mechanical calculation of the oscillating interlayer conductivity in a q2D metal at $W_\perp \ll \hbar\omega_c$. They have shown that the conductivity can be expressed as

$$\sigma_{zz} = \int [\sigma_B(\epsilon) + \sigma_Q(\epsilon)]\left(-\frac{df_0(\epsilon)}{d\epsilon}\right) d\epsilon \qquad (105)$$

where $\sigma_B(\epsilon)$ and $\sigma_Q(\epsilon)$ are respectively the semiclassical (Boltzmann) and purely quantum contributions to the total spectral conductivity $\sigma(\epsilon)$. At a relatively strong warping of the FS, $W_\perp > \hbar\omega_c$, or in the dirty limit, $\omega_c\tau < 1$, when the broadening of Landau levels is bigger than the distance between adjacent levels, the quantum term σ_Q gives a negligibly small cor-

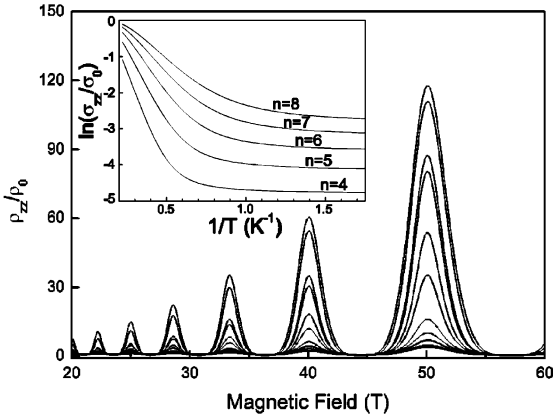

Figure 35. Theoretical simulations of the data in Figure 34 based on the quantum mechanical model. (Reproduced with permission from ref 293. Copyright 2002 American Physical Society.)

rection. The weak SdH oscillations can be quite well described by the semiclassical equation (eq 98). In particular, the simple relation between the SdH and dHvA oscillations, $\tilde{\sigma}_{zz} \propto B^2(\mathrm{d}\tilde{M}/\mathrm{d}B)$, like in the conventional 3D case, remains valid. However, when $\omega_c\tau > \pi$, both the Boltzmann and the quantum contributions are of the same order of magnitude.[293]

Figure 35 shows the SdH oscillations of the interlayer resistivity calculated on the basis of the model[293] with the substitution of the experimentally determined parameters: $F = 200$ T, $m_c = 1.96m_e$, $\tau = 1.2 \times 10^{-12}$ s, characteristic of the sample measured in ref 274. The theoretical temperature dependence at the resistivity peaks shown in the inset is in excellent agreement with the experimental data. To explain this behavior, it was noted[277,293] that, at the fields above 20 T, the clean limit, $\omega_c\tau > \pi$, is realized for this compound and a *pseudogap* develops in the spectral conductivity: the quantum term σ_Q almost exactly cancels the semiclassical term σ_B at energies around $\epsilon = n\hbar\omega_c$. This leads to a dramatic increase of the resistivity at the fields at which the chemical potential resides between the Landau levels, that is, in the vicinity of the integer fillings, $\epsilon_F/(\hbar\omega_c) = n$. At a finite temperature, the main contribution to the conductivity at such fields comes from the thermal excitation of quasiparticles at the edge of the pseudogap. At very low temperatures the small difference between $|\sigma_B|$ and $|\sigma_Q|$ is manifested in the saturation of the conductivity.

The calculations leading to the curves in Figure 35 have been made with the assumption of negligibly small chemical potential oscillations. This assumption is justified by the analysis of the dHvA oscillations,[232,275] as discussed in section 3.4.1. It should be noted that the model[293] gives reasonable results only under the condition of a finite electron reservoir, $n_R > 0$, which serves to stabilize the chemical potential ζ between Landau levels. In the absence of a reservoir, that is, when ζ is always pinned to the highest occupied Landau level, the theory fails to correctly describe the field-dependent density of states. The reason, as pointed out by the authors,[293] is that the model restricts the consideration of the scattering processes to those on pointlike scatterers only. It is possible that some disagreements between the theory and experiment (e.g., in the low-temperature behavior of the resistivity minima) are caused by this limitation. To develop a consistent theory taking into account specific contributions of the finite-range scattering in the material is a very difficult task and remains a challenging problem for future work.

4. Conclusion

This review is focused on the high-magnetic-field properties in the normal metallic state of layered organic conductors, avoiding complications related to various unusual electronic states. In particular, we did not touch the very interesting problem of phase transitions in a magnetic field, for example, the well-known field-induced SDW transitions[1,76] or recently observed field-induced CDW transitions.[280,304] Nevertheless, even in the normal metallic state these materials exhibit highly unusual behavior qualitatively different from that of conventional metals.

The key property underlying this behavior is the extremely high anisotropy of the electronic system. Relatively simple FS topologies in conjunction with typically very high crystal quality make the organic conductors ideal model objects for studying general physical phenomena characteristic of low-dimensional systems. In principle, the high-field effects presented here should also be observable in other types of q2D conductors such as, for example, superconducting and magnetic metal oxides, provided the sample quality is high enough. As mentioned at the end of section 2.2.1, the AMRO effect has already been found in a number of inorganic q2D materials.

The new phenomena introduced in this article prove high-magnetic-field experiments to be an exceptionally powerful tool in studying the FSs of the organic conductors.

The various oscillatory effects displayed by the semiclassical magnetoresistance, as the field is rotated with respect to the crystal axes, provide a direct means of precise determination of the size and shape of the FS. The warping of the FS in the least conducting direction determined by the interlayer transfer integral can be estimated from the magnetoresistance behavior at fields slightly tilting out of the highly conducting plane. Additionally to the dc magnetotransport, high-frequency (millimeter-wave) electrodynamics in high magnetic fields turns out to be very useful in studying the shape of the FS and other electronic parameters, such as cyclotron mass and Fermi velocity.

The peak feature observed in the angle-dependent dc magnetoresistance appears to be a good test for the coherence of the interlayer charge transport. It should be noted, however, that the behavior of the q2D conductors in the incoherent regime is not fully understood at present. It is possible that this behavior has a common nature with that observed on q1D conductors and associated[77] with field-induced deviations from the Fermi liquid model.

The magnetic quantum oscillations provide important complementary information on the electronic system in the organic conductors. The amplitude of the oscillations is generally strongly enhanced as

compared to 3D metals, making them easier to observe in the experiment. One should, however, take care when applying the standard 3D theory for analyzing the data. When the Landau level separation becomes comparable with or exceeds the interlayer bandwidth, the oscillations may significantly violate the conventional behavior and the low-dimensional nature of the conduction electrons should be explicitly taken into account. The theoretical models developed for 2D and q2D metals provide a consistent picture of the dHvA effect which, in principle, can be used for a quantitative analysis of the magnetization oscillations in layered organic metals. By contrast, the theoretical description of the q2D SdH effect has not yet been as successful. The reason is that the quantum oscillations of magnetoresistance crucially depend on details of the charge transfer and scattering processes, whose nature in the organic conductors is far from being well studied. Nevertheless, considerable progress has been recently achieved in at least the qualitative understanding of some remarkable anomalies of the SdH effect displayed by these materials.

5. Acknowledgment

I am very grateful to D. Andres and W. Biberacher for their helpful comments and assistance in the preparation of the manuscript. I greatly appreciate numerous illuminating discussions with P. Grigoriev, A. Lebed, V. Peschansky, I. Vagner, S. Pesotskii, V. Gvozdikov, E. Canadell, T. Champel, B. S. Chandrasekhar, and D. Einzel.

6. References

(1) Ishiguro, T.; Yamaji, K.; Saito, G. *Organic Superconductors*, 2nd ed.; Springer-Verlag: Berlin Heidelberg, 1998.
(2) Grant, P. M. *J. Phys. (Paris)* **1983**, *44*, C3−847.
(3) Kartsovnik, M. V.; Laukhin, V. N.; Pesotskii, S. I.; Schegolev, I. F.; Yakovenko, V. M. *J. Phys. I* **1992**, *2*, 89.
(4) Rousseau, R.; Gener, M.; Canadell, E. *Adv. Funct. Mater.* **2004**, *14*, 201.
(5) Oshima, K.; Mori, T.; Inokuchi, H.; Urayama, H.; Yamochi, H.; Saito, G. *Phys. Rev. B* **1988**, *38*, 938.
(6) Rousseau, R.; Doublet, M.-L.; Canadell, E.; Shibaeva, R. P.; Khasanov, S. S.; Rozenberg, L. P.; Kushch, N. D.; Yagubskii, E. B. *J. Phys. I* **1996**, *6*, 1527.
(7) Khasanov, S. S.; Narymbetov, B. Z.; Zorina, L. V.; Rozenberg, L. P.; Shibaeva, R. P.; Kushch, N. D.; Yagubskii, E. B.; Rousseau, R.; Canadell, E. *Eur. Phys. J. B* **1998**, *1*, 419.
(8) Jérome, D. *Science* **1991**, *252*, 1509.
(9) Bourbonnais, C.; Jérome, D. In *Advances in Synthetic Metals: Twenty Years of Progress in Science and Technology*; Bernier, P., Lefrant, S., Bidan, G., Eds.; Elsevier: Amsterdam, The Netherlands, 1999; p 206.
(10) Bourbonnais, C.; Jérome, D. *Chem. Rev.* **2004**, *104*, 5565.
(11) Kanoda, K. *Hyperfine Interact.* **1997**, *104*, 235.
(12) McKenzie, R. H. *Science* **1997**, *278*, 820.
(13) Limelette, P.; Wzietek, P.; Florens, S.; Georges, A.; Costi, T. A.; Pasquier, C.; Jérome, D.; Mézière, C.; Batail, P. *Phys. Rev. Lett.* **2003**, *91*, 016401.
(14) Uji, S.; Shinagawa, H.; Terashima, T.; Yakabe, T.; Terai, Y.; Tokumoto, M.; Kobayashi, A.; Tanaka, H.; Kobayashi, H. *Nature* **2001**, *410*, 908.
(15) Uji, S.; Terashima, T.; Terakura, C.; Yakabe, T.; Terai, Y.; Yasuzuka, S.; Imanaka, Y.; Tokumoto, M.; Kobayashi, A.; Sakai, F.; Tanaka, H.; Kobayashi, H.; Balicas, L.; Brooks, J. S. *J. Phys. Soc. Jpn.* **2003**, *72*, 369.
(16) Kobayashi, H.; Cui, H.; Kobayashi, A. *Chem. Rev.* **2004**, *104*, 5265.
(17) Mori, T.; Mori, H.; Tanaka, S. *Bull. Chem. Soc. Jpn.* **1999**, *72*, 179.
(18) Mori, T. *Chem. Rev.* **2004**, *104*, 4947.
(19) Rovira, C.; Novoa, J. J.; Mozos, J. L.; Ordejon, P.; Canadell, E. *Phys. Rev. B* **2002**, *65*, 081104.
(20) Lee, Y. J.; Nieminen, R. M.; Ordejon, P.; Canadell, E. *Phys. Rev. B* **2003**, *67*, 180505(R).
(21) Cracknell, A. P.; Wong, K. C. *The Fermi Surface*; Oxford University Press: London, 1973.
(22) Schoenberg, D. *Magnetic Oscillations in Metals*; Cambridge University Press: Cambridge, 1984.
(23) Pippard, A. B. *Magnetoresistance in Metals*; Cambridge University Press: Cambridge, 1989.
(24) Kartsovnik, M. V.; Laukhin, V. N.; Nizhankovskii, V. I.; Ignat'ev, A. A. *JETP Lett.* **1988**, *47*, 363.
(25) Wosnitza, J. *Fermi Surfaces of Low-Dimensional Organic Metals and Superconductors*; Springer-Verlag: Berlin Heidelberg, 1996.
(26) Singleton, J. *Rep. Prog. Phys.* **2000**, *63*, 1111.
(27) Lifshitz, I. M.; Azbel, M. Y.; Kaganov, M. I. *Electron Theory of Metals*; Consultants Bureau: New York, 1973.
(28) Abrikosov, A. A. *Fundamentals of the Theory of Metals*; Elsevier Science Publishers B.V.: Amsterdam, 1988.
(29) Ziman, J. M. *Principles of the Theory of Solids*, 2nd ed.; Cambridge University Press: Cambridge, 1972.
(30) Ziman, J. M. *Electrons and phonons: The Theory of Transport Phenomena in Solids*; Oxford University Press: London, 2001.
(31) Ashcroft, N. W.; Mermin, N. D. *Solid State Physics*; Saunders College: Philadelphia, PA, 1976.
(32) Lifshitz, I. M.; Azbel, M. Y.; Kaganov, M. I. *Sov. Phys. JETP* **1957**, *4*, 41.
(33) Lifshitz, I. M.; Peschansky, V. G. *Sov. Phys. JETP* **1959**, *8*, 875.
(34) Williams, J. M.; Ferraro, J. R.; Thorn, R. J.; Carlson, K. D.; Geiser, U.; Wang, H. H.; Kini, A. M.; Whangbo, M.-H. *Organic Superconductors (Including Fullerenes): Synthesis, Structure, Properties, and Theory*; Inorganic and Organometallic Chemistry Series; Prentice Hall: Englewood Cliffs, NJ, 1992.
(35) Mori, T. *Bull. Chem. Soc. Jpn.* **1999**, *72*, 2011.
(36) Buravov, L. I. *Technol. Phys.* **1994**, *39*, 743.
(37) Buravov, L. I.; Kushch, N. D.; Laukhin, V. N.; Khomenko, A. G.; Yagubskii, E. B.; Kartsovnik, M. V.; Kovalev, A. E.; Rozenberg, L. P.; Shibaeva, R. P.; Tanatar, M. A.; Yefanov, V. S.; Dyakin, V. V.; Bondarenko, V. A. *J. Phys. I* **1994**, *4*, 441.
(38) Kartsovnik, M. V.; Kononovich, P. A.; Laukhin, V. N.; Schegolev, I. F. *JETP Lett.* **1988**, *48*, 541.
(39) Kajita, K.; Nishio, Y.; Takahashi, T.; Sasaki, W.; Kato, R.; Kobayashi, H.; Kobayashi, A.; Iye, Y. *Solid State Commun.* **1989**, *70*, 1189.
(40) Kartsovnik, M. V.; Kononovich, P. A.; Laukhin, V. N.; Pesotskii, S. I.; Schegolev, I. F. *Sov. Phys. JETP* **1990**, *70*, 735.
(41) Yamaji, K. *J. Phys. Soc. Jpn.* **1989**, *58*, 1520.
(42) Yagi, R.; Iye, Y.; Osada, T.; Kagoshima, S. *J. Phys. Soc. Jpn.* **1990**, *59*, 3069.
(43) Peschansky, V. G.; Lopes, J. A. R.; Yao, T. G. *J. Phys. I* **1991**, *1*, 1469.
(44) Nam, M. S.; Blundell, S. J.; Ardavan, A.; Symington, J. A.; Singleton, J. *J. Phys.: Condens. Matter* **2001**, *13*, 2271.
(45) House, A. A.; Harrison, N.; Blundell, S. J.; Deckers, I.; Singleton, J.; Herlach, F.; Hayes, W.; Perenboom, J. A. A. J.; Kurmoo, M.; Day, P. *Phys. Rev. B* **1996**, *53*, 9127.
(46) Kurihara, Y. *J. Phys. Soc. Jpn.* **1992**, *61*, 975.
(47) Kartsovnik, M. V.; Laukhin, V. N. *J. Phys. I* **1996**, *6*, 1753.
(48) Shimojo, Y.; Trun, T.; Tanatar, M. A.; Ishiguro, T.; Toita, T.; Yamada, J. *Synth. Met.* **2003**, *137*, 1169.
(49) Choi, E. S.; Jobilong, E.; Wade, A.; Goetz, E.; Brooks, J. S.; Yamada, J.; Mizutani, T.; Kinoshita, T.; Tokumoto, M. *Phys. Rev. B* **2003**, *67*, 174511.
(50) Uji, S.; Terashima, T.; Yasuzuka, S.; Yamaura, J.; Yamamoto, H. M.; Kato, R. *Phys. Rev. B* **2003**, *68*, 064420.
(51) Kang, W.; Chung, O. H.; Jo, Y. J.; Kang, H.; Seo, I. S. *Phys. Rev. B* **2003**, *68*, 073101.
(52) Kato, K.; Oshima, K.; Kambe, T.; Nogami, Y.; Sasaki, T.; Motokawa, M.; Kato, R. *Synth. Met.* **2003**, *135−136*, 577.
(53) Hussey, N. E.; Abdel-Jawad, M.; Carrington, A.; Mackenzie, A. P.; Balicas, L. *Nature* **2003**, *425*, 814.
(54) Ohmichi, E.; Adachi, H.; Mori, Y.; Maeno, Y.; Ishiguro, T.; Oguchi, T. *Phys. Rev. B* **1999**, *59*, 7263.
(55) Yoshida, Y.; Mukai, A.; Settai, R.; Miyake, K.; Inada, Y.; Onuki, Y.; Betsuyaki, K.; Harima, H.; Tatsuma, T. D.; Aoki, Y.; Sato, H. *J. Phys. Soc. Jpn.* **1999**, *68*, 3041.
(56) Bergemann, C.; Mackenzie, A. P.; Julian, S. R.; Forsythe, D.; Ohmichi, E. *Adv. Phys.* **2003**, *52*, 639.
(57) Iye, Y.; Baxendale, M.; Mordkovich, V. Z. *J. Phys. Soc. Jpn.* **1994**, *63*, 1643.
(58) Baxendale, M.; Mordkovich, V. Z.; Yoshimura, S. *Solid State Commun.* **1998**, *107*, 165.
(59) Yagi, R.; Iye, Y.; Hashimoto, Y.; Odagiri, T.; Noguchi, H.; Sasaki, H.; Ikoma, T. *J. Phys. Soc. Jpn.* **1990**, *60*, 3784.
(60) Peschansky, V. G. *Low Temp. Phys.* **1997**, *23*, 35.
(61) Wosnitza, J.; Crabtree, G. W.; Williams, J. M.; Wang, H. H.; Carlson, K. D.; Geiser, U. *Synth. Met.* **1993**, *55−57*, 2891.
(62) Hanasaki, N.; Kagoshima, S.; Hasegawa, T.; Osada, T.; Miura, N. *Phys. Rev. B* **1998**, *57*, 1336.
(63) Laukhin, V. N.; Kostyuchenko, E. E.; Sushko, Y. V.; Shchegolev, I. F.; Yagubskii, E. B. *Sov. Phys. JETP Lett.* **1985**, *41*, 81.

(64) Schultz, A. J.; Wang, H. H.; Williams, J. M.; Filhol, A. *Physica B* **1986**, *143*, 354.
(65) Kang, W.; Montambaux, G.; Cooper, J. R.; Jérome, D.; Batail, P.; Lenoir, C. *Phys. Rev. Lett.* **1989**, *62*, 2559.
(66) Hanasaki, N.; Kagoshima, S.; Hasegawa, T.; Osada, T.; Miura, N. *Phys. Rev. B* **1999**, *60*, 11210.
(67) Kartsovnik, M. V.; Grigoriev, P. D.; Biberacher, W.; Kushch, N. D.; Wyder, P. *Phys. Rev. Lett.* **2002**, *89*, 126802.
(68) Peschansky, V. G.; Kartsovnik, M. V. *Phys. Rev. B* **1999**, *60*, 11207.
(69) Peschansky, V. G. *JETP* **1997**, *85*, 337.
(70) Wosnitza, J.; Goll, G.; Beckmann, D.; Wanka, S.; Schweitzer, D.; Strunz, W. *J. Phys. I* **1996**, *6*, 1597.
(71) Ohmichi, E.; Ito, H.; Ishiguro, T.; Komatsu, T.; Saito, G. *J. Phys. Soc. Jpn.* **1997**, *66*, 310.
(72) Kartsovnik, M. V. In *Molecular Molecular Low-Dimensional and Nanostructured Materials for Advanced Applications*; Graja, A., Bulka, B. R., Kajzar, F., Eds.; Kluwer Academic Publishers: Dordrecht, The Netherlands, 2002; p 159.
(73) Kartsovnik, M.; Grigoriev, P.; Biberacher, W.; Gröger, A.; Andres, D.; Pesotskii, S.; Kushch, N. *Synth. Met.* **2003**, *133*−*134*, 111.
(74) Lebed, A. G.; Bagmet, N. N. *Phys. Rev. B* **1997**, *55*, R8654.
(75) Schofield, A. J.; Cooper, J. R. *Phys. Rev. B* **2000**, *62*, 10779.
(76) Chaikin, P. M. *J. Phys. I* **1996**, *6*, 1875.
(77) Clarke, D. G.; Strong, S. P.; Chaikin, P. M.; Chashechkina, E. I. *Science* **1998**, *279*, 2071.
(78) Lee, I. J.; Brown, S. E.; Clark, W. G.; Strouse, M. J.; Naughton, M. J.; Kang, W.; Chaikin, P. M. *Phys. Rev. Lett.* **2002**, *88*, 017004.
(79) Lebed, A. G. *JETP Lett.* **1986**, *43*, 174.
(80) Naughton, M. J.; Chung, O. H.; Chiang, L. Y.; Brooks, J. S. *Mater. Res. Soc. Symp. Proc.* **1990**, *173*, 257.
(81) Naughton, M. J.; Chung, O. H.; Chaparala, M.; Bu, X.; Coppens, P. *Phys. Rev. Lett.* **1991**, *67*, 3712.
(82) Osada, T.; Kawasumi, A.; Kagoshima, S.; Miura, N.; Saito, G. *Phys. Rev. Lett.* **1991**, *66*, 1525.
(83) Kang, W.; Hannahs, S. T.; Chaikin, P. M. *Phys. Rev. Lett.* **1992**, *69*, 2827.
(84) Chashechkina, E. I.; Chaikin, P. M. *Phys. Rev. Lett.* **1998**, *80*, 2181.
(85) Lee, I. J.; Naughton, M. J. *Phys. Rev. B* **1998**, *58*, R13343.
(86) Kang, H.; Jo, Y. J.; Uji, S.; Kang, W. *Phys. Rev. B* **2003**, *68*, 132508.
(87) Biškup, N.; Brooks, J. S.; Kato, R.; Oshima, K. *Phys. Rev. B* **2000**, *62*, 21.
(88) Shimojo, Y.; Tanatar, M. A.; Ishiguro, T.; Kato, R. *J. Phys. Soc. Jpn.* **2002**, *71*, 393.
(89) Yasuzuka, S.; Terakura, C.; Yakabe, T.; Terai, Y.; Yamamoto, H. M.; Kato, R.; Uji, S. *Synth. Met.* **2003**, *135*−*136*, 647.
(90) Kartsovnik, M. V.; Kovalev, A. E.; Laukhin, V. N.; Ito, H.; Ishiguro, T.; Kushch, N.; Anzai, H.; Saito, G. *Synth. Met.* **1995**, *70*, 819.
(91) Nam, M.-S.; Honold, M. M.; Proust, C.; Harrison, N.; Mielke, C. H.; Blundell, S. J.; Singleton, J.; Hayes, W.; Kurmoo, M.; Day, P. *Synth. Met.* **1999**, *103*, 1905.
(92) Goddard, P. A.; Blundell, S. J.; Singleton, J.; McDonald, R. D.; Ardavan, A.; Narduzzo, A.; Schlueter, J. A.; Kini, A. M.; Sasaki, T. *cond-mat/0312197* **2003**, preprint.
(93) Pesotskii, S. I.; Lyubovskii, R. B.; Nizhankovskii, V. I.; Biberacher, W.; Kartsovnik, M. V.; Andres, K.; Perenboom, J. A. A. J.; Kushch, N. D.; Yagubskii, E. B.; Kobayashi, H. *JETP* **2000**, *90*, 527.
(94) Hanasaki, N.; Kagoshima, S.; Miura, N.; Saito, G. *Phys. Rev. B* **2001**, *63*, 245116.
(95) Hanasaki, N.; Kagoshima, S.; Miura, N.; Saito, G. *J. Phys. Soc. Jpn.* **1996**, *65*, 1010.
(96) Kartsovnik, M. V.; Kovalev, A. E.; Laukhin, V. N.; Pesotskii, S. I. *J. Phys. I* **1993**, *2*, 223.
(97) Kartsovnik, M. V.; Kovalev, A. E.; Kushch, N. D. *J. Phys. I* **1993**, *3*, 1187.
(98) Kovalev, A. E.; Kartsovnik, M. V.; Shibaeva, R. P.; Rozenberg, L. P.; Schegolev, I. F.; Kushch, N. D. *Solid State Commun.* **1994**, *89*, 575. Kartsovnik, M. V.; Kovalev, A. E.; Shibaeva, R. P.; Rozenberg, L. P.; Kushch, N. D. *Physica B* **1994**, *201*, 459.
(99) Iye, Y.; Yagi, R.; Hanasaki, N.; Kagoshima, S.; Mori, H.; Hujimoto, H.; Saito, G. *J. Phys. Soc. Jpn.* **1994**, *63*, 674.
(100) Sasaki, T.; Toyota, N. *Phys. Rev. B* **1994**, *49*, 10120.
(101) Caulfield, J.; Singleton, J.; Hendriks, P. T. J.; Perenboom, J. A. A. J.; Pratt, F. L.; Doporto, M.; Hayes, W.; Kurmoo, M.; Day, P. *J. Phys.: Condens. Matter* **1994**, *6*, L155.
(102) Kartsovnik, M. V.; Ito, H.; Ishiguro, T.; Mori, H.; Mori, T.; Saito, G.; Tanaka, S. *J. Phys.: Condens. Matter* **1994**, *6*, L479.
(103) Montambaux, G.; Littlewood, P. B. *Phys. Rev. Lett.* **1989**, *62*, 953.
(104) Chen, L.; Maki, K. *Synth. Met.* **1989**, *29*, F493.
(105) Lebed, A. G.; Bak, P. *Phys. Rev. Lett.* **1989**, *63*, 1315.
(106) Yakovenko, V. M. *Phys. Rev. Lett.* **1992**, *68*, 3607.
(107) Lebed, A. G. *J. Phys. I* **1994**, *4*, 351.
(108) Lebed, A. G. *J. Phys. I* **1996**, *6*, 1819.
(109) Chaikin, P. M. *Phys. Rev. Lett.* **1992**, *69*, 2831.
(110) Zheleznyak, A. T.; Yakovenko, V. M. *Synth. Met.* **1995**, *70*, 1005.
(111) Strong, S. P.; Clarke, D. G.; Anderson, P. W. *Phys. Rev. Lett.* **1994**, *73*, 1007.
(112) Danner, G. M.; Chaikin, P. M. *Phys. Rev. Lett.* **1995**, *75*, 4690.
(113) Osada, T.; Kagoshima, S.; Miura, N. *Phys. Rev. B* **1992**, *46*, 1812.
(114) Blundell, S. J.; Singleton, J. *Phys. Rev. B* **1996**, *53*, 5609.
(115) Kartsovnik, M. V.; Kovalev, A. E.; Laukhin, V. N.; Schegolev, I. F.; Ito, H.; Ishiguro, T.; Kushch, N. D.; Mori, H.; Saito, G. *Synth. Met.* **1995**, *70*, 811.
(116) Maki, K. *Phys. Rev. B* **1992**, *45*, 5111.
(117) Lebed, A. G.; Naughton, M. J. *J. Phys. IV* **2004**, *114*, 77. Lebed, A. G.; Bagmet, N. N.; Naughton, M. J. *Phys. Rev. Lett.* **2004**, *93*, 157006.
(118) Danner, G. M.; Kang, W.; Chaikin, P. M. *Phys. Rev. Lett.* **1994**, *72*, 3714.
(119) Yoshino, H.; Saito, K.; Kikuchi, K.; Nishikawa, H.; Kobayashi, K.; Ikemoto, I. *J. Phys. Soc. Jpn.* **1995**, *64*, 2307.
(120) Osada, T.; Kagoshima, S.; Miura, N. *Phys. Rev. Lett.* **1996**, *77*, 5261.
(121) Lee, I. J.; Naughton, M. J. *Phys. Rev. B* **1998**, *57*, 7423.
(122) Yoshino, H.; Murata, K. *J. Phys. Soc. Jpn.* **1999**, *68*, 3027.
(123) Yoshino, H.; Murata, K.; Saito, K.; Nishikawa, H.; Kikuchi, K.; Ikemoto, I. *Phys. Rev. B* **2003**, *67*, 035111.
(124) Yoshino, H.; Oda, A.; Murata, K.; Nishikawa, H.; Kikuchi, K.; Ikemoto, I. *Synth. Met.* **2001**, *120*, 885.
(125) Osada, T. *Physica E* **2002**, *12*, 272.
(126) Osada, T.; Kuraguchi, M. *Synth. Met.* **2003**, *133*−*134*, 75.
(127) Lebed, A. G.; Naughton, M. J. *J. Phys. IV* **2002**, *12*, Pr9-369. Lebed, A. G.; Naughton, M. J. *cond-mat/0304591* **2003**, preprint. Lebed, A. G.; Naughton, M. J. *Phys. Rev. Lett.* **2003**, *91*, 187003.
(128) McKenzie, R. H.; Moses, P. *Phys. Rev. B* **1999**, *60*, R11241.
(129) Hill, S. *Phys. Rev. B* **1997**, *55*, 4931.
(130) Blundell, S. J.; Ardavan, A.; Singleton, J. *Phys. Rev. B* **1997**, *55*, R6129.
(131) Ardavan, A.; Blundell, S. J.; Singleton, J. *Phys. Rev. B* **1999**, *60*, 15500.
(132) Hill, S. *Phys. Rev. B* **2000**, *62*, 8699.
(133) Peschansky, V. G. *Phys. Rep.* **1997**, *288*, 305.
(134) Peschanskiı, A. V.; Peschanskii, V. G. *JETP* **2000**, *91*, 416. Peschanskiı, V. G.; Pantoja, J. C. M. *Low Temp. Phys.* **2000**, *26*, 494.
(135) Kovalev, A. E.; Hill, S.; Kawano, K.; Tamura, M.; Naito, T.; Kobayashi, H. *Phys. Rev. Lett.* **2003**, *91*, 216402.
(136) Ardavan, A.; Schrama, J. M.; Blundell, S. J.; Singleton, J.; Hayes, W.; Kurmoo, M.; Day, P.; Goy, P. *Phys. Rev. Lett.* **1998**, *81*, 713.
(137) Mola, M.; Hill, S.; Goy, P.; Gross, M. *Rev. Sci. Instrum.* **2000**, *71*, 186.
(138) Schrama, J. M.; Singleton, J.; Edwards, R. S.; Ardavan, A.; Rzepniewski, E.; Harris, R.; Goy, P.; Gross, M.; Schlueter, J.; Kurmoo, M.; Day, P. *J. Phys.: Condens. Matter* **2001**, *13*, 2235.
(139) Palassis, C.; Mola, M.; Tritz, J.; Hill, S.; Uji, S.; Kawano, K.; Tamura, M.; Naito, T.; Kobayashi, H. *Synth. Met.* **2001**, *120*, 999.
(140) Edwards, R. S.; Narduzzo, A.; Ardavan, A.; Singleton, J. *Synth. Met.* **2003**, *133*−*134*, 117.
(141) Narduzzo, A.; Edwards, R. S.; Ardavan, A.; Singleton, J. *Synth. Met.* **2003**, *133*−*134*, 129. Rzepniewski, E.; Edwards, R. S.; Schrama, J. M.; Ardavan, A.; Singleton, J.; Kurmoo, M.; Day, P. *Synth. Met.* **2001**, *120*, 953.
(142) Oshima, Y.; Kimata, M.; Kishigi, K.; Ohta, H.; Koyama, K.; Motokawa, M.; Nishikawa, H.; Kikuchi, K.; Ikemoto, I. *Phys. Rev. B* **2003**, *68*, 054526; *Physica B* **2004**, *346*−*347*, 387.
(143) Oshima, Y.; Ohta, H.; Koyama, K.; Motokawa, M.; Yamamoto, H. M.; Kato, R.; Tamura, M.; Nishio, Y.; Kajita, K. *J. Phys. Soc. Jpn.* **2003**, *72*, 143.
(144) Kovalev, A. E.; Hill, S.; Qualls, J. S. *Phys. Rev. B* **2002**, *66*, 134513.
(145) McKenzie, R. H.; Moses, P. *Phys. Rev. Lett.* **1998**, *81*, 4492. Moses, P.; McKenzie, R. H. *Phys. Rev. B* **1999**, *60*, 7998.
(146) Soda, G.; Jérome, D.; Weger, M.; Alizon, J.; Gallice, J.; Robert, H.; Fabre, J. M.; Giral, L. *J. Phys. (Paris)* **1977**, *38*, 931. Shitkovsky, S.; Weger, M.; Gutfreund, H. *J. Phys. (Paris)* **1978**, *39*, 711.
(147) Jérome, D.; Schulz, H. J. *Adv. Phys.* **1982**, *31*, 299.
(148) Kumar, N.; Jayannavar, A. M. *Phys. Rev. B* **1992**, *45*, 5001.
(149) Osada, T.; Kobayashi, K.; Ohmichi, E. *Synth. Met.* **2003**, *135*−*136*, 653.
(150) Wosnitza, J.; Hagel, J.; Qualls, J. S.; Brooks, J. S.; Balthes, E.; Schweitzer, D.; Schlueter, J. A.; Geiser, U.; Mohtasham, J.; Winter, R. W.; Gard, G. L. *Phys. Rev. B* **2002**, *65*, 180506(R).
(151) Singleton, J.; Goddard, P. A.; Ardavan, A.; Harrison, N.; Blundell, S. J.; Schlueter, J. A.; Kini, A. M. *Phys. Rev. Lett.* **2002**, *88*, 037001.
(152) Singleton, J.; Mielke, C. H.; Hayes, W.; Schlueter, J. A. *J. Phys.: Condens. Matter* **2003**, *15*, L203.
(153) Kuraguchi, M.; Ohmichi, E.; Osada, T.; Shiraki, Y. *Synth. Met.* **2003**, *133*−*134*, 113.
(154) Landau, L. D. *Z. Phys.* **1930**, *64*, 629.
(155) Onsager, L. *Philos. Mag.* **1952**, *43*, 1006.

(156) Lifshitz, I. M.; Kosevich, A. M. *Sov. Phys. JETP* **1956**, *2*, 636.
(157) Peschansky, V. G.; Atalla, R. *Low Temp. Phys.* **2001**, *27*, 695.
(158) Kartsovnik, M. V. **2004**, unpublished.
(159) Adams, E. N.; Holstein, T. D. *J. Phys. Chem. Solids* **1959**, *10*, 254.
(160) Pippard, A. B. *The Dynamics of Conduction Electrons*; Gordon and Breach: New York, 1965.
(161) Merino, J.; McKenzie, R. H. *Phys. Rev. B* **2000**, *62*, 2416.
(162) Merino, J.; McKenzie, R. H. *Phys. Rev. B* **2000**, *61*, 7996.
(163) Dingle, R. B. *Proc. R. Soc. A* **1952**, *211*, 517.
(164) Bychkov, Y. A. *Sov. Phys. JETP* **1961**, *12*, 977.
(165) Harrison, N.; Bogaerts, R.; Reinders, P. H. P.; Singleton, J.; Blundell, S. J.; Herlach, F. *Phys. Rev. B* **1996**, *54*, 9977.
(166) Harrison, N.; Mielke, C. H.; Rickel, D. G.; Wosnitza, J.; Qualls, J. S.; Brooks, J. S.; Balthes, E.; Schweitzer, D.; Heinen, I.; Strunz, W. *Phys. Rev. B* **1998**, *58*, 10248.
(167) Wosnitza, J.; Wanka, S.; Hagel, J.; Häussler, R.; v. Löhneysen, H.; Schlueter, J. A.; Geiser, U.; Nixon, P. G.; Winter, R. W.; Gard, G. L. *Phys. Rev. B* **2000**, *62*, R11973.
(168) Balthes, E.; Schiller, M.; Schweitzer, D.; Heinen, I.; Strunz, W.; Steep, E.; Jansen, A. G. M.; Wyder, P. *Europhys. Lett.* **1999**, *47*, 70.
(169) Balthes, E.; Schweitzer, D.; Heinen, I.; Keller, H. J.; Strunz, W.; Biberacher, W.; Jansen, A. G. M.; Steep, E. *Z. Phys. B* **1996**, *99*, 163.
(170) Balthes, E.; Wyder, P.; Schweitzer, D. *Solid State Commun.* **2002**, *124*, 141.
(171) Powell, B. J.; McKenzie, R. H. *Phys. Rev. B* **2004**, *69*, 024519.
(172) Wosnitza, J.; Goll, G.; Beckmann, D.; Wanka, S.; Schlueter, J. A.; Williams, J. M.; Nixon, P. G.; Winter, R. W.; Gard, G. L. *Physica B* **1998**, *246*−*247*, 104.
(173) Kobayashi, A.; Udagawa, T.; Tomita, H.; Naito, T.; Kobayashi, H. *Chem Lett.* **1993**, 2179.
(174) Goze, F.; Laukhin, V. N.; Brossard, L.; Audouard, A.; Ulmet, J. P.; Askenazy, S.; Naito, T.; Kobayashi, H.; Kobayashi, A.; Tokumoto, M.; Cassoux, P. *Europhys. Lett.* **1994**, *28*, 427.
(175) Brossard, L.; Clerac, R.; Coulon, C.; Tokumoto, M.; Ziman, T.; Petrov, D. K.; Laukhin, V. N.; Naughton, M. J.; Audouard, A.; Goze, F.; Kobayashi, A.; Kobayashi, H.; Cassoux, P. *Eur. Phys. J. B* **1998**, *1*, 439.
(176) Balicas, L.; Brooks, J. S.; Storr, K.; Uji, S.; Tokumoto, M.; Tanaka, H.; Kobayashi, H.; Kobayashi, A.; Barzykin, V.; Gor'kov, L. P. *Phys. Rev. Lett.* **2001**, *87*, 067002.
(177) Lebed, A. G. *JETP Lett.* **1986**, *44*, 114.
(178) Lebed, A. G.; Yamaji, K. *Phys. Rev. Lett.* **1998**, *80*, 2697.
(179) Dupuis, N.; Montambaux, G.; Sá de Melo, C. A. R. *Phys. Rev. Lett.* **1993**, *70*, 2613.
(180) Dupuis, N.; Montambaux, G. *Phys. Rev. B* **1994**, *49*, 8993.
(181) Sá de Melo, C. A. R. *Physica C* **1996**, *260*, 224.
(182) Shimahara, H. *J. Phys. Soc. Jpn.* **2000**, *69*, 1966.
(183) Jaccarino, V.; Peter, M. *Phys. Rev. Lett.* **1962**, *9*, 290.
(184) Uji, S.; Shinagawa, H.; Terakura, C.; Terashima, T.; Yakabe, T.; Terai, Y.; Tokumoto, M.; Kobayashi, A.; Tanaka, H.; Kobayashi, H. *Phys. Rev. B* **2001**, *64*, 024531.
(185) Cépas, O.; McKenzie, R. H.; Merino, J. *Phys. Rev. B* **2002**, *65*, 100502.
(186) Uji, S.; Terakura, T.; Terashima, T.; Yakabe, T.; Terai, Y.; Tokumoto, M.; Kobayashi, A.; Sakai, F.; Tanaka, H.; Kobayashi, H. *Phys. Rev. B* **2002**, *65*, 113101.
(187) Balicas, L.; Brooks, J. S.; Storr, K.; Graf, D.; Uji, S.; Shinagawa, H.; Ojima, E.; Fujiwara, H.; Kobayashi, H.; Kobayashi, A.; Tokumoto, M. *Solid State Commun.* **2000**, *116*, 557.
(188) Uji, S.; Shinagawa, H.; Terai, Y.; Yakabe, T.; Terakura, C.; Terashima, T.; Balicas, L.; Brooks, J. S.; Ojima, E.; Fujiwara, H.; Kobayashi, H.; Kobayashi, A.; Tokumoto, M. *Physica B* **2001**, *298*, 557.
(189) Ojima, E.; Fujiwara, H.; Kato, K.; Kobayashi, H.; Tanaka, H.; Kobayashi, A.; Tokumoto, M.; Cassoux, P. *J. Am. Chem. Soc.* **1999**, *121*, 5581.
(190) Kobayashi, H.; Kobayashi, A.; Cassoux, P. *Chem. Soc. Rev.* **2000**, *29*, 325.
(191) Fujiwara, H.; Fujiwara, E.; Nakazawa, Y.; Narymbetov, B. Z.; Kato, K.; Kobayashi, H.; Kobayashi, A.; Tokumoto, M.; Cassoux, P. *J. Am. Chem. Soc.* **2001**, *123*, 306.
(192) Kobayashi, H.; Zhang, B.; Tanaka, H.; Fujiwara, H.; Otsuka, T.; Fujiwara, E.; Kobayashi, A. *Synth. Met.* **2003**, *137*, 1157.
(193) Fujiwara, H.; Kobayashi, H.; Fujiwara, E.; Kobayashi, A. *J. Am. Chem. Soc.* **2002**, *124*, 6816.
(194) Tanatar, M. A.; Suzuki, M.; Ishiguro, T.; Tanaka, H.; Fujiwara, H.; Kobayashi, H.; Toito, T.; Yamada, J. *Synth. Met.* **2003**, *137*, 1291.
(195) Konoike, T.; Fujiwara, H.; Zhang, B.; Kobayashi, H.; Nishimura, M.; Yasuzuka, S.; Enomoto, K.; Uji, S. *J. Phys. IV* **2004**, *114*, 223.
(196) Cohen, M. H.; Falicov, L. M. *Phys. Rev. Lett.* **1961**, *7*, 231.
(197) Blount, E. I. *Phys. Rev.* **1962**, *126*, 1636.
(198) Kaganov, M. I.; Slutskin, A. A. *Phys. Rep.* **1983**, *98*, 189.
(199) Falicov, L. M.; Stachowiak, H. *Phys. Rev.* **1966**, *147*, 505.
(200) Pippard, A. B. *Proc. R. Soc. London* **1962**, *A270*, 1.
(201) Pippard, A. B. *Philos. Trans. R. Soc. London* **1964**, *A256*, 317.
(202) Honold, M. M.; Harrison, N.; Nam, M.-S.; Singleton, J.; Mielke, C. H.; Kurmoo, M.; Day, P. *Phys. Rev. B* **1998**, *58*, 7560.
(203) Meyer, F. A.; Steep, E.; Biberacher, W.; Christ, P.; Lerf, A.; Jansen, A. G. M.; Joss, W.; Wyder, P.; Andres, K. *Europhys. Lett.* **1995**, *32*, 681.
(204) Vignolles, D.; Audouard, A.; Brossard, L.; Pesotskii, S.; Lyubovskii, R.; Nardone, M.; Haanappel, E.; Lyubovskaya, R. *Eur. Phys. J. B* **2003**, *31*, 53.
(205) Audouard, A.; Vignolles, D.; Proust, C.; Brossard, L.; Nardone, M.; Haanappel, E.; Pesotskii, S.; Lyubovskii, R.; Lyubovskaya, R. *Physica B* **2004**, *346*−*347*, 377.
(206) Stark, R. W.; Friedberg, C. B. *J. Low Temp. Phys.* **1974**, *14*, 111. Stark, R. W.; Reifenberger, R. *J. Low Temp. Phys.* **1977**, *26*, 763. Stark, R. W.; Reifenberger, R. *J. Low Temp. Phys.* **1977**, *26*, 819. Reifenberger, R. *J. Low Temp. Phys.* **1977**, *26*, 827. Sandesara, N. B.; Stark, R. W. *Phys. Rev. Lett.* **1984**, *53*, 1681.
(207) Müller, H.; Heidmann, C.-P.; Lerf, A.; Biberacher, W.; Sieburger, R.; Andres, K. *The Physics and Chemistry of Organic Superconductors*, Proceedings of the ISSP International Symposium, Tokyo, Japan, August 28−30, 1989; Springer-Verlag: Berlin, Heidelberg, 1990. Heidmann, C.-P.; Müller, H.; Biberacher, W.; Neumaier, K.; Probst, Ch.; Andres, K.; Jansen, A. G. M.; Joss, W. *Synth. Met.* **1991**, *41*−*43*, 2029. Andres, K.; Heidmann, C.-P.; Müller, H.; Himmelsbach, S.; Biberacher, W.; Probst, Ch.; Joss, W. *Synth. Met.* **1991**, *41*−*43*, 1893.
(208) Sasaki, T.; Sato, H.; Toyota, N. *Solid State Commun.* **1990**, *76*, 507.
(209) Caulfield, J.; Singleton, J.; Pratt, F. L.; Doporto, M.; Lyubczynski, W.; Hayes, W.; Kurmoo, M.; Day, P.; Hendriks, P. T. J.; Perenboom, J. A. A. J. *Synth. Met.* **1993**, *61*, 63.
(210) Uji, S.; Chaparala, M.; Hill, S.; Sandhu, P. S.; Qualls, J.; Seger, L.; Brooks, J. S. *Synth. Met.* **1997**, *85*, 1573.
(211) Kartsovnik, M. V.; Logvenov, G. Y.; Ishiguro, T.; Biberacher, W.; Anzai, H.; Kushch, N. *Phys. Rev. Lett.* **1996**, *77*, 2530.
(212) Harrison, N.; Caulfield, J.; Singleton, J.; Reinders, P. H. P.; Herlach, F.; Hayes, W.; Kurmoo, M.; Day, P. *J. Phys.: Condens. Matter* **1996**, *8*, 5415.
(213) Harrison, N.; Goodrich, R. G.; Vuillemin, J. J.; Fisk, Z.; Rickel, D. G. *Phys. Rev. Lett.* **1998**, *80*, 4498.
(214) Proust, C.; Audouard, A.; Brossard, L.; Pesotskii, S.; Lyubovskii, R.; Lyubovskaya, R. *Phys. Rev. B* **2002**, *65*, 155106.
(215) Fortin, J.-Y.; Ziman, T. *Phys. Rev. Lett.* **1999**, *82*, 4149.
(216) Tan, Y.; Ziman, T. In *Physical Phenomena at High Magnetic Fields-II*; Fisk, Z., Gorkov, L., Meltzer, D., Schrieffer, R., Eds.; World Scientific: Singapore, 1996; p 110.
(217) Kartsovnik, M. V.; Logvenov, G. Y.; Biberacher, W.; Ishiguro, T.; Christ, P.; Andres, K.; Steep, E.; Jansen, A. G. M.; Kushch, N. D.; Müller, H. *Synth. Met.* **1997**, *86*, 2061.
(218) Weiss, H.; Kartsovnik, M. V.; Biberacher, W.; Steep, E.; Jansen, A. G. M.; Kushch, N. D. *JETP Lett.* **1997**, *66*, 202.
(219) Mielke, C. H.; Harrison, N.; Rickel, D. G.; Lacerda, A. H.; Vestal, R. M.; Montgomery, L. K. *Phys. Rev. B* **1997**, *56*, 4309.
(220) Weiss, H.; Kartsovnik, M. V.; Biberacher, W.; Steep, E.; Balthes, E.; Jansen, A.; Andres, K.; Kushch, N. *Phys. Rev. B* **1999**, *59*, 12370.
(221) Weiss, H.; Kartsovnik, M. V.; Biberacher, W.; Balthes, E.; Jansen, A. G. M.; Kushch, N. D. *Phys. Rev. B* **1999**, *60*, 16259(R).
(222) Kartsovnik, M. V.; Logvenov, G. Y.; Ito, H.; Ishiguro, T.; Saito, G. *Phys. Rev. B* **1995**, *52*, R15715.
(223) Nogami, Y.; Pouget, J.-P.; Ito, H.; Ishiguro, T.; Saito, G. *Solid State Commun.* **1994**, *89*, 113.
(224) Kartsovnik, M. V.; Biberacher, W.; Andres, K.; Kushch, N. D. *JETP Lett.* **1995**, *62*, 905.
(225) Yamauchi, Y.; Kartsovnik, M. V.; Ishiguro, T.; Kubota, M.; Saito, G. *J. Phys. Soc. Jpn.* **1996**, *65*, 354.
(226) Lyubovskii, R. B.; Pesotskii, S. I.; Gilewski, A.; Lyubovskaya, R. N. *JETP* **1995**, *80*, 946.
(227) Vieros, L. F.; Canadell, E. *J. Phys. I* **1994**, *4*, 939.
(228) Laukhin, V. N.; Audouard, A.; Rakoto, H.; Broto, J.; Goze, F.; Coffe, G.; Brossard, L.; Redoules, J.; Kartsovnik, M.; Kushch, N.; Buravov, L.; Khomenko, A.; Yagubskii, E.; Askenazy, S.; Pari, P. *Physica B* **1995**, *211*, 282.
(229) Sandhu, P. S.; Athas, G. J.; Brooks, J. S.; Haanappel, E. G.; Goettee, J. D.; Rickel, D. W.; Tokumoto, M.; Kinoshita, N.; Tanaka, Y. *Surf. Sci.* **1996**, *361*/*362*, 913.
(230) Tokumoto, M.; Swanson, A. G.; Brooks, J. S.; Agosta, C. C.; Hannahs, S. T.; Kinoshita, N.; Anzai, H.; Tamura, M.; Tajima, H.; Kuroda, H.; Ugawa, A.; Yakushi, K. *Physica B* **1993**, *184*, 508.
(231) Harrison, N.; House, A.; Deckers, I.; Singleton, J.; Herlach, F.; Hayes, W.; Kurmoo, M.; Day, P. *Phys. Rev. B* **1995**, *52*, 5584.
(232) Wosnitza, J.; Wanka, S.; Hagel, J.; Balthes, E.; Harrison, N.; Schlueter, J. A.; Kini, A. M.; Geiser, U.; Mohtasham, J.; Winter, R. W.; Gard, G. L. *Phys. Rev. B* **2000**, *61*, 7383.
(233) Shoenberg, D. *J. Low Temp. Phys.* **1984**, *56*, 417.
(234) Champel, T.; Mineev, V. P. *Philos. Mag. B* **2001**, *81*, 55.
(235) Grigoriev, P. D.; Vagner, I. D. *cond-mat*/*0009409* **2000**, preprint.
(236) Peierls, R. *Z. Phys.* **1933**, *81*, 186.

(237) Vagner, I. D.; Maniv, T.; Ehrenfreund, E. *Phys. Rev. Lett.* **1983**, *51*, 1700.
(238) Vagner, I. D.; Maniv, T. *Phys. Rev. B* **1985**, *32*, 8398.
(239) Jauregui, K.; Marchenko, V. I.; Vagner, I. D. *Phys. Rev. B* **1990**, *41*, 12922.
(240) Grigoriev, P. D. *JETP* **2001**, *92*, 1090.
(241) Itskovsky, M. A.; Maniv, T.; Vagner, I. D. *Phys. Rev. B* **2000**, *61*, 14616.
(242) Vagner, I. D.; Maniv, T.; Joss, W.; van Ruitenbeek, J. M.; Jauregui, K. *Synth. Met.* **1989**, *34*, 393.
(243) Itskovsky, M. A.; Maniv, T. *Phys. Rev. B* **2001**, *64*, 174421.
(244) Champel, T. *Phys. Rev. B* **2001**, *64*, 054407.
(245) Shepherd, R. A.; Elliott, M.; Herrenden-Harker, W. G.; Zervos, M.; Morris, P. R.; Beck, M.; Ilegems, M. *Phys. Rev. B* **1999**, *60*, R11277.
(246) Yoshida, Y.; Mukai, A.; Miyake, K.; Watanabe, N.; Settai, R.; Ōnuki, Y.; Matsuda, T. D.; Aoki, Y.; Sato, H.; Miyamoto, Y.; Wada, N. *Physica B* **2000**, *281−282*, 959.
(247) Machida, K.; Kishigi, K.; Hori, Y. *Phys. Rev. B* **1995**, *51*, 8946.
(248) Kishigi, K.; Nakano, M.; Machida, K.; Hori, Y. *J. Phys. Soc. Jpn.* **1995**, *64*, 3043.
(249) Alexandrov, A. S.; Bratkovsky, A. M. *Phys. Rev. Lett.* **1996**, *76*, 1308.
(250) Alexandrov, A. S.; Bratkovsky, A. M. *Phys. Lett. A* **1997**, *234*, 53.
(251) Nakano, M. *J. Phys. Soc. Jpn.* **1997**, *66*, 19.
(252) Kishigi, K. *J. Phys. Soc. Jpn.* **1997**, *66*, 910.
(253) Fortin, J.-Y.; Ziman, T. *Phys. Rev. Lett.* **1998**, *80*, 3117.
(254) Kishigi, K.; Hasegawa, Y.; Miyazaki, M. *J. Phys. Soc. Jpn.* **2000**, *69*, 821.
(255) Bratkovsky, A. M.; Alexandrov, A. S. *Phys. Rev. B* **2002**, *65*, 035418. Alexandrov, A. S.; Bratkovsky, A. M. *Phys. Rev. B* **2001**, *63*, 033105.
(256) Champel, T. *Phys. Rev. B* **2002**, *65*, 153403.
(257) Kishigi, K.; Hasegawa, Y. *Phys. Rev. B* **2002**, *65*, 205405.
(258) Itskovsky, M. A. *Phys. Rev. B* **2003**, *68*, 054423.
(259) Fortin, J.-Y.; Perez, E.; Audouard, A. *Physica B* **2004**, *346−347*, 373.
(260) Alexandrov, A. S.; Bratkovsky, A. M. *Phys. Rev. B* **2004**, *69*, 167401.
(261) Champel, T. *Phys. Rev. B* **2004**, *69*, 167402.
(262) Grigoriev, P. D.; Vagner, I. D. *JETP* **1999**, *69*, 156.
(263) Grigoriev, P. D. Magnetic Quantum oscillations in Quasi-Two-Dimensional Metals. Ph.D. Thesis; Hartung-Gorre Verlag: Konstanz, 2002.
(264) Nakano, M. *J. Phys. Soc. Jpn.* **1999**, *68*, 1801.
(265) Gvozdikov, V. M.; Jansen, A. G. M.; Pesin, D. A.; Vagner, I. D.; Wyder, P. *Phys. Rev. B* **2003**, *68*, 155107.
(266) Ohmichi, E.; Maeno, Y.; Ishiguro, T. *J. Phys. Soc. Jpn.* **1999**, *68*, 24.
(267) Potts, A.; Shepherd, R.; Herrenden-Harker, W. G.; Elliot, M.; Jones, C. L.; Usher, A.; Jones, G. A. C.; Ritchie, D. A.; Linfield, E. H.; Grimshaw, M. *J. Phys.: Condens. Matter* **1996**, *8*, 5189.
(268) Maniv, T.; Vagner, I. D. *Phys. Rev. B* **1988**, *38*, 6301.
(269) Ando, T.; Uemura, Y. *J. Phys. Soc. Jpn.* **1974**, *36*, 959.
(270) Geiser, U.; Schlueter, J. A.; Wang, H. H.; Kini, A. M.; Williams, J. M.; Sche, P. P.; Zakowicz, H. I.; VanZile, M. L.; Dudek, J. D. *J. Am. Chem. Soc.* **1996**, *118*, 9996.
(271) Beckmann, D.; Wanka, S.; Wosnitza, J.; Schlueter, J. A.; Williams, J. M.; Nixon, P. G.; Winter, R. W.; Gard, G. L.; Ren, J.; Whangbo, M.-H. *Eur. Phys. J. B* **1998**, *1*, 295.
(272) Wosnitza, J.; Wanka, S.; Qualls, J. S.; Brooks, J. S.; Mielke, C. H.; Harrison, N.; Schlueter, J. A.; Williams, J. M.; Nixon, P. G.; Winter, R. W.; Gard, G. L. *Synth. Met.* **1999**, *103*, 2000.
(273) Zuo, F.; Su, X.; Zhang, P.; Brooks, J. S.; Wosnitza, J.; Schlueter, J. A.; Williams, J. M.; Nixon, P. G.; Winter, R. W.; Gard, G. L. *Phys. Rev. B* **1999**, *60*, 6296.
(274) Nam, M.-S.; Ardavan, A.; Symington, J. A.; Singleton, J.; Harrison, N.; Mielke, C. H.; Schlueter, J. A.; Winter, R. W.; Gard, G. L. *Phys. Rev. Lett.* **2001**, *87*, 117001.
(275) Hagel, J.; Wanka, S.; Wosnitza, J.; Balthes, E.; Schlueter, J. A.; Kini, A. M.; Geiser, U.; Mohtasham, J.; Winter, R. W.; Gard, G. L. *Synth. Met.* **2001**, *120*, 813.
(276) Harrison, N. *Phys. Rev. Lett.* **1999**, *83*, 1395.
(277) Champel, T.; Mineev, V. P. *Physica B* **2004**, *346−347*, 392.
(278) Alekseevskii, N. E.; Nizhankovskii, V. I. *Sov. Phys. JETP* **1985**, *61*, 1051.
(279) Harrison, N.; Balicas, L.; Brooks, J. S.; Tokumoto, M. *Phys. Rev. B* **2000**, *62*, 14212. Harrison, N.; Singleton, J.; Bangura, A.; Ardavan, A.; Goddard, P. A.; McDonald, R. D.; Montgomery, L. K. *Phys. Rev. B* **2004**, *69*, 165103.
(280) Andres, D.; Kartsovnik, M. V.; Biberacher, W.; Weiss, H.; Balthes, E.; Müller, H.; Kushch, N. D. *Phys. Rev. B* **2001**, *64*, 161104(R). Andres, D.; Kartsovnik, M. V.; Grigoriev, P. D.; Biberacher, W.; Müller, H. *Phys. Rev. B* **2003**, *68*, 201101. Kartsovnik, M. V.; Andres, D.; Biberacher, W.; Grigoriev, P. D.; Schuberth, E. A.; Müller, H. *J. Phys. IV* **2004**, *114*, 191.
(281) Choi, E. S.; Brooks, J. S.; Qualls, J. S. *Phys. Rev. B* **2002**, *65*, 205119.
(282) Steep, E.; Nguyen, L. H.; Biberacher, W.; Müller, H.; Jansen, A. G. M.; Wyder, P. *Physica B* **1999**, *259−261*, 1079.
(283) Nguyen, L. H. De Haas-van Alphen Effect in a Low-Dimensional Organic Superconductor and Boro-carbide Superconductors. Ph.D. Thesis; Hartung-Gorre Verlag: Konstanz, 1998.
(284) Sandhu, P. S.; Kim, J. H.; Brooks, J. S. *Phys. Rev. B* **1997**, *56*, 11566.
(285) Kim, J. H.; Han, S. Y.; Brooks, J. S. *Phys. Rev. B* **1999**, *60*, 3213.
(286) Han, S. Y.; Brooks, J. S.; Kim, J. H. *Phys. Rev. Lett.* **2000**, *85*, 1500.
(287) Gvozdikov, V. M.; Pershin, Y. V.; Steep, E.; Jansen, A. G. M.; Wyder, P. *Phys. Rev. B* **2002**, *65*, 165102.
(288) Datars, A. E.; Sipe, J. E. *Phys. Rev. B* **1995**, *51*, 4312.
(289) Gvozdikov, V. M. *Low Temp. Phys.* **2001**, *27*, 704.
(290) Averkiev, N. S.; Golub, L. E.; Tarasenko, S. A.; Willander, M. *J. Phys.: Condens. Matter* **2001**, *13*, 2517.
(291) Grigoriev, P. D.; Kartsovnik, M. V.; Biberacher, W.; Kushch, N. D.; Wyder, P. *Phys. Rev. B* **2002**, *65*, 060403(R).
(292) Grigoriev, P. D. *Phys. Rev. B* **2003**, *67*, 144401.
(293) Champel, T.; Mineev, V. P. *Phys. Rev. B* **2002**, *66*, 195111.
(294) Whangbo, M.-H.; Williams, J. M.; Leung, P. C. W.; Beno, M. A.; Emge, T. J.; Wang, H. H.; Carlson, K. D.; Crabtree, G. W. *J. Am. Chem. Soc.* **1985**, *107*, 5815.
(295) Kasowski, R. V.; Whangbo, M.-H. *Inorg. Chem.* **1990**, *29*, 360.
(296) Kartsovnik, M. V.; Kononovich, P. A.; Laukhin, V. N.; Pesotskii, S. I.; Schegolev, I. F. *JETP Lett.* **1989**, *49*, 519.
(297) Wosnitza, J.; Beckmann, D.; Goll, G.; Schweitzer, D. *Synth. Met.* **1997**, *85*, 1479.
(298) Ohmichi, E.; Ito, H.; Ishiguro, T.; Saito, G.; Komatsu, T. *Phys. Rev. B* **1998**, *57*, 7481.
(299) Togonidze, T. G.; Kartsovnik, M. V.; Perenboom, J. A. A. J.; Kushch, N. D.; Kobayashi, H. *Physica B* **2001**, *294−295*, 435.
(300) Gvozdikov, V. M. *Sov. Phys. Solid State* **1984**, *26*, 1560.
(301) Schiller, M.; Schmidt, W.; Balthes, E.; Schweitzer, D.; Koo, H.; Whangbo, M. H.; Heinen, I.; Klausa, T.; Kircher, P.; Strunz, W. *Europhys. Lett.* **2000**, *51*, 82.
(302) Wosnitza, J.; Crabtree, G. W.; Wang, H. H.; Geiser, U.; Williams, J. M.; Carlson, K. D. *Phys. Rev. B* **1992**, *45*, 3018.
(303) Brooks, J.; Sandhu, P.; Qualls, J. S.; Hill, S.; Tokumoto, M. *Physica B* **1998**, *246−247*, 307.
(304) Kartsovnik, M.; Andres, D.; Grigoriev, P.; Biberacher, W.; Müller, H. *Physica B* **2004**, *346−347*, 368.

CR0306891